FP7-ICT Future Networks
SPECIFIC TARGETTED RESEARCH PROJECT
Project Deliverable

PHYDYAS Doc. Number	PHYDYAS_006
Project Number	**ICT - 211887**
Project Acronym+Title	PHYDYAS – PHYsical layer for DYnamic AccesS and cognitive radio
Deliverable Nature	Report
Deliverable Number	D4.1
Contractual Delivery Date	January 1st, 2009
Actual Delivery Date	January 28, 2009
Title of Deliverable	MIMO channel matrix estimation and tracking
Contributing Workpackage	WP4. MIMO TRANSMIT AND RECEIVE PROCESSING
Project starting date; Duration	01/01/2008 ; 30 months
Dissemination Level	RE
Author(s)	Montse Nájar, Carlos Bader, Francisco Rubio, Eleftherios Kofidis, Mario Tanda, Jérôme Louveaux, Markku Renfors, Didier Le Ruyet

Abstract: The techniques developed for initialization in the single antenna case are extended to MIMO systems: joint CFO and timing estimation, use of auxiliary pilots, filter bank memory preloading. Associated channel matrix estimation methods are investigated and the adaptation to WiMAX is considered. Multi-coefficient sub-channel equalization exploits the channel matrix measurements. Successive interference cancellation approaches are proposed to improve the performance of the equalizers. For the multiantenna receiver, diversity equalization is combined with maximum ratio combining. Finally, a brief introduction to MIMO techniques is provided, as a transition to the theme of the next deliverable.

TABLE OF CONTENTS

Notations

$\angle\{x\}$ the argument of a complex number x in [0,2π),

$\mathrm{Re}\{.\}$ real part

$\mathrm{Im}\{.\}$ imaginary part

$(.)^*$ complex conjugation

$|.|$ absolute value

$\lfloor x \rfloor$ integer part of x

$*$ convolution operator

$\otimes$ element –by-element multiplication

M overall number of subcarriers, FFT size

M_u^i number of used subcarriers of the ith user (in single-user case, index i is dropped)

M_u^i set of used subcarriers of the ith user

M_v number of virtual (unused) subcarriers

K overlapping factor in prototype filter design

α roll-off factor in prototype filter design

L_p prototype filter length

L_{eq} subcarrier equalizer length

T_s sampling interval (at SFB output and AFB input)

f_s sampling rate (at SFB output and AFB input) $f_s = 1/T_s$

T OQAM symbol duration; $T = MT_s$

Δf subcarrier spacing, $\Delta f = 1/T = f_s/M$

k subcarrier index (k=0, …, M-1; k=0 corresponds to center subcarrier)

l time index at OQAM symbol rate (→ T)

n time index at OQAM subsymbol rate (→ $T/2$)

m time index at SFB output/AFB input (→ T/M)

i user index in multiuser cases

U number of users

$v^R[n]$ real part of (arbitrary) complex sequence $v[n]$

$v^I[n]$ imaginary part of (arbitrary) complex sequence $v[n]$

$p(t)$ prototype filter impulse response, continuous-time model

$p[m]$ prototype filter impulse response, discrete-time [(1)]

$$p[m] = \sqrt{T_s}\, p\left(mT_s\right)$$

$P(z)$ prototype filter transfer function

$f_k[m]$ analysis filter impulse response for subchannel k

$F_k(z)$ analysis filter transfer function for subchannel k

$G_k(z)$ synthesis filter transfer function for subchannel k

$g_k[m]$ synthesis filter impulse response for subchannel k

$$g_k[m] = p[m] e^{j\frac{2\pi}{M}k\left(m-\frac{L_p-1}{2}\right)}$$

$p_{k,n}[m]$ SFB impulse response for real symbol $d_{k,n}$ (see also definition of $s[m]$)

$$p_{k,n}[m] = \theta_{k,n}\beta_{k,n} g_k[m - nM/2]$$

$$= \theta_{k,n}\beta_{k,n} p[m - nM/2] e^{j\frac{2\pi}{M}km}$$

$\theta_{k,n}$ phase mapping between real data sequence and complex samples at the SFB input

In general,

$$\theta_{k,n} = \begin{cases} \pm 1 & \text{for } k+n \text{ even} \\ \pm j & \text{for } k+n \text{ odd} \end{cases}$$

The recommended choice (following Siohan's papers) is [2]:

$$\theta_{k,n} = j^{k+n}$$

$$\beta_{k,n} = e^{j2\pi k\left(-\frac{n}{2}-\frac{L_p-1}{2M}\right)}$$

$d_{k,n}^{i}$ transmitted sequence of the *i*th user (data & pilots) (real)

$x_{k,n}$ observed ideal (without channel) complex sample sequence at AFB output,

$$\theta_{k,n}^{*} x_{k,n} = d_{k,n} + j u_{k,n}$$

Here $u_{k,n}$ is the un-interesting part of the received complex samples.

$\tilde{x}_{k,n}$ $\theta_{k,n}^{*} x_{k,n}$

$y_{k,n}$ observed channel-distorted complex sample sequence at AFB output

$\tilde{y}_{k,n}$ $\theta_{k,n}^{*} y_{k,n}$

$\tilde{d}_{k,n}$ real part of the subcarrier sequence after equalization and multiplication by $\theta_{k,n}^{*}$

$\hat{d}_{k,n}$ detected sequence (real)

$s[m]$ transmitted sequence at SFB output, single user case

$$\begin{aligned} s[m] &= \sum_{k\in \mathsf{M}_u} \sum_{n=-\infty}^{\infty} d_{k,n}\theta_{k,n} g_k\left[m - nM/2\right] \\ &= \sum_{k\in \mathsf{M}_u} \sum_{n=-\infty}^{\infty} d_{k,n}\theta_{k,n} p\left[m - nM/2\right] e^{j\frac{2\pi}{M}k\left(m - n\frac{M}{2} - \frac{L_p-1}{2}\right)} \\ &= \sum_{k\in \mathsf{M}_u} \sum_{n=-\infty}^{\infty} d_{k,n}\theta_{k,n} (-1)^{kn}\, p\left[m - nM/2\right] e^{j\frac{2\pi}{M}k\left(m - \frac{L_p-1}{2}\right)} \\ &= \sum_{k\in \mathsf{M}_u} \sum_{n=-\infty}^{\infty} d_{k,n}\theta_{k,n}\beta_{k,n} p\left[m - nM/2\right] e^{j\frac{2\pi}{M}km} \\ &= \sum_{k\in \mathsf{M}_u} \sum_{n=-\infty}^{\infty} d_{k,n} p_{k,n}[m] \end{aligned}$$

$s_i[m]$ transmitted sequence at SFB output in the uplink multiuser FBMC system, e.g.,

$$s_i[m] = \sum_{k\in \mathsf{M}_u^{i}} \sum_{n=-\infty}^{\infty} d_{k,n} p_{k,n}[m]$$

$s(t)$ transmitted continuous-time signal ($s_i(t)$ correspondingly for user *i* in multiuser case)

$$s(t) = \sum_{k\in \mathsf{M}_u} \sum_{n=-\infty}^{\infty} d_{k,n}\theta_{k,n}(-1)^{kn} p\left(t - n\frac{T}{2}\right) e^{j2\pi k\left(\Delta f t - \frac{L_p-1}{2M}\right)}$$

$r(t)$ received continuous-time signal in the uplink multiuser FBMC system

$$r(t) = \sum_{i=1}^{U} e^{j2\pi(\frac{\varepsilon_i}{T}t)} h_i(t,\tau) * s_i(t) + \eta(t) \qquad \text{general case}$$

$$r(t) = \sum_{i=1}^{U} e^{j2\pi(\frac{\varepsilon_i}{T}t)} \sum_{p=0}^{P_i-1} c_{i,p} s_i(t-\tau_{i,p}) + \eta(t) \qquad \text{discrete multipath case}$$

$$r(t) = \sum_{i=1}^{U} e^{j2\pi(\frac{\varepsilon_i}{T}t)} c_i s_i(t-\tau_i) + \eta(t) \qquad \text{AWGN case}$$

$$= \sum_{i=1}^{U} e^{j2\pi(\frac{\varepsilon_i}{T}t+\phi_i)} |c_i| s_i(t-\tau_i) + \eta(t)$$

ε_i carrier frequency offset of the *i*th user, normalized to subcarrier spacing

ϕ_i carrier phase offset (radians) of the *i*th user in the AWGN model

$h_i(t,\tau)$ time-variant channel impulse response of *i*th user

P_i number of paths in the multipath channel model of user *i*

$c_{i,p}$ complex gain of the *p*th path of the channel of user *i*

$\tau_{i,p}$ delay of the *p*th path of the channel of user *i*

τ_i timing offset of the *i*th user in the AWGN model

$\eta(t)$ complex envelope of white (Gaussian) noise whose real and imaginary parts are statistically independent and have a power spectral density level of N_0

σ_η^2 channel noise variance

N_0 one-sided noise power spectral density of white channel noise

$r[m]$ received complex sequence at AFB input

$\eta[m]$ channel noise

$h_i[m]$ discrete-time channel impulse response for user *i* in block-fading model

$H_i(e^{j\omega})$ channel frequency response for user *i*

H_k channel response of subcarrier *k* (assuming flat-fading and time invariant/block-fading case)

$H_{k,n}$ channel response for subcarrier *k* and symbol *n* (assuming flat-fading and time variant case)

$H_{k,n}^{p,q}$ channel response for subcarrier *k* and symbol *n* from TX antenna *p* to RX antenna *q*

$w_k[n]$ subcarrier-wise channel equalizer impulse response for subchannel *k*

Notes:

(1) This assumes causal continuous-time prototype filter impulse response, which is different from Siohan's continuous-time model.

(2) The choice of $\theta_{k,n}$, i.e., the signs in mapping real data sequence to complex samples at the SFB input is an internal choice of the filter bank module (i.e., the definition of $x_{k,n}$ above can be assumed to be valid in any case). However, it has an effect on the signal models at the SFB output and for the complex sequences at the AFB output. In the receiver side, $\beta_{k,n}^*$ is implemented before the subband processing, and $\theta_{k,n}^*$ after it. With this choice, all the subchannels are centered at DC at the subchannel processing stage.

1 Introduction: MIMO in FBMC

The use of multiple antennas at the transmitter and/or at the receiver has led to the MIMO (multiple input multiple output) concept. With multiple antennas at the transmitter and the receiver, the following functions can be realized:

a) space diversity, to make the radio Rayleigh channel behave more like a stationary Gaussian channel, which allows for a reduction of transmission margins and improved quality of service,
b) multiplexing, i.e., parallel transmission over several propagation paths simultaneously, in order to increase the total bit rate in a given frequency bandwidth,
c) beam forming at the transmitter, at the receiver or jointly at both ends, to improve the link budget and control multi-user interference.

MIMO techniques combined with multicarrier (MC) transmission yield memoryless and flat sub-channels that can be accurately represented by a single complex matrix-valued coefficient. The properties of this matrix transfer function and, in particular, its eigenvalue/eigenvector decomposition are exploited to increase the data throughput and the quality of service. Therefore, it is crucial that the channel matrix elements be accurately and robustly estimated.

1.1 Initialization with FBMC

In burst transmission, the channel matrix estimation is part of the initialization process, which includes also frequency and time synchronization. The techniques developed for OFDM (orthogonal frequency division multiplexing) can apply to FBMC (filter bank based multicarrier) transmission and they will not be repeated here [51]. Instead, this document is focussed on the specific aspects of FBMC/OQAM (Offset Quadrature Amplitude Modulation), namely the prototype filter impulse response, the independence of the sub-channels and multi-tap sub-channel equalization. Of course, conventional OFDM techniques will be invoked whenever appropriate for comparison purposes, in terms of performance and complexity for example.

The prototype filter impulse response introduces a transition phase at the beginning and the end of the transmitted burst. It is crucial in cognitive radio, where the transmission system must insert its signal in a spectrum hole without disturbing other systems which operate in the immediate spectral vicinity. In these conditions, in order to limit the reduction in global throughput, parallelization of the synchronization and measurement operations is seeked. Of course, if a spectral gap is present between systems, maximizing the throughput is an objective and OFDM compatible techniques can be employed, as in the single antenna case, namely memory preloading and impulse response shortening.

In FBMC, any sub-channel overlaps with its neighbours only and orthogonality is limited to these neighbouring sub-channels. The property can be exploited in the measurement process. Moreover, since groups of sub-channels are independent as soon as there is an empty sub-channel in-between, many techniques developed for the downlink case (full group of sub-channels) apply to the uplink case (groups of sub-channels) as well. However, an important difference remains concerning the timing offset.

With the presence of multi-tap sub-channel equalizers, the timing offset is not a critical parameter for FBMC. However, if a single tap equalizer is desirable, which is the case for MIMO, then, the timing offset must be estimated and compensated. In multi-user uplink, it is not possible to compensate the timing offsets, unless ranging and distant timing alignment is performed as in OFDMA. Therefore, multitap sub-channel equalizers are necessary. Fortunately, in the MIMO context, the multiple antennas of a transmitter lead to received signals which have a common timing offset and, then, a

common timing offset equalizer can serve for all the received signals, while the various channel elements are modelled as a single tap coefficient.

1.2 System model for FBMC transmission

Following the notation in D2.1 [2], we express the discrete-time sequence of the baseband signal synthesized at the FBMC transmitter as

$$s[m] = \sum_{k \in M_u} \sum_{n=-\infty}^{\infty} d_{k,n} \theta_{k,n} \beta_{k,n} p[m - n\frac{M}{2}] e^{j\frac{2\pi}{M}km}, \tag{1.1}$$

where

$$\theta_{k,n} = e^{j\frac{\pi}{2}(k+n)} = j^{k+n}$$

and

$$\beta_{k,n} = (-1)^{kn} \cdot e^{-j\frac{2\pi k}{M}(\frac{L_p-1}{2})}.$$

Recall, that $d_{k,n}, \theta_{k,n}$, and $p[m]$ denote the complex-to-real transformed data symbol modulated (at rate $2/T$) on the kth subcarrier during the nth OQAM sub-symbol period, the phase mapping between the real-valued data sequence and the complex-valued input samples of the synthesis filter bank (SFB), and the impulse response of a real-valued symmetric lowpass prototype filter, respectively. Moreover, M, M_u, k, and m denote the overall number of subcarriers (=IFFT/FFT size), the number of active subcarriers, the subcarrier index, and the high rate (at the output of SFB) sample index, respectively. Coefficients $\beta_{k,n}$ are due to the applied modulation sequence in (1.1) and L_p denotes the length of the prototype filter.

The sequence $s[m]$ is transmitted over the mobile channel. A baseband equivalent time-variant tapped delay line (FIR filter with time-varying coefficients) is used to model the channel. The received sequence then writes

$$r[m] = \sum_{p=0}^{P-1+D} h_{p,m} s[m-p] + \eta[m],$$

where the channel transfer function

$$\begin{aligned} H(z) &= h_{0,m} + h_{1,m} z^{-1} + \ldots, h_{P-1+D,m} z^{-(P-1+D)} \\ &= \left[\tilde{h}_{0,m} + \tilde{h}_{1,m} z^{-1} + \ldots, \tilde{h}_{P-1,m} z^{-(P-1)}\right] \cdot z^{-D} \\ &= \tilde{H}(z) \cdot z^{-D} \end{aligned}$$

is expressed as a cascade of a 0-delay multipath response denoted by $\tilde{H}(z)$ (corresponding to a receiver perfectly time synchronized to the first multipath component) and a delay term z^{-D} for modelling a possible timing offset of D samples. Moreover, P, $h_{p,m}$, and $\eta[m]$ denote the number of resolvable multipaths, the complex-valued time-varying channel coefficients and the thermal noise samples, respectively. A timing offset normalized with respect to the OQAM sub-symbol period and denoted by $\tau = 2D/M$ will later be referred to as a fractional time delay (FTD).

In the FBMC receiver, the time domain sequence $r[m]$ is converted into the frequency domain by means of the analysis filter bank (AFB). Let us now denote the channel distorted OQAM sub-symbol rate (i.e., of rate $2/T$) sample sequence at the output of the kth analysis filter as

$$y_k[n] = \bar{y}_k[nM/2]$$

where

$$\bar{y}_k[m] = \sum_{l=0}^{L_p-1} f_k[l] r[m-l]$$

and $f_k[l]$ denotes the impulse response of the kth subchannel filter in the analysis bank.

We now consider a communication link with a single transmit and Q receive antennas (i.e., $1 \times Q$ SIMO model) and therefore extend the notation to

$$r^q[m] = \sum_{p=0}^{P^q-1} h_{p,m}^q s[m-p] + \eta^q[m]$$

for $q = 1, \ldots, Q$ and

$$y_k^q[n] = \bar{y}_k^q[nM/2]$$

where

$$\bar{y}_k^q[m] = \sum_{l=0}^{L_p-1} f_k[l] r^q[m-l]$$

Here, the superscript q is used to define the respective receive antenna. Moreover, the thermal noise on each antenna is assumed to have a pdf of zero-mean Gaussian with variance $\sigma^2 = N_o/2$. Furthermore, the noise components at each receive antenna are assumed to be uncorrelated with the noise components at the other receive antennas.

Finally, we consider a MIMO-FBMC system with N_t transmit antennas and N_r receive antennas. The block diagram of the system is depicted in Figure 1.1. Note that the SFB and AFB can be efficiently implemented using the modified discrete Fourier transform (MDFT) filter bank based multicarrier system [12][5].

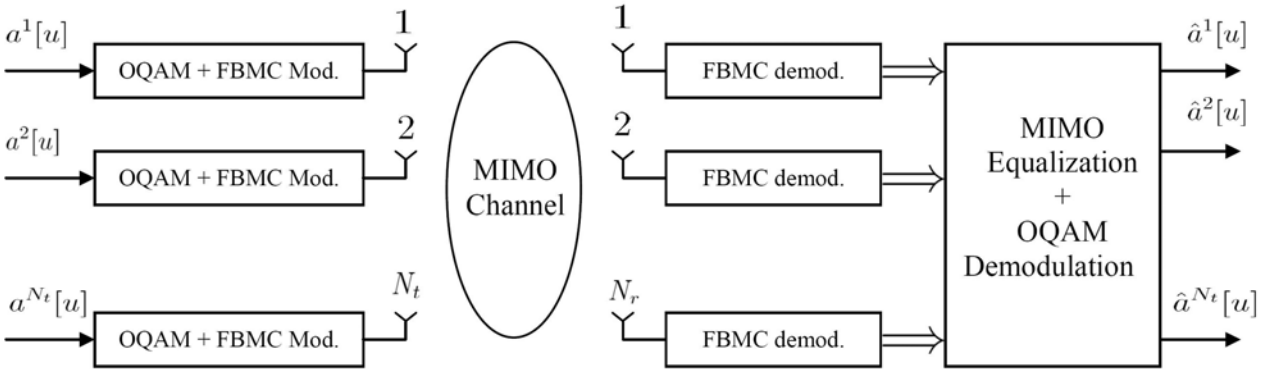

Figure 1.1. MIMO-FBMC system

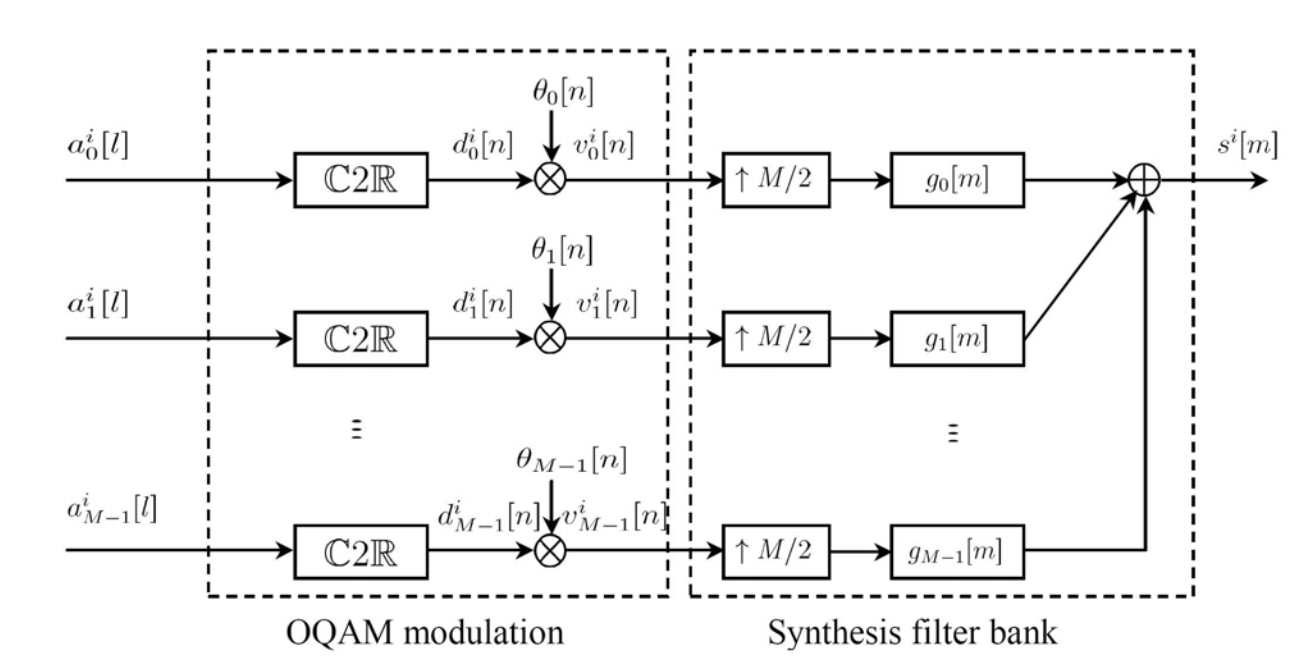

Figure 1.2. OQAM and FBMC modulation at the transmitter

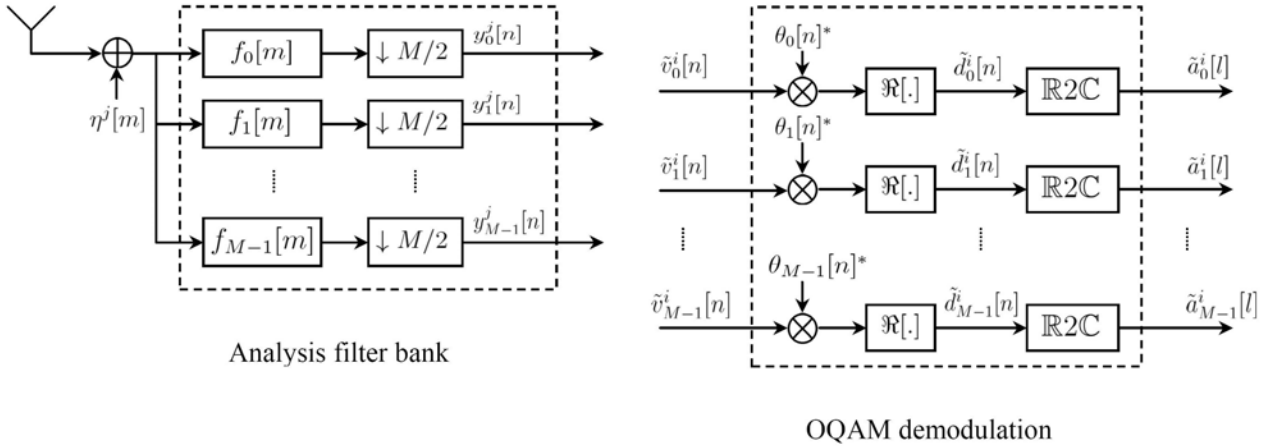

Figure 1.3. OQAM and FBMC demodulation at the receiver

Under the assumptions of good time-frequency localization for the prototype filter and relatively low frequency selectivity for the channel, the sample received at the q th antenna, $q = 1,2,\ldots,N_r$, at the subcarrier k and time n, *after* phase rotations ($\theta_{k,n}^*$) will be written as:

$$\tilde{y}_{k,n}^q = H_{k,n}^{1,q}\tilde{x}_{k,n}^1 + H_{k,n}^{2,q}\tilde{x}_{k,n}^2 + \cdots + H_{k,n}^{N_t,q}\tilde{x}_{k,n}^{N_t} + \eta_{k,n}^q$$

where $\tilde{x}_{k,n}^p = \theta_{k,n}^* x_{k,n}^p = d_{k,n}^p + ju_{k,n}^p$ is the ideal AFB output corresponding to the p th transmit antenna, called the virtually transmitted symbol, and $\eta_{k,n}^q$ the noise component at the q th receive antenna. $u_{k,n}^i$ is the intrinsic interference that depends on the data symbols at positions (k',n') around the symbol $d_{k,n}^i$.

Collecting the receive antenna array outputs for subcarrier k and time n results in

$$\underbrace{\begin{bmatrix} \tilde{y}_{k,n}^{1} \\ \tilde{y}_{k,n}^{2} \\ \vdots \\ \tilde{y}_{k,n}^{N_r} \end{bmatrix}}_{\tilde{\mathbf{y}}_{k,n}} = \underbrace{\begin{bmatrix} H_{k,n}^{1,1} & H_{k,n}^{2,1} & \cdots & H_{k,n}^{N_t,1} \\ H_{k,n}^{1,2} & H_{k,n}^{2,2} & \cdots & H_{k,n}^{N_t,2} \\ \vdots & \vdots & \ddots & \vdots \\ H_{k,n}^{1,N_r} & H_{k,n}^{2,N_r} & \cdots & H_{k,n}^{N_t,N_r} \end{bmatrix}}_{\mathbf{H}_{k,n}} \underbrace{\begin{bmatrix} \tilde{x}_{k,n}^{1} \\ \tilde{x}_{k,n}^{2} \\ \vdots \\ \tilde{x}_{k,n}^{N_t} \end{bmatrix}}_{\tilde{\mathbf{x}}_{k,n}} + \underbrace{\begin{bmatrix} \eta_{k,n}^{1} \\ \eta_{k,n}^{2} \\ \vdots \\ \eta_{k,n}^{N_r} \end{bmatrix}}_{\boldsymbol{\eta}_{k,n}}$$

that is,

$$\tilde{\mathbf{y}}_{k,n} = \mathbf{H}_{k,n}\tilde{\mathbf{x}}_{k,n} + \boldsymbol{\eta}_{k,n} \tag{1.2}$$

1.3 Organization of the document

The present document is organized as follows. Section 2 is dedicated to synchronization and a specific symbol timing and carrier frequency offset (CFO) estimation technique is described and evaluated, for the two cases of preambles and pilot symbols. Channel matrix estimation is investigated in Section 3, first with preambles and, then, with a pilot symbol allocation as in WiMAX. Also in Section 3, channel tracking techniques specific to FBMC are developed and the application of the memory preloading technique to the MIMO context is presented. In Section 4, equalization is dealt with, taking into account various situations, namely spatial multiplexing, receiver and diversity. A successive interference cancellation scheme is also introduced. Finally, in Section 5, the MIMO techniques which will be developed in the next deliverable are briefly discussed.

2 Synchronization

The prototype filter impulse response has an impact on timing offset estimation, as in the single antenna case. The frequency domain techniques described in documents D2.1 and D2.2 can be extended to the multiantenna case. However, if time domain processing is desired, the joint estimation approach of the single antenna case can be adapted.
In fact, only one carrier frequency offset and one timing offset have to be estimated, because the transmitter and the receiver are each assumed synchronized. However, exploiting multiple antennas can result in improved estimations, particularly with the maximum likelihood (ML) technique, which is known to be sensitive to the channel.

Two different situations are considered in two sections. In Section 2.1, the ML-based symbol timing and and CFO estimators are presented [1]. Precisely, in the case of an N_t transmit and single receive (N_t x 1) MIMO FBMC/OQAM system, N_t interleaved groups of subchannels or N_t FBMC/OQAM symbols can be allocated to the N_t transmitted signals. In this way, the waveforms of the different antennas are nearly orthogonal. Then, under the assumption of a non-dispersive channel, by exploiting the ML approach, we obtain N_t different estimators without significantly increasing the complexity of the derived synchronization algorithm for SISO FBMC/OQAM systems.

In Section 2.2, timing and CFO estimation using auxiliary pilot is discussed. The auxiliary pilot idea was first introduced in [4] as a way to construct FBMC pilots which can be used basically in the same way as pilots in OFDM. Scattered pilot schemes utilizing the auxiliary pilot idea were investigated in deliverable D2.1 [2] in the synchronization context and in Deliverable D3.1 [5] in the channel estimation context. Here we first state the basic auxiliary pilot model, considering the case where the pilots are scattered among the data symbols. Then we show how the auxiliary pilot scheme can be used in FBMC-based multiantenna configurations. The quality of scattered pilots is then examined in some basic multiantenna configurations using WiMAX-like system parameters.

2.1 ML symbol timing and CFO estimation

Let us consider a MIMO FBMC/OQAM system with N_t transmit antennas and a single receiver. In the presence of AWGN channel and under the assumption that the transmitted signals are synchronous and affected by a common CFO, the received signal can be written as

$$r[m]=\sum_{i=1}^{N_t}\gamma_i e^{j\left(\frac{2\pi}{M}m\varepsilon+2\pi\phi_i\right)}s_i[m-\tau/T_s]+\eta[m] \tag{2.1.1}$$

where $\eta[m]$ is the noise term and $s_i[m]$ the signal transmitted by the *i*th antenna whose expression is given by (see section 2 in [2] and (1.1) above)

$$s_i[m]=\sum_{k\in M_u{}^i}\sum_{n=-\infty}^{\infty}d_{k,n}\theta_{k,n}\beta_{k,n}p\left[m-nM/2\right]e^{j\frac{2\pi}{M}km}. \tag{2.1.2}$$

In this section we derive the joint ML CFO and timing estimator for the considered MIMO FBMC/OQAM scenario, by exploiting the transmission of a training sequence, embedded in the transmitted burst. In particular, let us consider a preamble of N_{TR} FBMC/OQAM symbols, the training sequence of the *i*th antenna, is given by

$$z_i[m]=\sum_{k\in M_u{}^i}\sum_{n=0}^{2N_{TR}-1}d_{k,n}\theta_{k,n}\beta_{k,n}p\left[m-nM/2\right]e^{j\frac{2\pi}{M}km}. \tag{2.1.3}$$

where M_u^i is the set of training subcarriers of each antenna such that $\bigcup_{i=1}^{N_t}M_u^i=M$ and $M_u^i\cap M_u^j=\varnothing$ for $i\neq j$.

By considering an observation window of total length $M\lambda$ containing the non-zero support of the preamble received from each antenna, the likelihood function in AWGN channel for the unknown parameters $\{\tau,\varepsilon\}$, $\{\gamma_i\}_{i=1}^{N_t}$ and $\{\phi_i\}_{i=1}^{N_t}$ is given by (up to an irrelevant multiplicative factor)

$$\Lambda\left(\tilde{\tau},\tilde{\varepsilon},\underline{\tilde{\gamma}},\underline{\tilde{\phi}}\right)=\exp\left\{-\frac{T_s}{N_0}\sum_{m=0}^{\lambda M-1}\left|r[m]-\sum_{i=1}^{N_t}\tilde{\gamma}_i e^{j2\pi\tilde{\phi}_i}\tilde{z}_i^{\tilde{\tau},\tilde{\varepsilon}}[m]\right|^2\right\} \tag{2.1.4}$$

where $\underline{\tilde{\phi}}=\left(\tilde{\phi}_1,\tilde{\phi}_2,...,\tilde{\phi}_{N_t}\right)$, $\underline{\tilde{\gamma}}=\left(\tilde{\gamma}_1,\tilde{\gamma}_2,...,\tilde{\gamma}_{N_t}\right)$

$$\begin{aligned}\tilde{z}_i^{\tilde{\tau},\tilde{\varepsilon}}[m]&=z_i[m-\tilde{\tau}/T_s]e^{j\frac{2\pi}{M}m\tilde{\varepsilon}}\\&=\sum_{k\in M_u{}^i}\sum_{n=0}^{2N_{TR}-1}d_{k,n}\theta_{k,n}\beta_{k,n}p[m-nM/2-\tilde{\tau}/T_s]e^{j\frac{2\pi}{M}k(m-\tilde{\tau}/T_s)}e^{j\frac{2\pi}{M}m\tilde{\varepsilon}}\end{aligned} \tag{2.1.5}$$

and the notation of the type $\tilde{x}$ indicates trial value of x. By replacing (2.1.5) in (2.1.4) after simple algebraic manipulation and dropping irrelevant multiplicative and additive factors, we obtain

$$\begin{aligned}\ln\Lambda\left(\tilde{\tau},\tilde{\varepsilon},\underline{\tilde{\gamma}},\underline{\tilde{\phi}}\right)=&-\frac{T_s}{N_0}\sum_{m=0}^{\lambda M-1}\sum_{i=1}^{N_t}\left|\tilde{\gamma}_i z_i[m-\tilde{\tau}/T_s]\right|^2\\&+\frac{2T_s}{N_0}\sum_{i=1}^{N_t}\mathrm{Re}\left[\tilde{\gamma}_i e^{-j2\pi\tilde{\phi}_i}\alpha_i(\tilde{\varepsilon},\tilde{\tau})\right]\end{aligned} \tag{2.1.6}$$

where

$$\alpha_i\left(\tilde{\varepsilon},\tilde{\tau}\right)=\sum_{k\in M_u{}^i}\sum_{n=0}^{2N_{TR}-1}d_{k,n}\theta_{k,n}{}^*\beta_{k,n}{}^*w_n^{(k)}\left(\tilde{\varepsilon},\tilde{\tau}\right) \tag{2.1.7}$$

with

$$w_n^{(k)}\left(\tilde{\varepsilon},\tilde{\tau}\right)=\sum_{m=0}^{\lambda M-1} r[m]p[m-nM/2-\tilde{\tau}/T_s]e^{-j\frac{2\pi}{M}m(\tilde{\varepsilon}+k)}e^{j\frac{2\pi}{T}k\tilde{\tau}}. \quad (2.1.8)$$

In the derivation of (2.1.6) we have neglected the quantity

$$C_1=-\frac{2T_s}{N_0}\mathrm{Re}\left\{\sum_{m=0}^{\lambda M-1}\sum_{i_1=1}^{N_t}\sum_{i_1=1}^{N_t-i_1}\tilde{\gamma}_{i_1}\tilde{\gamma}_{i_1+i_2}e^{j2\pi(\tilde{\phi}_{i_1}-\tilde{\phi}_{i_2+i_1})}e^{j\frac{2\pi}{M}m(\tilde{\varepsilon}_{i_1}-\tilde{\varepsilon}_{i_1+i_2})}z_{i_1}[m-\tilde{\tau}/T_s]\,z_{i_1+i_2}[m-\tilde{\tau}/T_s]^*\right\} \quad (2.1.9)$$

since it depends on the scalar product between the signals of the different antennas whose spectra essentially do not overlap.

Therefore, for a given value of the parameters $\{\tilde{\tau},\tilde{\varepsilon}\}$ the ML estimator of $\underline{\tilde{\phi}}$ and $\underline{\tilde{\gamma}}$ is equal to

$$\hat{\gamma}_{iML}(\tilde{\varepsilon},\tilde{\tau})=\frac{\left|\alpha_i(\tilde{\varepsilon},\tilde{\tau})\right|}{\sum_{m=0}^{\lambda M-1}\left|z_i[m-\tilde{\tau}/T_s]\right|^2},\quad i=1,...,N_t \quad (2.1.10)$$

$$\hat{\phi}_{i_{ML}}(\tilde{\varepsilon},\tilde{\tau})=\frac{1}{2\pi}\angle\left\{\alpha_i(\tilde{\varepsilon},\tilde{\tau})\right\},\quad i=1,...,N_t \quad (2.1.11)$$

and, moreover,

$$\left(\hat{\tau}_{ML},\hat{\varepsilon}_{ML}\right)=\arg\max_{(\tilde{\tau},\tilde{\varepsilon})}\left[\sum_{i=1}^{N_t}\frac{\left|\alpha_i(\tilde{\varepsilon},\tilde{\tau})\right|^2}{\sum_{m=0}^{\lambda M-1}\left|z_i[m-\tilde{\tau}/T_s]\right|^2}\right]. \quad (2.1.12)$$

Note that the solution of the considered two-dimensional maximization problem can be found only by numerical methods. Therefore, due to the computational complexity of the joint ML estimator, we consider a more feasible synchronization scheme that requires two one-dimensional maximization procedures.

Specifically, let us suppose that the CFO is sufficiently small that within a time ΔQ comparable with the length of the prototype filter $e^{-j\frac{2\pi}{M}\tilde{\varepsilon}\,\Delta Q}\approx 1$ and in the case of a training sequence of total length $N_{TR}=1$ it follows that

$$w_n^{(k)}\left(\tilde{\varepsilon},\tilde{\tau}\right)\approx e^{-j\pi\tilde{\varepsilon}n}w_n^{(k)}\left(0,\tilde{\tau}\right)=e^{-j\pi\tilde{\varepsilon}n}\sum_{m=0}^{\lambda M-1}r[m]p[m-nM/2-\tilde{\tau}/T_s]e^{j\frac{2\pi}{T}k(\tilde{\tau}-m)} \quad (2.1.13)$$

and, moreover,

$$\alpha_i\left(\tilde{\varepsilon},\tilde{\tau}\right)=\underbrace{\sum_{k\in M_u{}^i}d_{k,0}\theta_{k,0}{}^*\beta_{k,0}{}^*w_0^{(k)}\left(0,\tilde{\tau}\right)}_{A_i(\tilde{\tau})}+e^{-j\pi\tilde{\varepsilon}}\underbrace{\sum_{k\in M_u{}^i}d_{k,n}\theta_{k,n}{}^*\beta_{k,n}{}^*w_1^{(k)}\left(0,\tilde{\tau}\right)}_{B_i(\tilde{\tau})} \quad (2.1.14)$$

Therefore, the joint ML estimator in (2.1.12) can be simplified as

$$\hat{\tau}_{AML}=\arg\max_{\tilde{\tau}}\left[\sum_{i=1}^{N_t}\frac{\left|A_i(\tilde{\tau})\right|^2+\left|B_i(\tilde{\tau})\right|^2}{\sum_{m=0}^{\lambda M-1}\left|z_i[m-\tilde{\tau}/T_s]\right|^2}+2\left|\sum_{i=1}^{N_t}\frac{A_i^*(\tilde{\tau})B_i(\tilde{\tau})}{\sum_{m=0}^{\lambda M-1}\left|z_i[m-\tilde{\tau}/T_s]\right|^2}\right|\right]. \quad (2.1.15)$$

and

$$\hat{\varepsilon}_{AML}(\hat{\tau}_{AML}) = \frac{1}{\pi}\angle\left\{\sum_{i=1}^{N_t}\left[\frac{A_i^*(\hat{\tau}_{AML})B_i(\hat{\tau}_{AML})}{\sum_{m=0}^{\lambda M-1}\left|z_i[m-\hat{\tau}_{AML}/T_s]\right|^2}\right]\right\}. \quad (2.1.16)$$

2.1.1 Performance Evaluation

The performance of the proposed AML estimator is assessed via computer simulations. A number of 10^2 Monte Carlo trials have been performed under the following conditions:

- We have considered the MIMO FBMC/OQAM system with the diversity allocation strategy proposed in [3] composed by 2 transmitting antennas and a single receiver.
- The value of the normalized CFO and of the timing offset are uniformly distributed in [-0.5, 0.5) and T_s\{-M/2,-M/2+1,…,M/2-1,M/2}, respectively. In particular, the symbol timing is supposed to be an integer multiple of the sampling period T_s.
- The size of the set of subcarriers is M=1024.
- The preamble is made up of N_{TR} = 1 FBMC/OQAM symbol. Moreover, we assume that the training sequences of the transmitting antennas are orthogonal, in particular the first antenna's training symbols are transmitted on subcarriers with even index while those of the second antenna are allocated on odd subcarriers
- The prototype filter is that described in [2] with an overlapping factor K=4.
- Numerical results have been obtained by considering two different scenarios: AWGN channel and multipath channel modelled using the Vehicular-A channel model of ITU-R. Moreover, the channel is fixed in each run but it is independent from one run to another.

Figure 2.1.1 and Figure 2.1.2 show the root mean squared error (RMSE) of the considered joint CFO and symbol timing estimators in AWGN (solid lines) and multipath channel (dashed lines) as a function of the SNR in dB. The results show that in multipath channel the proposed AML symbol timing estimator exhibits a significant performance degradation while the considered CFO estimator assures nearly the same RMSE.

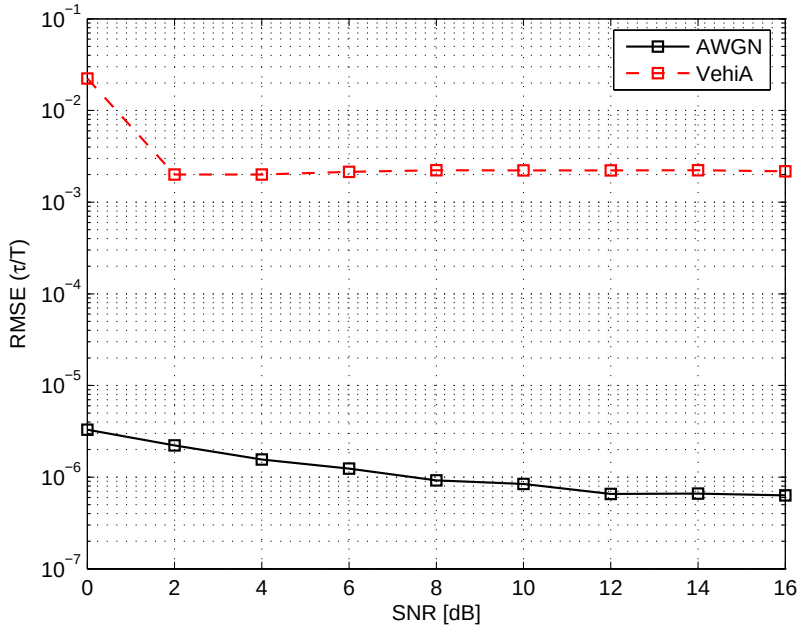

Figure 2.1.1. Performance of the considered symbol timing estimator in AWGN and multipath channel.

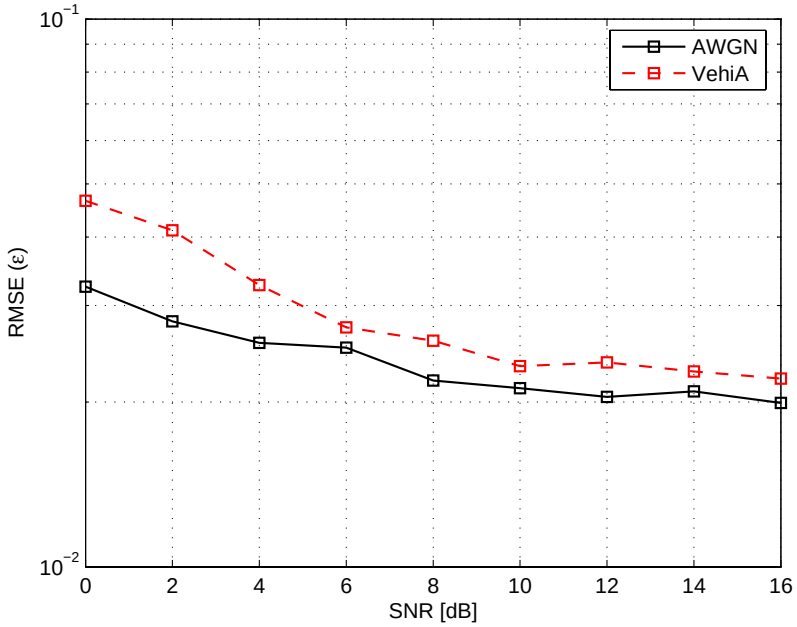

Figure 2.1.2. Performance of the considered CFO estimator in AWGN and multipath channel.

2.2 CFO and FTD estimation using auxiliary pilot

In an FBMC/OQAM system, either real or imaginary parts of the complex subcarrier symbols are used for data transmission in a staggered fashion. When a real (imaginary) part of a subcarrier symbol is used, the unused imaginary (real) part is, at the receiver, a fairly complicated function of surrounding data symbols. In the following, we refer to these two parts of the complex samples as primary and secondary parts, respectively. With a well-designed filter bank system, like the PHYDYAS reference bank, the crosstalk effects between the primary parts are small enough to be neglected.

The nature of FBMC systems makes it impossible to construct pilot symbols for channel estimation and synchronization purposes in the same way as in OFDM. The approach taken in [6] is based on the observation that it is sufficient to select one of the subcarrier symbols surrounding a pilot symbol as an associated auxiliary pilot. Adjusting the primary part of the auxiliary pilot depending on the surrounding data symbols, the secondary part of the actual pilot can be forced to take any desired value. For example, the secondary part of the complex pilot symbol can be forced to zero. Utilizing this idea, pilots can be used in FBMC systems in a similar way as in OFDM. It should be noticed that the relative pilot overhead using this idea is the same as the pilot overhead in OFDM.

In the following, the pilot and auxiliary pilot positions are denoted as (k_p, n_p) and (k_a, n_a), respectively. Typically, the auxiliary pilot is the subcarrier symbol immediately preceding or following the pilot in the same subcarrier, i.e., $(k_a, n_a) = (k_p, n_p \pm 1)$.

Based on Section 2.4 of [2], the secondary part of the pilot sample can be forced to zero by choosing the primary part of the auxiliary pilot as

$$d_{k_a,n_a} = -\frac{\sum_{\substack{(k,n)\in\Omega_{k_p,n_p} \\ (k,n)\neq(k_p,n_p) \\ (k,n)\neq(k_a,n_a)}} d_{k,n}\hat{t}_{k_p-k,n_p-n}}{\hat{t}_{k_p-k_a,n_p-n_a}} \tag{2.2.1}$$

Here $\hat{t}_{k,n}$ is obtained from the transmultiplexer response $t_{k,n}$ as follows:

$$\hat{t}_{k,n} = \mathrm{Im}\left[(-j)^{k+n} t_{k,n}\right].$$

Equation (2.2.1) uses the data symbols $d_{k,n}$ in a specified window Ω_{k_p,n_p} around the pilot. This window is chosen to include those symbols which have significant effect on the secondary part of the pilot. The window typically used with the PHYDYAS reference filter bank includes subcarriers *k*-1, *k*, and *k*+1 and sample indices *n*-3, *n*-2, … , *n*+3.

When scattered pilots are used in multi-antenna transmission schemes for channel estimation and synchronization, the usual model is the following: When a pilot is transmitted from antenna *p*, zero symbols are transmitted from all the other antennas in the corresponding subcarrier(s). In this way, it is possible to obtain a clean pilot observation for each transmission link. To apply this idea in FBMC-based multi-antenna schemes, it is important to realize that zero-pilots have to be constructed by utilizing the auxiliary pilot idea to make the secondary parts of the pilot symbols equal to zero. With this modification, the basic scattered pilot multiplexing scheme can be applied also in FBMC transmission. If clean pilot observations are obtained, the same scattered pilot based methods, which have developed in WP2 and WP3 for synchronization and channel estimation in the SISO/SIMO case, can be used for the same purpose in MISO/MIMO cases.

In multicarrier systems, the pilots are naturally sensitive to carrier frequency offset (CFO) due to the induced intercarrier interference. In FBMC reception, the sensitivity to CFO is expected to be similar or slightly improved, compared to OFDM. Regarding timing offsets, or fractional time delays (FTDs), the OFDM is quite robust as long as the cyclic prefix is long enough to accommodate the delay spread extended by the FTD. FBMC is expected to show higher sensitivity to FTD, but on the other hand, it is possible to compensate significant timing offsets using the subcarrier equalizers, after successful estimation of the FTD value. In the following, the sensitivity of scattered pilots on the CFO, FTD, and number of transmit antennas is investigated.

The signal transmitted by antenna *i* is defined by

$$s_i(t) = \sum_{k\in\mathsf{M}_u}\sum_{n=-\infty}^{\infty} d_{k,n}^{\{i\}}\theta_{k,n}(-1)^{kn}\, p\left(t - n\frac{T}{2}\right)e^{j2\pi k\left(\Delta f t - \frac{L_p-1}{2M}\right)}, \tag{2.2.2}$$

and the combined received signal, assuming independent channel paths for each antenna can be expressed as

$$r(t) = \sum_{i=1}^{U} e^{j2\pi(\frac{\varepsilon_i}{T}t)} \sum_{p=0}^{P_i-1} c_{i,p}\, s_i(t-\tau_{i,p}). \tag{2.2.3}$$

2.2.1 Performance evaluation

The quality of scattered pilots based on the auxiliary pilot model was tested using the PHYDYAS reference filter bank with overlapping factor *K*=4 and WiMAX-like parameters:

- FFT-size: 1024
- Bandwidth: 10 MHz
- Subcarrier spacing: 10.94 kHz
- Pilot pattern: DL-PUSC

- 1, 2 or 4 transmit antennas
  - Ideal channel
  - Vehicular A channel model (independent instances from the delay profile are used for different transmit antennas).
- Both channel models are noiseless.

The performance metric is the mean-squared error between observed pilot value and ideal pilot value $H_{k_p,n_p} d_{k_p,n_p}$ where H_{k_p,n_p} is the channel response for symbol n_p of subcarrier k_p and d_{k_p,n_p} is the corresponding transmitted pilot symbol value. The channel is assumed to be noise free and stationary, so the error is predominantly due to loss of orthogonality due to CFO and FTD. For zero CFO and FTD, the error is partly due to frequency selectivity of the channel within the subcarrier bandwidth and the neighboring subcarriers and also due to the limited window size in auxiliary pilot configurations. The data symbols are QPSK modulated. The total energy of each pilot/auxiliary pilot pair is, on the average, 4.5 dB above the data symbol energy.

The pilot MSE is shown in Figure 2.2.1 as a function of CFO and in Figure 2.2.2 as a function of FTD for 1, 2, and 4 transmitter antennas transmitting in an ideal channel. Figure 2.2.3 and Figure 2.2.4 show the corresponding results in the Vehicular A channel. Here the synchronized case is considered, i.e., the different transmit antennas physically connected, so that the CFO's and FTD's can be assumed to be perfectly matched. In this case $\tau_i = \tau$ and $\varepsilon_i = \varepsilon, \forall i$. Figure 2.2.5 and Figure 2.2.6 show the pilot MSE as a function of both, CFO and FTD, in the ideal channel and Vehicular A channel, respectively.

The residual distortion due to the limited interference cancellation window when calculating the auxiliary pilot with (2.2.1) is seen when both CFO and FTD are 0, i.e. when the signal is perfectly synchronized. Here the interference grows proportionally to the number of antennas used in the MISO link. This proportion is maintained with increasing FTD, but not with increasing CFO, where already with 1% offset of the pilot MSE converges to a similar value for different numbers of transmit antennas. With 4 antennas in the ideal channel, a CFO of 1.5% (@ FTD = 0) and FTD of less than 5% (@ CFO = 0) is needed to keep the error level below -20 dB. With 2 antennas, up to 7% FTD can be tolerated. With the Vehicular A channel model, a somewhat smaller FTD can be tolerated. Figure 2.2.5 and Figure 2.2.6 show the area in which the combination of FTD and CFO yields an error below -20dB with both channel models.

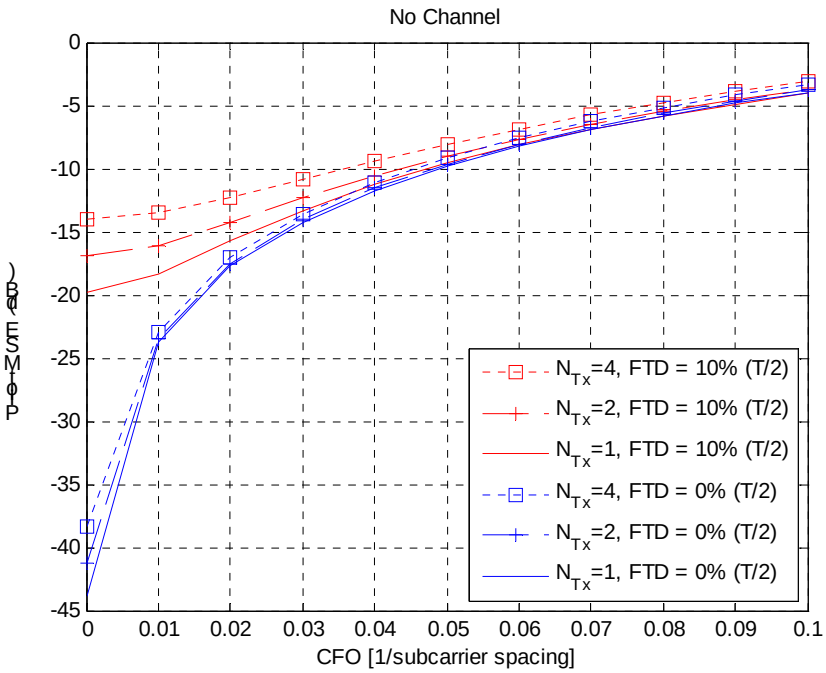

Figure 2.2.1. Pilot MSE as a function of CFO for 1, 2, and 4 transmit antennas. Synchronized case in ideal channel.

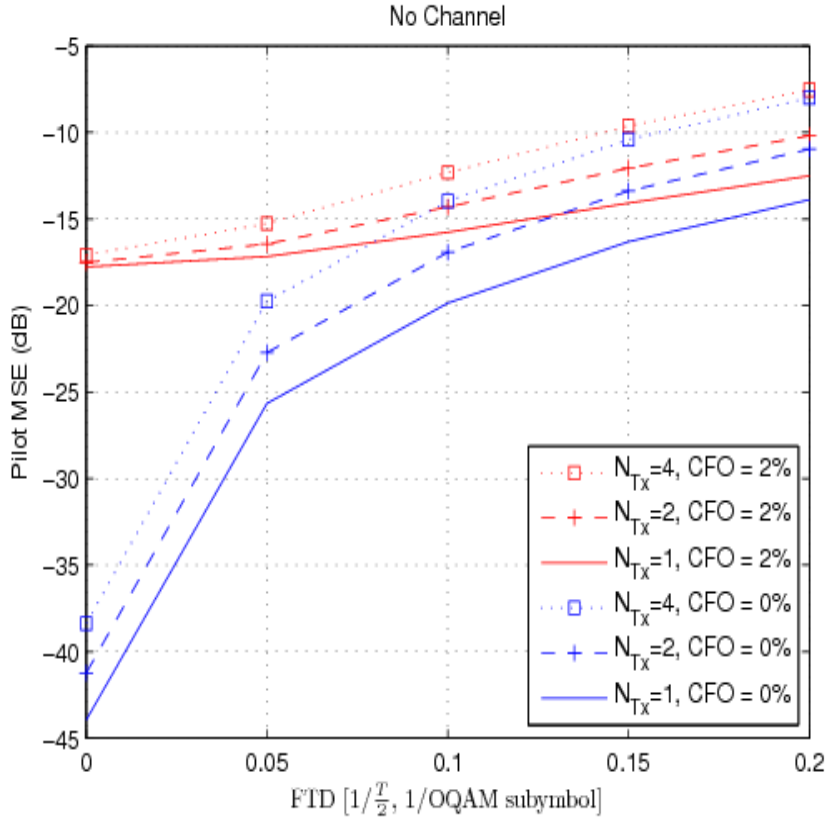

Figure 2.2.2. Pilot MSE as a function of FTD for 1, 2, and 4 transmit antennas. Synchronized case in ideal channel.

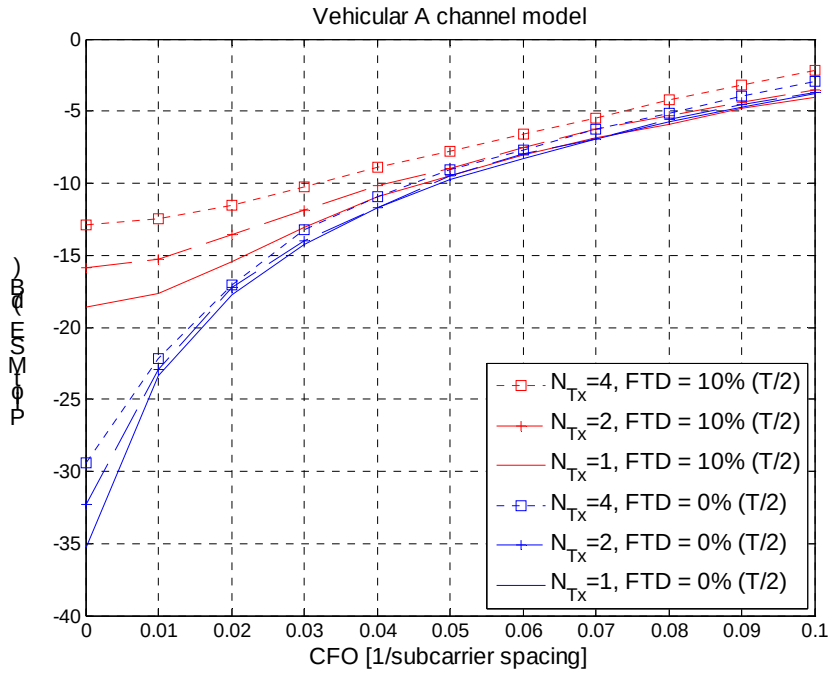

Figure 2.2.3. Pilot MSE as a function of CFO for 1, 2, and 4 transmit antennas. Synchronized case in Vehicular A channel.

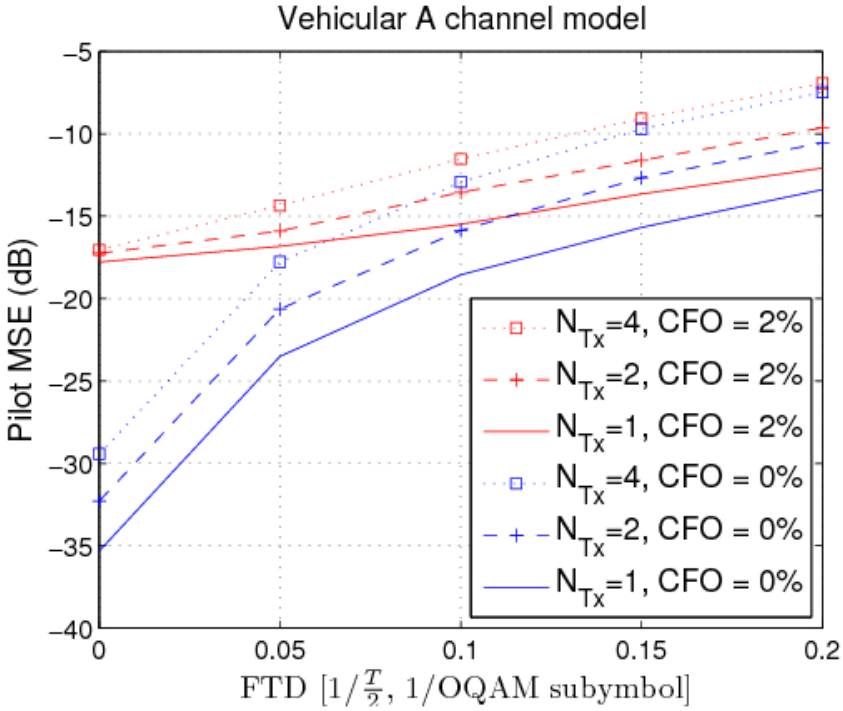

Figure 2.2.4. Pilot MSE as a function of FTD for 1, 2, and 4 transmit antennas. Synchronized case in Vehicular A channel.

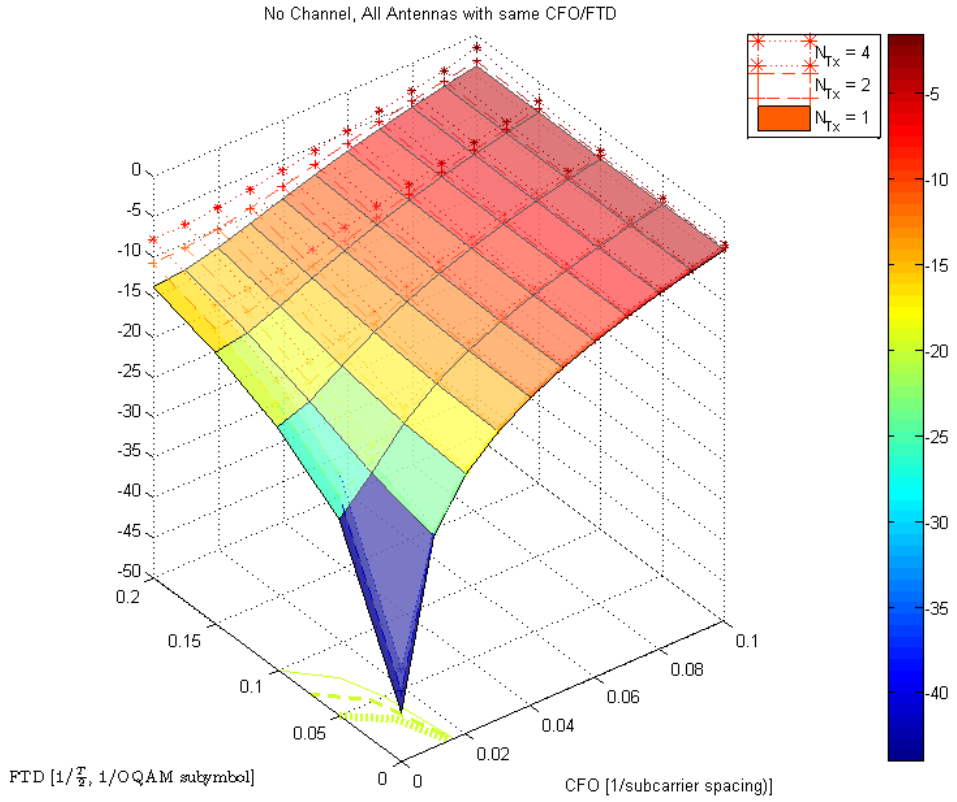

Figure 2.2.5. Pilot MSE as a function of FTD and CFO for 1, 2, and 4 transmit antennas. Synchronized case in ideal channel. On the xy-plane the limits for the -20 dB distortion are depicted.

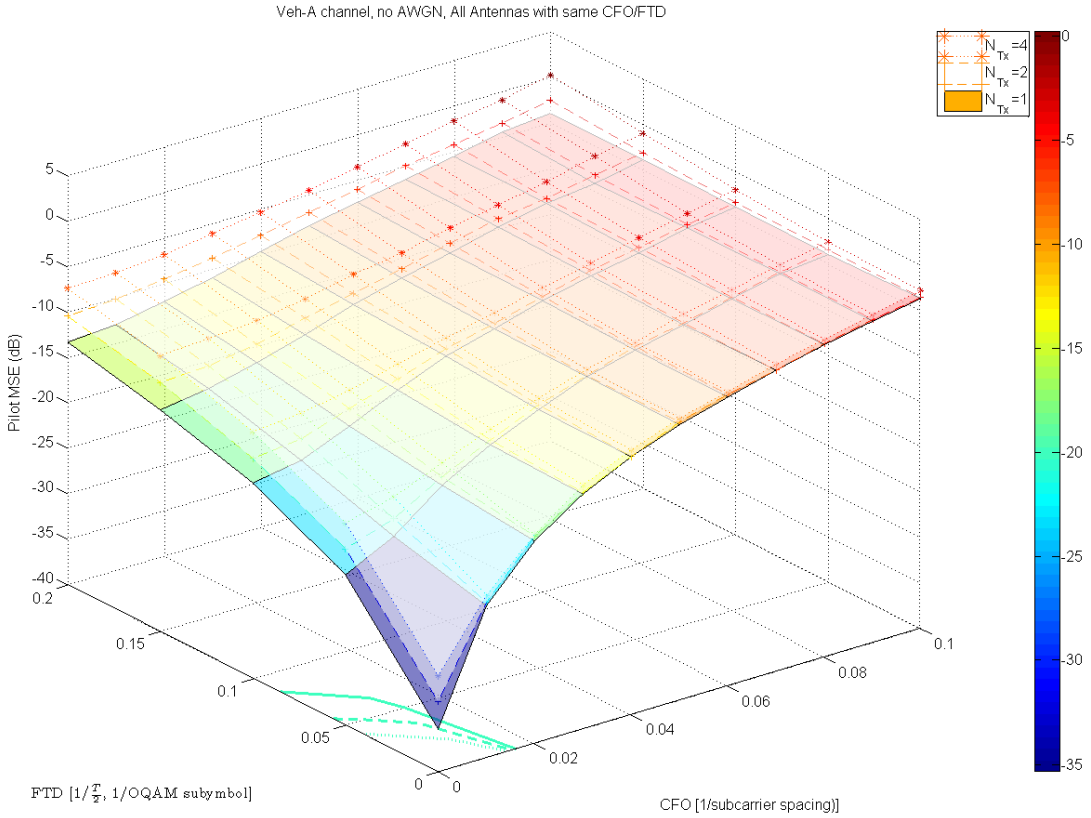

Figure 2.2.6. Pilot MSE as a function of FTD and CFO for 1, 2, and 4 transmit antennas. Synchronized case in Veh-A channel. On the xy-plane the limits for the -20 dB distortion are depicted.

In uplink multiuser MIMO, different mobile stations are transmitting waveforms which are processed jointly by the base-station as a multi-antenna signal. The collaborative spatial multiplexing of WiMAX is one example of this approach. In this configuration, the different user signals cannot be assumed to be perfectly synchronized. In Figure 2.2.7 and Figure 2.2.8, the pilot quality is expressed as a function of the CFO and FTD difference, respectively, in the case of 2 transmit antennas in an ideal channel and in the Vehicular A model. It is assumed here that the signal carrying the pilots is ideally synchronized, and the other user's signal has the given CFO or FTD, i.e., $\tau_1 = 0$ and $\varepsilon_1 = 0$ and $\tau_2 = \tau$ and $\varepsilon_2 = \varepsilon$ in (2.2.3). Figure 2.2.9 presents again the pilot distortion with respect to both variables and the region, in which the distortion is below -20 dB in the ideal channel case. It can be seen that, when the transmitter with the pilots is synchronized, the distortion is lower than in the previous case. FTD's of 10% and CFO's of up to almost 7% can be supported with a reasonable pilot MSE. Figure 2.2.10 presents similar results for the Vehicular A channel model.

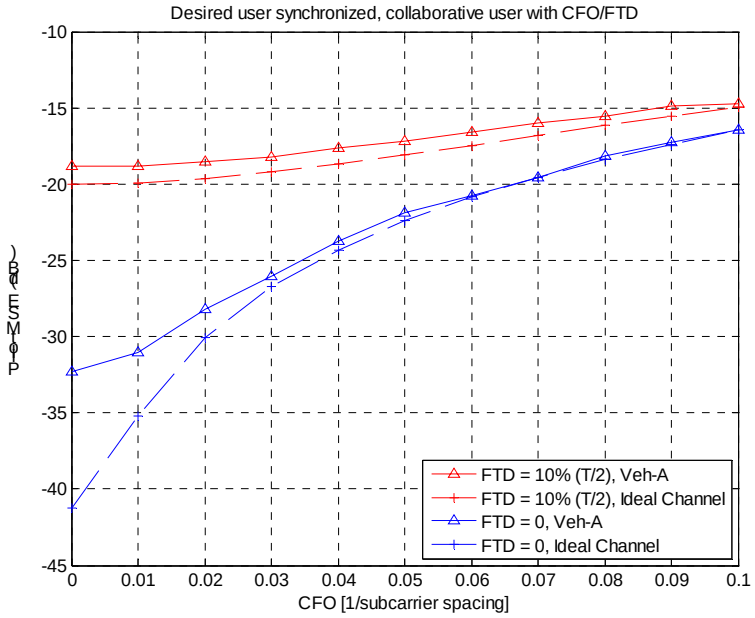

Figure 2.2.7. Pilot MSE as a function of CFO difference between 2 collaborative uplink users. Ideal and Vehicular A channel models.

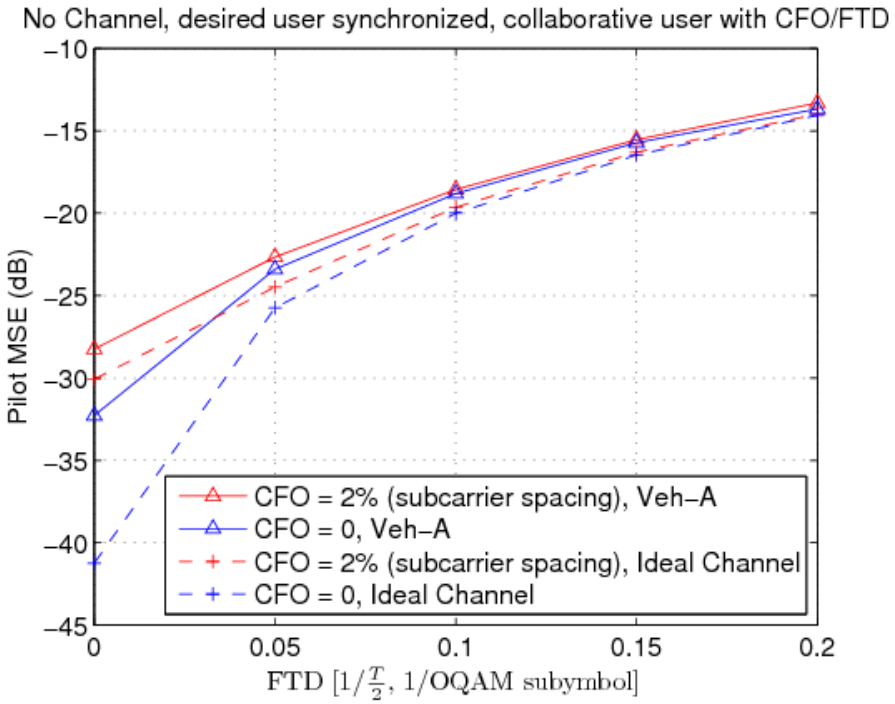

Figure 2.2.8. Pilot MSE as a function of FTD difference between 2 collaborative uplink users. Ideal and Vehicular A channel models.

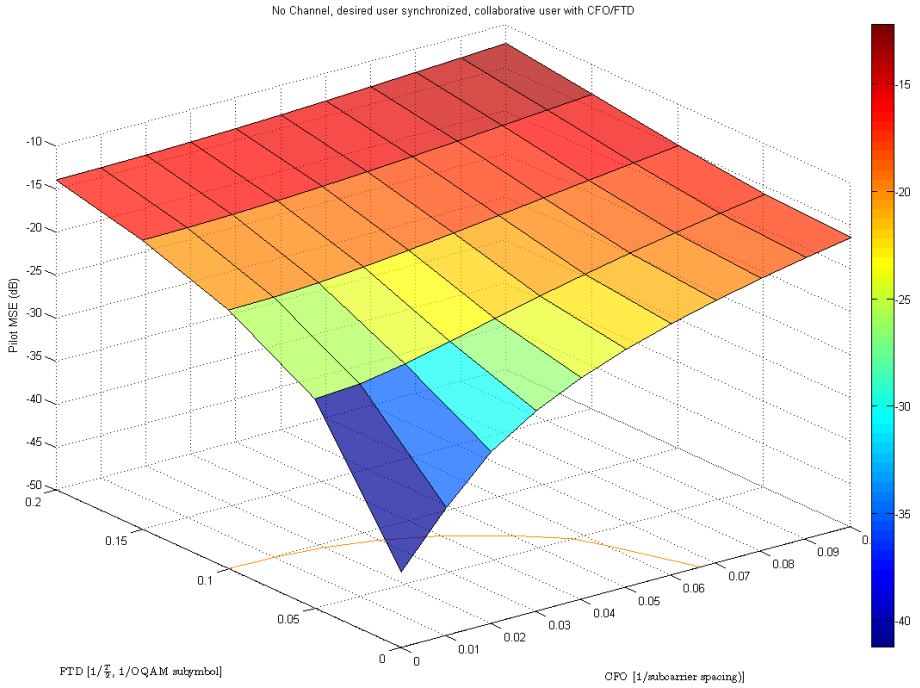

Figure 2.2.9. Pilot MSE as a function of FTD- and CFO-difference between 2 collaborative uplink users in ideal channel. On the xy-plane the limits for the -20 dB distortion are depicted.

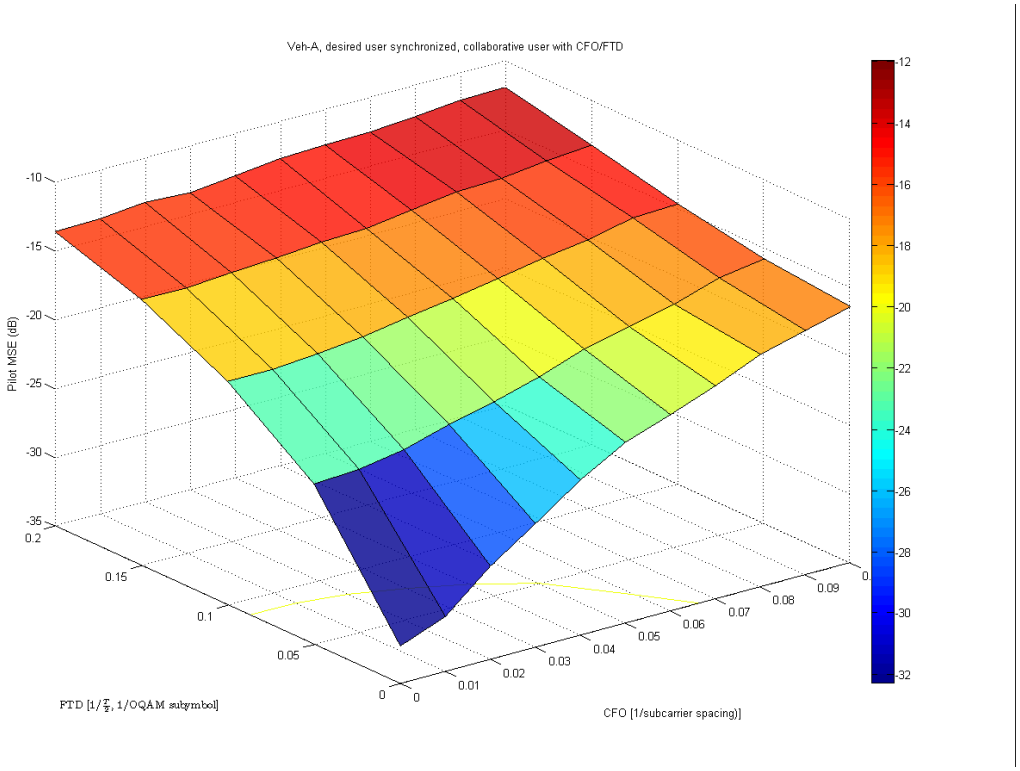

Figure 2.2.10. Pilot MSE as a function of FTD- and CFO-difference between 2 collaborative uplink users in Vehicular A channel. On the xy-plane the limits for the -20 dB distortion are depicted.

In summary, the quality of the pilots is logically affected by the synchronization accuracy. With reasonable synchronization, the error of the pilots can be kept at an acceptable level even in the multiantenna case, as can be seen from the results. We expect that advanced but relatively simple equalization techniques based on multitap FIR equalizers and iterative distortion reduction will improve the quality of the pilots when the transmitted signals are synchronous, i.e., they arrive at the receiver with similar FTD and CFO. Also the effects of the common CFO and timing errors on the data symbols can be compensated using the same methods as in the single-antenna case.

In cases where the multiuser elements of the MIMO-signal are non-synchronous (like collaborative spatial multiplexing), the situation is somewhat different. Based on the above results, it is seen that such a multiuser MIMO system is not very sensitive to the synchronization errors, allowing CFO error of 6 % of subcarrier spacing and FTD error of 10 % of FBMC/OQAM subsymbol duration with 20 dB pilot MSE. This indicates that the zero-pilot model works well, and there are good possibilities to estimate the carrier frequency and timing differences using scattered pilots. However, simple methods are not expected to be effective for compensating excessive carrier frequency or timing offsets in the collaborative spatial multiplexing case.

3 Channel Matrix estimation

To begin with, Section 3.1 presents and evaluates methods for preamble-based channel estimation. These include the schemes reported in D3.1 [5] for SISO channels and extended here to the MIMO case, as well as a number of new preambles and associated methods. The downlink (DL) partial usage of subcarriers (PUSC) configuration for data and pilot allocation in the CP-OFDM system has been adapted for MIMO FBMC in Section 3.2. In Section 3.3, a Kalman filter to track the evolutions

of the radio channel matrix components, in the FBMC context, is proposed. Finally, in Section 3.4, memory preloading in MIMO is presented.

3.1 Preamble based estimation

In this section, the preamble based methods proposed in [5] for SISO FBMC are extended to the MIMO case. The first method, Pairs of Pilots (POP), relies on simple algebraic relations for the input / output samples in a number of (in practice consecutive) time instants. The second one, Interference Approximation Method (IAM), aims at approximating the intrinsic imaginary interference from neighboring pilots and hence constructing complex pilots, to accommodate the complex channel. A number of variants of IAM are considered. In these schemes, all subcarriers are used (*full* preamble) to directly estimate the corresponding channel frequency response values. One may instead activate only part of the subcarriers, with the rest of them carrying nulls (*sparse* preamble), and use frequency-domain interpolation to estimate the channel at the inactive frequencies. Four such alternatives are considered in this section.

3.1.1 Pair of Pilots (POP)

Consider (1.2) with noise being neglected and assume $\mathbf{H}_{k,n}$ is (left-) invertible for all k,n (hence $N_r \geq N_t$). Denote by $\mathbf{W}$ the (per sub-carrier) zero forcing (ZF) equalization matrix, that is, $\mathbf{W}_{k,n} = \mathbf{H}_{k,n}^{\dagger}$, with $\mathbf{H}_{k,n}^{\dagger}$ being the left inverse of $\mathbf{H}_{k,n}$. Write (1.2) in the form $\mathbf{W}_{k,n}\tilde{\mathbf{y}}_{k,n} = \tilde{\mathbf{x}}_{k,n}$ for $2N_r$ different (and assumed consecutive) time instants, $n = 0,1,\ldots,2N_r - 1$, assuming that the channel (and hence $\mathbf{W}$) can be viewed as invariant in this time period. Then:

$$\mathbf{W}_{k,0}^{R}\tilde{\mathbf{y}}_{k,0}^{R} - \mathbf{W}_{k,0}^{I}\tilde{\mathbf{y}}_{k,0}^{I} = \mathbf{d}_{k,0}$$

and similarly for $n = 1,2,\ldots,2N_r - 1$. Collecting these equations into one, one can write

$$\begin{bmatrix}\mathbf{W}_{k,0}^{R} & \mathbf{W}_{k,0}^{I}\end{bmatrix}\underbrace{\begin{bmatrix}\tilde{\mathbf{y}}_{k,0}^{R} & \tilde{\mathbf{y}}_{k,1}^{R} & \cdots & \tilde{\mathbf{y}}_{k,2N_r-1}^{R} \\ -\tilde{\mathbf{y}}_{k,0}^{I} & -\tilde{\mathbf{y}}_{k,1}^{I} & \cdots & -\tilde{\mathbf{y}}_{k,2N_r-1}^{I}\end{bmatrix}}_{\tilde{\mathbf{Y}}_k} = \underbrace{\begin{bmatrix}\mathbf{d}_{k,0} & \mathbf{d}_{k,1} & \cdots & \mathbf{d}_{k,2N_r-1}\end{bmatrix}}_{\mathbf{D}_k}$$

or

$$\begin{bmatrix}\mathbf{W}_{k,0}^{R} & \mathbf{W}_{k,0}^{I}\end{bmatrix}\tilde{\mathbf{Y}}_k = \mathbf{D}_k$$

Assuming all symbols at times $n = 0,1,\ldots,2N_r - 1$ are known, the ZF equalizer can be computed as

$$\begin{bmatrix}\mathbf{W}_{k,0}^{R} & \mathbf{W}_{k,0}^{I}\end{bmatrix} = \mathbf{D}_k\tilde{\mathbf{Y}}_k^{-1}$$

The channel matrix can then be found as the right inverse of $\mathbf{D}_k\tilde{\mathbf{Y}}_k^{-1}\left(\begin{bmatrix}1\\ j\end{bmatrix}\otimes\mathbf{I}_{N_r}\right)$.

Remark: The above scheme is developed along the same line with the SISO POP method [31]. Nevertheless, it must be noted that it is no longer associated to the concept of "pairs of pilots" and the name "POP" is only used as a reminder of its SISO counterpart.

3.1.2 Interference Approximation Method (IAM)

The idea behind the IAM methods for SISO channels is to approximate the intrinsic interference $ju_{k,n}$ at a pilot position (k,n), based on the assumption that contributions only come from the first-order neighboring time-frequency points. Moreover, these contributions can be known if the pilot in question is surrounded by known training symbols. The so-called 'pseudo-pilot', $\hat{\tilde{x}}_{k,n} = d_{k,n} + j\hat{u}_{k,n}$,

can then be constructed and used as a complex pilot to estimate the channel frequency response: $\hat{H}_{k,n} = \tilde{y}_{k,n} / \hat{\tilde{x}}_{k,n}$.

3.1.2.1 IAM-R

Consider first the IAM2 variant of the IAM method [6][31], which consists of choosing the neighboring training symbols in such a way that $\left|\hat{\tilde{x}}_{k,n}\right|$ is maximized, in order to minimize noise enhancement. Moreover, [6] suggests that the FBMC symbols at times $n-1, n+1$ be set to all zeros, so as to null any interference from those symbols (and hence simplify the task of properly selecting the training symbols of interest). Such a training input was provided in [6] for SISO channels, based on the configuration of the first-order neighborhood of a given time-frequency point (k_0, n_0) which turns out to be as follows for odd n_0:

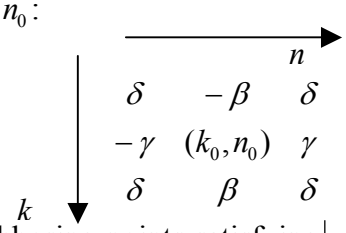

with the contributions from neighboring points satisfying $|\gamma| > |\beta| > |\delta|$. Since the preamble structure is such that (nonnegligible) interference only comes from the points $(k_0 - 1, n_0), (k_0 + 1, n_0)$, it suffices to choose the corresponding training symbols so as to have different signs, thus maximizing their contribution to the resulting pseudo-pilot modulus. A preamble that satisfies this requirement is built for a SISO channel using alternating pairs of 1's and -1's for the middle FBMC symbol, as shown below for the example of $M = 8$, with QPSK modulation:

$$\begin{matrix} 0 & 1 & 0 \\ 0 & -1 & 0 \\ 0 & -1 & 0 \\ 0 & 1 & 0 \\ 0 & 1 & 0 \\ 0 & -1 & 0 \\ 0 & -1 & 0 \\ 0 & 1 & 0 \end{matrix} \qquad (3.1.1)$$

Let us consider extending that scheme to the MIMO case. For the sake of simplicity, consider the case of two transmit antennas. The first antenna can use the same preamble employed in the SISO case, but with a repetition. An example for $M = 8$:

$$\begin{matrix} 0 & 1 & 0 & 1 & 0 \\ 0 & -1 & 0 & -1 & 0 \\ 0 & -1 & 0 & -1 & 0 \\ 0 & 1 & 0 & 1 & 0 \\ 0 & 1 & 0 & 1 & 0 \\ 0 & -1 & 0 & -1 & 0 \\ 0 & -1 & 0 & -1 & 0 \\ 0 & 1 & 0 & 1 & 0 \end{matrix}$$

At the second antenna, use the same preamble, but change the signs in the second column of ± 1's. For the above example:

$$\begin{matrix} 0 & 1 & 0 & -1 & 0 \\ 0 & -1 & 0 & 1 & 0 \\ 0 & -1 & 0 & 1 & 0 \\ 0 & 1 & 0 & -1 & 0 \\ 0 & 1 & 0 & -1 & 0 \\ 0 & -1 & 0 & 1 & 0 \\ 0 & -1 & 0 & 1 & 0 \\ 0 & 1 & 0 & -1 & 0 \end{matrix}$$

Assume, moreover, that the channel is invariant in this time period. Write then (1.2) at times $n = 1,3$:

$$\begin{aligned} \left[\tilde{\mathbf{y}}_{k,1} \quad \tilde{\mathbf{y}}_{k,3}\right] &= \mathbf{H}_{k,1}\begin{bmatrix} \tilde{x}_k & \tilde{x}_k \\ \tilde{x}_k & -\tilde{x}_k \end{bmatrix} + \left[\boldsymbol{\eta}_{k,1} \quad \boldsymbol{\eta}_{k,3}\right] \\ &= \mathbf{H}_{k,1}\tilde{x}_k\begin{bmatrix} 1 & 1 \\ 1 & -1 \end{bmatrix} + \left[\boldsymbol{\eta}_{k,1} \quad \boldsymbol{\eta}_{k,3}\right] \end{aligned}$$

where the "pseudo-pilot" $\tilde{x}_k$ can be pre-calculated as in the SISO case. An estimate of the channel matrix at the sub-carrier k can then be computed as

$$\hat{\mathbf{H}}_{k,1} = \left[\tilde{\mathbf{y}}_{k,1} \quad \tilde{\mathbf{y}}_{k,3}\right]\frac{1}{\tilde{x}_k}\begin{bmatrix} 1 & 1 \\ 1 & -1 \end{bmatrix}^{-1} = \mathbf{H}_{k,1} + \left[\boldsymbol{\eta}_{k,1} \quad \boldsymbol{\eta}_{k,3}\right]\frac{1}{2\tilde{x}_k}\begin{bmatrix} 1 & 1 \\ 1 & -1 \end{bmatrix} \tag{3.1.2}$$

In view of the fact that the matrix $\begin{bmatrix} 1 & 1 \\ 1 & -1 \end{bmatrix}$ is unitary, noise enhancement is again controlled by the magnitude of the pseudo-pilot $\tilde{x}_k$.

Remarks:

1) The above IAM scheme requires, for an $N_t \times N_r$ system, $2N_t + 1$ (real) training FBMC symbols (that is, for square systems, one more than POP).
2) The preamble is easily generalized to the $N_t \times N_r$ case with N_t a power of 2: Select the signs so that a Hadamard matrix results. Thus, for $N_t = 4$, we can choose the signs in the antenna outputs so as to get e.g. the following matrix in (3.1.2):

$$\begin{bmatrix} 1 & 1 & 1 & 1 \\ 1 & -1 & 1 & -1 \\ 1 & 1 & -1 & -1 \\ 1 & -1 & -1 & 1 \end{bmatrix}$$

   It is of interest to note that a similar preamble structure, based on a Hadamard matrix, has been also used in IEEE 802.11n for channel matrix estimation [34]
3) One can consider three different patterns for preamble training (see, e.g., [33], Section 5.7, for MIMO-OFDM): independent (one antenna at a time), scattered (transmitting at different frequencies), and orthogonal (transmitting *orthogonal* signals at the same times and frequencies). The preamble proposed above belongs to the third category. The second category is treated later on in this section.
4) Eq. (3.1.2) relies on the assumption that the prototype filter is sufficiently well localized in time so that interference from times other than the previous and next is negligible. If this is

not the case, the 'pseudo-pilot' matrix in (3.1.2) should instead be $\begin{bmatrix} \widetilde{x}_k^1 & \widetilde{x}_k^1 \\ \widetilde{x}_k^2 & -\widetilde{x}_k^2 \end{bmatrix}$ with $\widetilde{x}_k^p$ (in general $\widetilde{x}_k^1 \neq \widetilde{x}_k^2$) corresponding to the p th transmit antenna.

3.1.2.2 IAM-I

In the previous training scheme, all pseudo-pilots $\widetilde{x}_{k,n} = d_{k,n} + ju_{k,n}$ are complex, with modulus squared equal to $\left|\widetilde{x}_{k,n}\right|^2 = d_{k,n}^2 + u_{k,n}^2$ and $\left|u_{k,n}\right| \cong 2|\beta|$. A modification to this scheme, aiming at further increasing this modulus, was proposed in [34]. The idea is to use *imaginary* pilot symbols, $jd_{k,n}$, at certain frequencies in order to result in purely imaginary pseudo-pilots, $j\left(d_{k,n} + u_{k,n}\right)$, with modulus squared $\left(d_{k,n} + u_{k,n}\right)^2 = d_{k,n}^2 + u_{k,n}^2 + 2d_{k,n}u_{k,n}$. The latter is increased compared to IAM2, provided that $d_{k-1,n}, d_{k,n}, d_{k+1,n}$ are so chosen that $d_{k,n}u_{k,n}$ is positive. The new scheme is called *IAM-I*, to signify the presence of imaginary pilots, as contrasted to the use of only real pilots in IAM2, called *IAM-R* henceforth.

With the preamble proposed in [34], imaginary pseudo-pilots will result in only one third of the subcarriers used, whereas the rest of the subcarriers will deliver complex pseudo-pilots. With a slight modification, one can overcome this and obtain pseudo-pilots that are either pure imaginary or real at *all* the subcarriers. Simply set the middle FBMC symbol equal to that in (3.1.1) with the pilots at the odd subcarriers multiplied by j. For the $M = 8$ example, this will result in:

$$\begin{matrix} 0 & 1 & 0 \\ 0 & -j & 0 \\ 0 & -1 & 0 \\ 0 & j & 0 \\ 0 & 1 & 0 \\ 0 & -j & 0 \\ 0 & -1 & 0 \\ 0 & j & 0 \end{matrix}$$

This preamble can easily be extended to the MIMO case in a manner analogous with IAM-R.

Remark: The above preamble is, strictly speaking, *not* OQAM. Nevertheless, it can still be fed to the synthesis filter bank and perfectly reconstructed at the analysis bank.

3.1.2.3 Averaged IAM-I (aIAM-I)

Assuming that the channel frequency response is almost invariant beyond the first-order neighborhood, one can try to improve the estimates obtained by IAM-I through an averaging procedure. For example, using a second-order neighborhood centered at (k,n), the corresponding channel estimate will be computed as $\dfrac{\hat{\mathbf{H}}_{k-1,n} + \hat{\mathbf{H}}_{k,n} + \hat{\mathbf{H}}_{k+1,n}}{3}$ where the three estimates have resulted as previously. This method, called henceforth *aIAM-I*, can also be seen to be equivalent to summing the corresponding received samples and dividing by the sum of the corresponding pseudo-pilots.

3.1.3 Using sparse preambles

3.1.3.1 Estimation based on only one subcarrier set

In WiMAX, the subcarriers in the preamble are divided into three sets, one for each sector in DL-PUSC with segmentation (cf. Section 8.7 in [33]). In each sector, only one of these sets is active, modulating every third subcarrier [36]. For example, for the first sector, only subcarriers 0, 3, 6, … are modulated, while the rest of them are nulled. We have tested this scenario in our experiments, using the same preamble as previously at the active frequencies and employing linear interpolation to determine the channel at the inactive ones.

3.1.3.2 Using as many frequencies as channel taps

Alternatively, one may use only L_h subcarriers, with L_h being the channel length (or an upper bound). It is well known that, in OFDM, these L_h pilots should be equispaced and equipowered [36][37][38]. The same principle was used in our experiments for FBMC/OQAM. Note that, in the practical case of $L_h << M$, there won't be any intrinsic interference among these pilots and hence the estimation can be performed in the same way as in CP-OFDM. Let $\mathbf{H}^{p,q}$ contain the frequency response values of the channel from transmit antenna p to receive antenna q, estimated (as previously) at the L_h active subcarriers. Then the corresponding impulse response can be computed as $\mathbf{h}^{p,q} = \mathbf{F}_{L_h}^{-1}\mathbf{H}^{p,q}$, where $\mathbf{F}_{L_h}$ is the $L_h \times L_h$ submatrix of the M th-order DFT matrix built from its first L_h columns and its L_h rows corresponding to the used subcarriers.

3.1.3.3 Using Frequency-Division Multiplexed (FDM) pilots

In all of the schemes presented above, the transmit antennas transmit simultaneously at the *same* frequencies. Moreover, at least as many nonzero FBMC symbols as transmit antennas are included in the preamble. An alternative preamble-based training pattern consists of sharing the subcarriers among the antennas, as suggested in [39]. This kind of preamble training has been known as *frequency-division multiplexing (FDM)* [40] and results in a preamble of a shorter duration. FDM allows, for a given receive antenna, to separately estimate the channels from each of the transmit antennas. The frequency response values at the inactive frequencies are found via interpolation in the frequency direction.

This subsection focuses on the example of two transmit antennas, with the first antenna transmitting on the even and the second on the odd subcarriers, for the duration of *one* symbol. Active subcarriers carry randomly chosen real symbols. Consider first cyclic prefix based OFDM (CP-OFDM) and let the preamble symbols be chosen as $d_0,0,d_2,0,\ldots,0,d_{M-2},0$ and $0,d_1,0,d_3,\ldots,0,d_{M-1}$ for the first and second antenna, respectively, with real d_i's. Then the received samples at the q th receive antenna can be written as

$$y_k^q = \begin{cases} H_k^{1,q} d_k + \eta_k^q, & k \text{ even} \\ H_k^{2,q} d_k + \eta_k^q, & k \text{ odd} \end{cases}$$

whereby one can easily compute the two channels at the active subcarriers and then interpolate for the rest of them.

The same preamble is used in FBMC/OQAM, preceded and followed by all-zero symbols as previously (i.e., 1.5 complex symbols in total). Then one can write for the received signal at the q th antenna:

$$\underbrace{\begin{bmatrix} \widetilde{y}_0^q \\ \widetilde{y}_2^q \\ \vdots \\ \widetilde{y}_{M-2}^q \\ \widetilde{y}_1^q \\ \widetilde{y}_3^q \\ \vdots \\ \widetilde{y}_{M-1}^q \end{bmatrix}}_{\tilde{\mathbf{y}}^q} = \underbrace{\begin{bmatrix} d_0 & 0 & \cdots & 0 & \beta d_1 & 0 & \cdots & -\beta d_{M-1} \\ 0 & d_2 & \cdots & 0 & -\beta d_1 & \beta d_3 & \cdots & 0 \\ \vdots & \vdots & \ddots & \vdots & \vdots & \vdots & \ddots & \vdots \\ 0 & 0 & \cdots & d_{M-2} & 0 & 0 & \cdots & \beta d_{M-1} \\ -\beta d_0 & \beta d_2 & \cdots & 0 & d_1 & 0 & \cdots & 0 \\ 0 & -\beta d_2 & \cdots & 0 & 0 & d_3 & \cdots & 0 \\ \vdots & \vdots & \ddots & \vdots & \vdots & \vdots & \ddots & \vdots \\ \beta d_0 & 0 & \cdots & -\beta d_{M-2} & 0 & 0 & \cdots & d_{M-1} \end{bmatrix}}_{\mathbf{D}_\beta} \cdot \underbrace{\begin{bmatrix} H_0^{1,q} \\ H_2^{1,q} \\ \vdots \\ H_{M-2}^{1,q} \\ H_1^{2,q} \\ H_3^{2,q} \\ \vdots \\ H_{M-1}^{2,q} \end{bmatrix}}_{\mathbf{H}^q} + \underbrace{\begin{bmatrix} \eta_0^q \\ \eta_2^q \\ \vdots \\ \eta_{M-2}^q \\ \eta_1^q \\ \eta_3^q \\ \vdots \\ \eta_{M-1}^q \end{bmatrix}}_{\eta^q}$$

or

$$\tilde{\mathbf{y}}^q = \mathbf{D}_\beta \mathbf{H}^q + \boldsymbol{\eta}^q, \tag{3.1.3}$$

where $\mathbf{H}^q$ contains the frequency responses of the channels from the first and second transmit antennas to the qth receive antenna at even and odd subcarriers, respectively, and

$$\mathbf{D}_\beta = \begin{bmatrix} \mathbf{I}_{M/2} & \mathbf{B} \\ \mathbf{B}^H & \mathbf{I}_{M/2} \end{bmatrix} \cdot \begin{bmatrix} \mathbf{D}_e & \mathbf{0} \\ \mathbf{0} & \mathbf{D}_o \end{bmatrix},$$

with $\mathbf{B}$ denoting the $M/2 \times M/2$ circulant matrix

$$\mathbf{B} = \begin{bmatrix} \beta & 0 & 0 & \cdots & -\beta \\ -\beta & \beta & 0 & \cdots & 0 \\ 0 & -\beta & \beta & \cdots & 0 \\ \vdots & \vdots & \vdots & \ddots & \vdots \\ 0 & 0 & 0 & \cdots & \beta \end{bmatrix},$$

and $\mathbf{D}_e = \mathrm{diag}(d_0, d_2, \ldots, d_{M-2})$, $\mathbf{D}_o = \mathrm{diag}(d_1, d_3, \ldots, d_{M-1})$. Again, one can compute $\mathbf{H}^q$ from (3.1.3) as $\mathbf{H}^q = \mathbf{D}_\beta^{-1}\tilde{\mathbf{y}}^q$, $q = 1,2,\ldots,N_r$, and use interpolation in the frequency axis to estimate the channels at the missing subcarriers.

3.1.3.4 Optimal one-symbol preamble

An alternative to FDM pilots, while still using *one* symbol per antenna, is to use only a set of subcarriers (the *same* for all antennas) with the pilot symbols so chosen as to achieve orthogonality among the transmitting antennas. Such a preamble training scheme was proposed in [41] for MIMO-OFDM and was shown to result in a least squares (LS) channel estimate of *minimum MSE*. When transmitting nulls (instead of data) at the remaining subcarriers and hence no interference results for the pilot tones, this scheme can be extended to FBMC/OQAM in a straightforward manner; namely, by preceding and following the pilot symbol with all-zeros symbols, as previously.

Let $N = \dfrac{M}{L_h}$ be an integer[1], greater than or equal to N_t.[2] Consider N_t sets of L_h pilots each, placed at subcarriers $\{P_p, P_p + N, P_p + 2N, \ldots, P_p + (L_h - 1)N\}$, $p = 1,2,\ldots,N_t$, with user-chosen starting

[1] If not, one can use for L_h the smallest power of 2 that is not smaller than L_h, that is, $2^{\lceil \log_2 L_h \rceil}$.

[2] The latter has to be true anyway, since the number of unknown parameters ($N_t N_r L_h$) cannot exceed the number of received signals (MN_r).

positions $P_1, P_2, \ldots, P_{N_t} \in \{0,1,\ldots,N-1\}$. Thus, the pilot subcarriers within each set are equispaced. Moreover, the pilot symbols are chosen to be equipowered.

Let $\tilde{\mathbf{y}}^{(P)} = \begin{bmatrix} \tilde{\mathbf{y}}_P^T & \tilde{\mathbf{y}}_{P+N}^T & \cdots & \tilde{\mathbf{y}}_{P+(L_h-1)N}^T \end{bmatrix}^T$, with $\tilde{\mathbf{y}}_k = \begin{bmatrix} \tilde{y}_k^1 & \tilde{y}_k^2 & \cdots & \tilde{y}_k^{N_r} \end{bmatrix}^T$, contain the received signals at the P th pilot-tone set. Then one can readily verify that

$$\tilde{\mathbf{y}}^{(P)} = \mathbf{D}_1^{(P)} \overline{\mathbf{F}}_{L_h} \mathbf{W}^{(P)} \mathbf{h}^{1,\cdot} + \mathbf{D}_2^{(P)} \overline{\mathbf{F}}_{L_h} \mathbf{W}^{(P)} \mathbf{h}^{2,\cdot} + \cdots + \mathbf{D}_{N_t}^{(P)} \overline{\mathbf{F}}_{L_h} \mathbf{W}^{(P)} \mathbf{h}^{N_t,\cdot} \tag{3.1.4}$$

where

$$\mathbf{D}_p^{(P)} = \mathrm{diag}\left(d_P^p, d_{P+N}^p, \ldots, d_{P+(L_h-1)N}^p\right) \otimes \mathbf{I}_{N_r},$$

with d_k^p again denoting the pilot symbol transmitted at frequency k from antenna p,

$$\overline{\mathbf{F}}_{L_h} = \mathbf{F}(1:N:M, 1:L_h) \otimes \mathbf{I}_{N_r},$$

with $\mathbf{F}(1:N:M, 1:L_h)$ being the submatrix of the M th order DFT matrix consisting of its first L_h columns and every N th of its rows,

$$\mathbf{W}^{(P)} = \mathrm{diag}\left(1, W^P, W^{2P}, \ldots, W^{(L_h-1)P}\right)$$

with $W = e^{-j\frac{2\pi}{M}}$ denoting the M th root of unity, and $\mathbf{h}^{p,\cdot}$ contains the impulse responses of the channels from transmit antenna p to all receive antennas. Then one can compute an estimate for the impulse response $\mathbf{h}$ by solving the $N_t N_r L_h \times N_t N_r L_h$ system of equations

$$\underbrace{\begin{bmatrix} \tilde{\mathbf{y}}^{(P_1)} \\ \tilde{\mathbf{y}}^{(P_2)} \\ \vdots \\ \tilde{\mathbf{y}}^{(P_{N_t})} \end{bmatrix}}_{\tilde{\mathbf{y}}} = \underbrace{\begin{bmatrix} \mathbf{D}_1^{(P_1)} \overline{\mathbf{F}}_{L_h} \mathbf{W}^{(P_1)} & \mathbf{D}_2^{(P_1)} \overline{\mathbf{F}}_{L_h} \mathbf{W}^{(P_1)} & \cdots & \mathbf{D}_{N_t}^{(P_1)} \overline{\mathbf{F}}_{L_h} \mathbf{W}^{(P_1)} \\ \mathbf{D}_1^{(P_2)} \overline{\mathbf{F}}_{L_h} \mathbf{W}^{(P_2)} & \mathbf{D}_2^{(P_2)} \overline{\mathbf{F}}_{L_h} \mathbf{W}^{(P_2)} & \cdots & \mathbf{D}_{N_t}^{(P_2)} \overline{\mathbf{F}}_{L_h} \mathbf{W}^{(P_2)} \\ \vdots & \vdots & \ddots & \vdots \\ \mathbf{D}_1^{(P_{N_t})} \overline{\mathbf{F}}_{L_h} \mathbf{W}^{(P_{N_t})} & \mathbf{D}_2^{(P_{N_t})} \overline{\mathbf{F}}_{L_h} \mathbf{W}^{(P_{N_t})} & \cdots & \mathbf{D}_{N_t}^{(P_{N_t})} \overline{\mathbf{F}}_{L_h} \mathbf{W}^{(P_{N_t})} \end{bmatrix}}_{\mathbf{C}} \cdot \underbrace{\begin{bmatrix} \mathbf{h}^{1,\cdot} \\ \mathbf{h}^{2,\cdot} \\ \vdots \\ \mathbf{h}^{N_t,\cdot} \end{bmatrix}}_{\mathbf{h}} + \underbrace{\begin{bmatrix} \boldsymbol{\eta}^{(P_1)} \\ \boldsymbol{\eta}^{(P_2)} \\ \vdots \\ \boldsymbol{\eta}^{(P_{N_t})} \end{bmatrix}}_{\boldsymbol{\eta}}$$

or

$$\tilde{\mathbf{y}} = \mathbf{C}\mathbf{h} + \boldsymbol{\eta} \tag{3.1.5}$$

A sufficient condition for the matrix $\mathbf{C}$ above to be unitary is that $d_P^p = d_{P+N}^p = \cdots = d_{P+(L_h-1)N}^p$ for all P, p and the matrix

$$\mathbf{D} = \begin{bmatrix} d_{P_1}^1 & d_{P_1}^2 & \cdots & d_{P_1}^{N_t} \\ d_{P_2}^1 & d_{P_2}^2 & \cdots & d_{P_2}^{N_t} \\ \vdots & \vdots & \ddots & \vdots \\ d_{P_{N_t}}^1 & d_{P_{N_t}}^2 & \cdots & d_{P_{N_t}}^{N_t} \end{bmatrix}$$

be unitary. For example, with $M = 8$, $N_t = 2$ and $L_h = 2$, we have $N = 4$. Choosing $\mathbf{D} = \begin{bmatrix} 1 & 1 \\ 1 & -1 \end{bmatrix}$ and $P_1 = 0, P_2 = 2$, the (nonzero) symbols at the two transmit antennas will be

$$\begin{matrix} 1 & 1 \\ 0 & 0 \\ 1 & -1 \\ 0 & 0 \\ 1 & 1 \\ 0 & 0 \\ 1 & -1 \\ 0 & 0 \end{matrix}$$

Clearly, the above analysis holds only if N is sufficiently greater than N_t and the prototype filter is sufficiently well localized in frequency so that one can ignore interference among pilot tones. Moreover, the corresponding noise signals can then be considered as being uncorrelated and LS channel estimation attains the minimum MSE.

3.1.4 Simulation results

We have simulated the above schemes for 2×2 systems. The channel taps are modeled in accordance with the Kronecker model [42], that is

$$\mathbf{H}[m] = \mathbf{R}_r^{1/2}[m]\mathbf{H}_w[m]\mathbf{R}_t^{1/2}[m],$$

where the receive and transmit correlation matrices $\mathbf{R}_r[m], \mathbf{R}_t[m]$ are generated according to the exponential model [44][33], and $\mathbf{H}_w[m]$ is a matrix of i.i.d. zero mean circularly symmetric Gaussian entries with their variance following a given (Veh-A or Veh-B) power delay profile.

CP-OFDM is also included in the comparisons. The CP used is of the *minimum* length, i.e., equal to the channel order. QPSK modulation is adopted.

3.1.4.1 Full preambles

The training input for CP-OFDM is chosen to be orthogonal among the antennas [44], following the same pattern as above. For example, with 2 transmitting antennas and $M = 4$ subcarriers, the two antennas will send

$$\begin{matrix} 1 & 1 \\ -1 & -1 \\ 1 & 1 \\ -1 & -1 \end{matrix} \quad \text{and} \quad \begin{matrix} 1 & -1 \\ -1 & 1 \\ 1 & -1 \\ -1 & 1 \end{matrix}.$$

The same preamble was used by POP, albeit in the real/imaginary OQAM format. That is:

$$\begin{matrix} 1 & 0 & 1 & 0 \\ -1 & 0 & -1 & 0 \\ 1 & 0 & 1 & 0 \\ -1 & 0 & -1 & 0 \end{matrix} \quad \text{and} \quad \begin{matrix} 1 & 0 & -1 & 0 \\ -1 & 0 & 1 & 0 \\ 1 & 0 & -1 & 0 \\ -1 & 0 & 1 & 0 \end{matrix}.$$

As expected, POP exhibited a quite bad performance (significantly worse than that observed in the SISO case (D3.1) [5]). There was no noticeable difference in the results when a random preamble was used. Therefore, POP will not be further considered in our comparative study.

200 channel realizations were used in all the experiments. The *relative* MSE, namely $E\left[\left\|\mathbf{H}-\hat{\mathbf{H}}\right\|^2 \Big/ \left\|\mathbf{H}\right\|^2\right]$, is plotted, with respect to the per-receive antenna SNR. Note that, in each experiment, all preambles are appropriately scaled so as to result in the *same* power for the channel input. Noise power is then varied to obtain the SNR range. The abscissas represent the average SNR per receive antenna at the channel *output*. Notice that the energy wasted in the CP for CP-OFDM was taken into account when computing the corresponding SNR. Weak spatial correlation was assumed for both transmit and receive fading.

2×2 channels of the Veh-A and Veh-B types are considered in Figure 3.1.1. In Figure 3.1.1(a)-(d), perfect reconstruction (PR) filter banks are used, with $K=3$ and $M=256$ and 512, respectively. Results from using the PHYDYAS reference filter bank [17][38] with $M=1024$ and $K=3$ are depicted in Figure 3.1.1(e), (f).

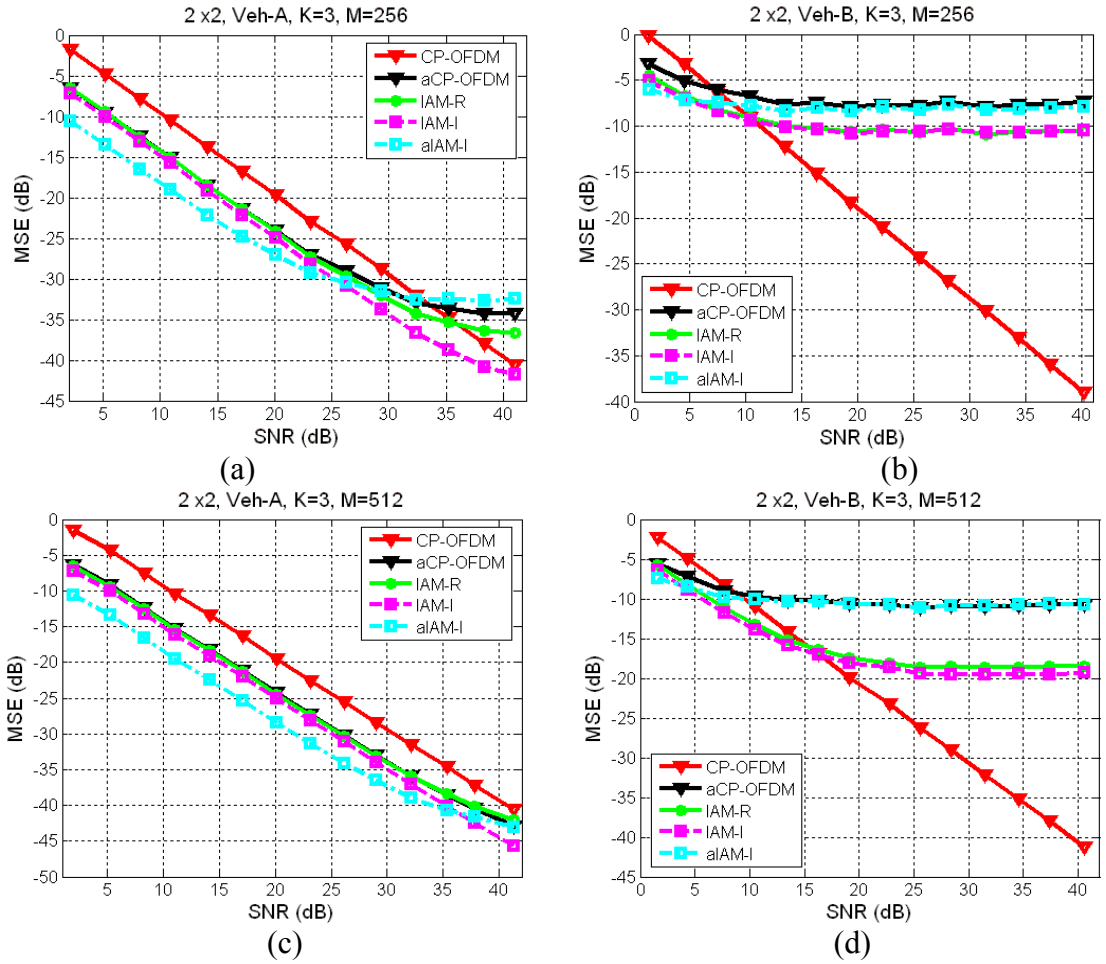

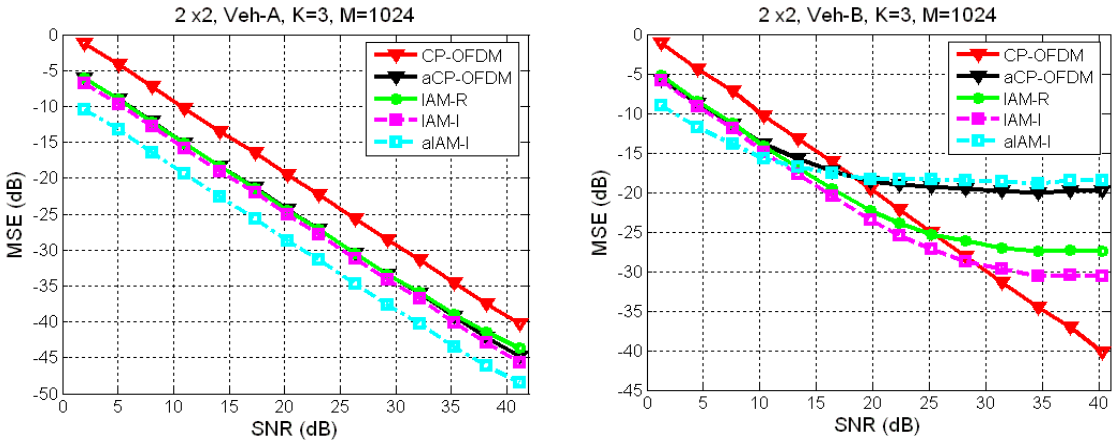

Figure 3.1.1. MSE performance for 2x2 Veh-A and Veh-B channels. PR filter banks with (a), (b) M=256 and (c), (d) M=512. (e), (f) PHYDYAS reference filter bank, M=1024. K=3 in all cases.

It is observed that the IAM-based schemes perform significantly better than CP-OFDM only at sufficiently low SNR values. The well-known (from SISO systems) error floor of IAM at high SNR's is observed here too, due to the unavoidable intrinsic interference, which shows up at the weak noise regime.

The crossing point, where CP-OFDM starts outperforming the FBMC methods, is, as expected, moved to the right as the number of subcarriers increases, with fixed overlapping factor. This is particularly noticeable for channels of higher frequency selectivity (Veh-B). As one would expect, the improvement over CP-OFDM also increases with increasing K (see Figure 3.1.2 for an example).

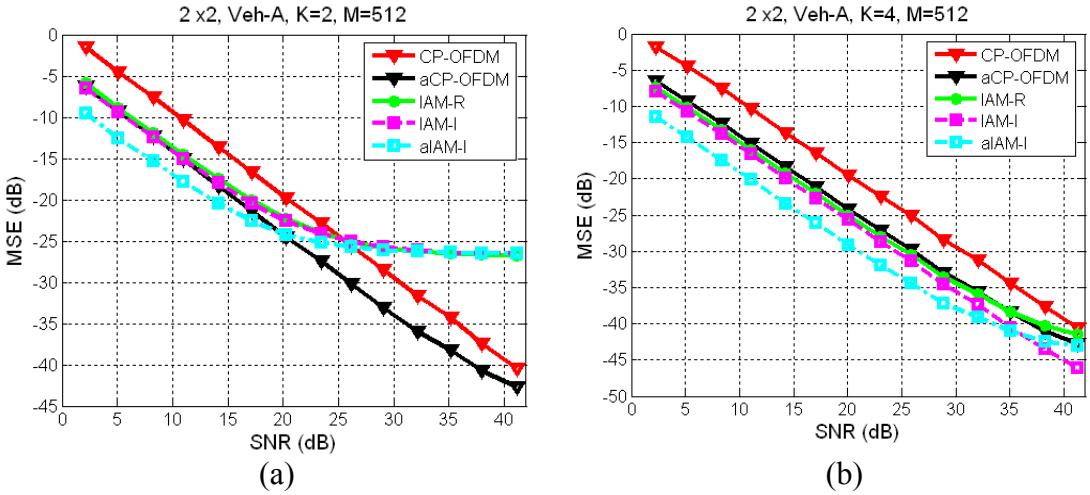

Figure 3.1.2. Effect of overlapping factor: 2x2 Veh-A channels. PR filter bank with M=512 and (a) K=2, (b) K=4.

For the sake of the comparison, CP-OFDM with averaging in the frequency domain (*aCP-OFDM*) was also tested. It is seen to generally perform similarly with IAM-R, for Veh-A channels. For Veh-B channels, where the assumption of locally flat frequency response is no longer valid, its performance deteriorates similarly with that of aIAM-I. The averaged IAM-I scheme exhibits a significant performance gain with respect to all the other methods, at practical SNR values, in Veh-A

channels. We have not observed any significant effect of the fading correlation strength on the estimation performance.

3.1.4.2 Sparse preambles

The following figures depict the estimation accuracy resulting from using one carrier set with the other two being zero (Figure 3.1.3), a set of equispaced and equipowered L_h pilots (Figure 3.1.4), and a single-symbol preamble with FDM pilots (Figure 3.1.5). The results are for 2×2 Veh-A channels, for both CP-OFDM and FBMC/OQAM, using random QPSK symbols.

PR filter banks of size $M = 512$ and the PHYDYAS reference NPR filter bank with $M = 1024$ are used. The overlapping factor is $K = 3$ in all cases. Linear interpolation is carried out with the aid of the Matlab function `interp1`. The CP-OFDM transmitted signal was again scaled in each experiment so as to be of the same power with the channel input in the corresponding FBMC/OQAM system.

It is seen that FBMC/OQAM offers a significant improvement in estimation accuracy, for low and moderate SNR values. With the exception of Figure 3.1.6, one can see that, at high values of SNR, the well-known error floor again prevails and FBMC/OQAM is then outperformed by CP-OFDM. As expected, the crossing point is moved to the right as the number of subcarriers increases. With the optimal one-symbol preamble (Figure 3.1.6), there is no significant interference neither in frequency nor in time[3] direction, hence the error floor is not an issue. Moreover, although only 1.5 complex symbols are used, the obtained estimation performance is significantly better than all the other schemes considered.

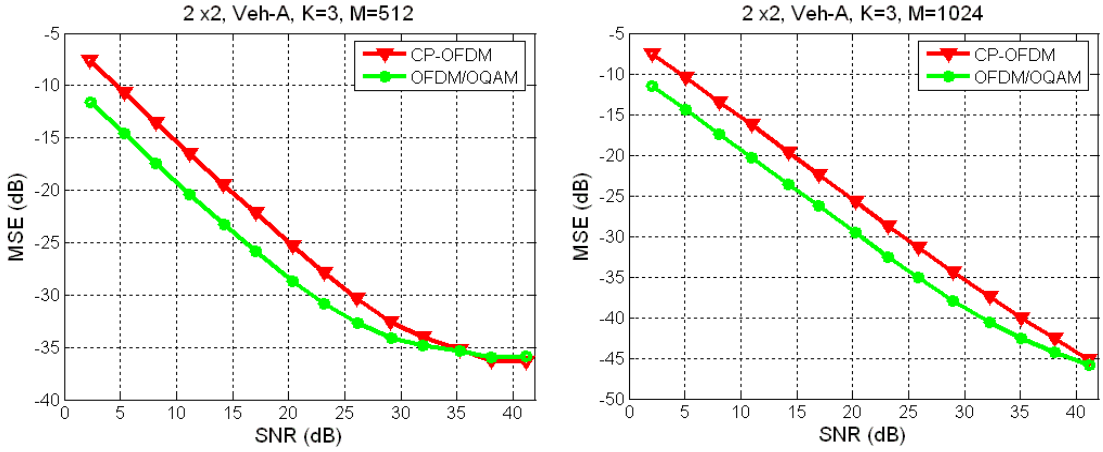

(a) (b)

Figure 3.1.3. Preamble with only one active carrier set: 2x2 Veh-A channels. (a) PR filter bank with M=512, K=3. (b) PHYDYAS reference filter bank with M=1024, K=3.

[3] In practice, there will be some interference from the symbols following the preamble. This can be greatly reduced by using two zero symbols instead of one at the right-hand side of the preamble. In view of the fact that a guard time interval (as in WiMAX [33]) will be present between frames, the left-hand side zero symbol could be omitted, thus keeping the preamble length the same.

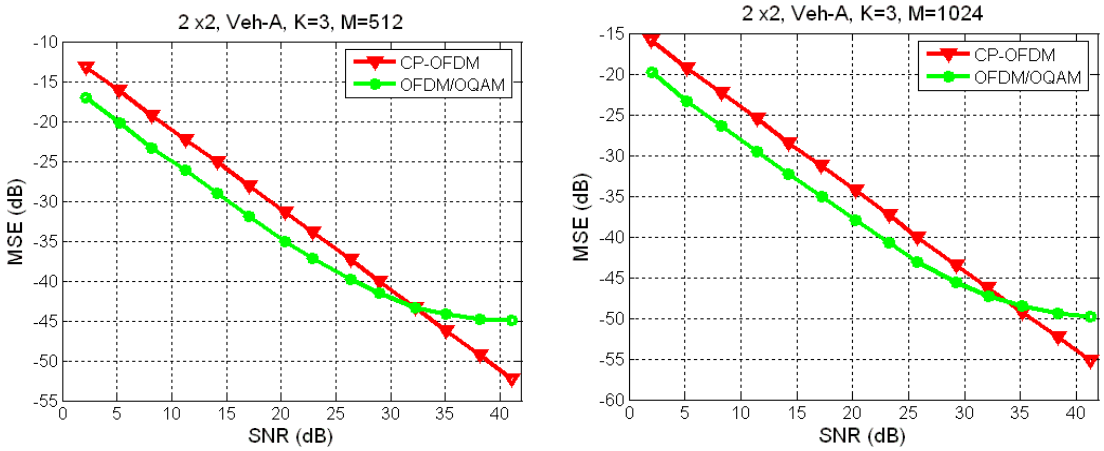

(a) (b)

Figure 3.1.4. Using only L_h pilots: 2x2 Veh-A channels. (a) PR filter bank with M=512, K=3. (b) PHYDYAS reference filter bank with M=1024, K=3.

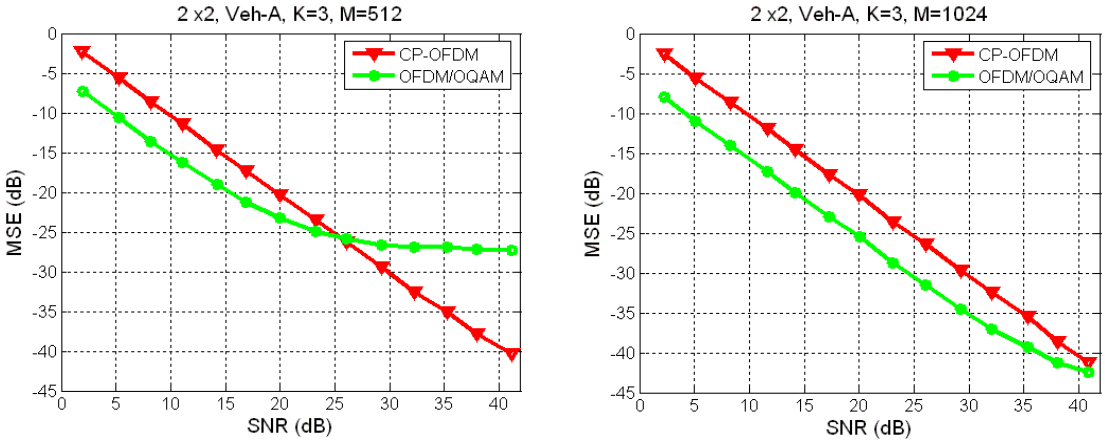

(a) (b)

Figure 3.1.5. FDM preamble for 2x2 Veh-A channels. (a) PR filter bank with M=512, K=3. (b) PHYDYAS reference filter bank with M=1024, K=3.

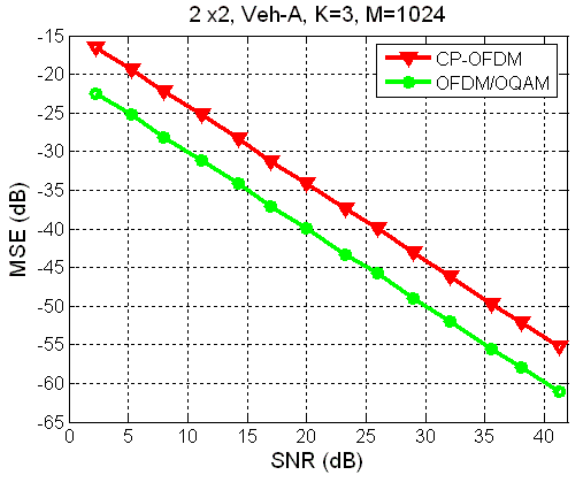

Figure 3.1.6. Optimum preamble for 2x2 Veh-A channels. PHYDYAS reference filter bank with M=1024, K=3.

3.2 Adaptation to WiMAX DL-PUSC communication mode

The general frame structure in WiMAX systems for the TDD scheme can be found in [7]. To ensure compatibility, these principles should be taken as basis for framing within PHYDYAS. As explained in [7], WiMAX offers three different subcarrier permutation schemes. First, the Full Usage of the Subcarriers (FUSC) scheme allocates first the pilots on fixed positions, and the remaining subcarriers are used to transmit the data. On the other hand, Partial Usage of the Subcarriers (PUSC) and Band Adaptive Modulation and Coding scheme (henceforth referred to as AMC), divide the whole frame (excluding the Preamble, the frame control header (FCH) and downlink/uplink maps (DL/UL-MAPs)) into minimal data units, named slots, where dedicated pilots and data are jointly allocated. Each slot is defined as a 2-dimensional unit which spans in both frequency and time directions. This section describes different slot definitions as a function of the permutation scheme described in [8] and [9], and how the dedicated pilots are inserted in the case of a multiple antenna transmitter.

3.2.1 A general overview of pilot allocation structures in WiMAX systems

The transmission of the preamble and the control channels in SISO case (i.e. FCH, DLMAP and ULMAP) shall be performed from only one antenna (Antenna 0) using the PUSC scheme, while applying transmit diversity shall be performed considering any of the schemes resumed hereafter.

3.2.1.1 Pilot and data allocation for the PUSC permutation scheme (Downlink)

For the PUSC permutation scheme, the set of used subcarriers is divided into clusters. Pilots and data carriers are allocated within each cluster. Each cluster is formed by 14 adjacent subcarriers where 2 subcarriers are dedicated to pilots. In case of single antenna transmission, the position of the pilots is changed between odd and even symbols. In case of two and four transmitting antennas, the pilots are placed as defined in Figure 3.2.1(a) and Figure 3.2.1(b), respectively. In both cases, the pilot pattern allocation has a period of 4 OFDM symbols. For the 4 transmitting antennas case, one can observe that pilot subcarriers for antenna 2 and antenna 3 override data subcarriers, hence the puncturing rate in case of convolutional coding (CC) or the data truncation rate in case of convolutional turbo coding (CTC) must be modified accordingly.

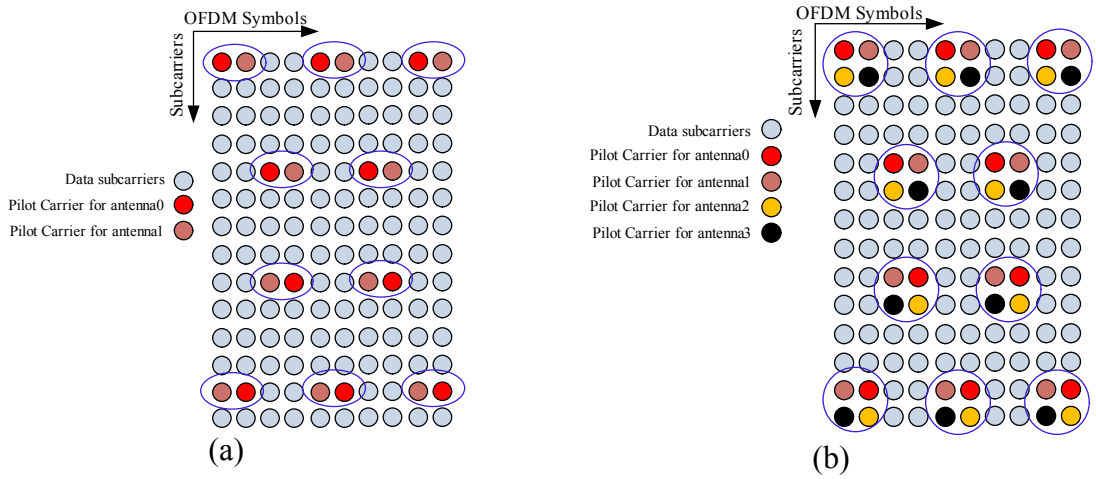

Figure 3.2.1 Cluster structure for STC downlink PUSC using 2 antennas in (a), and 4 antennas in (b).

The shape of one slot in the PUSC scheme is 2 clusters in frequency direction and two OFDM symbols in the time direction. Hence, the number of data subcarriers is 48. Due to subchannel permutation the clusters are transmitted at distant positions in the spectrum, although each cluster is transmitted as a whole in adjacent subcarriers. Consequently, the PUSC permutation scheme increases frequency diversity.

3.2.1.2 Pilot and data allocation for the PUSC permutation scheme (Uplink)

In the uplink case, the PUSC permutation scheme divides the uplink frame into structures of 4 subcarriers lasting for 3 OFDM symbols. This structure, formed by 12 subcarriers (4 pilot subcarriers and 8 data subcarriers), is referred to as a tile.

In order to obtain one slot, 6 tiles are packed together in frequency, thus giving the required 48 data subcarriers. In case of two transmit antennas, the pilots are located for each antenna as shown in Figure 3.2.2. The case of four transmitting antennas is not considered within the IEEE 802.16e standard [8].

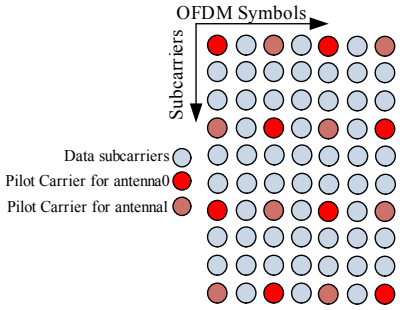

Figure 3.2.2: Cluster structure for STC uplink PUSC using 2 antennas.

.

3.2.1.3 Pilot and data allocation for the AMC permutation scheme (Downlink and Uplink)

The AMC permutation scheme is characterized by mapping adjacent subcarriers to each slot. By doing so, although frequency diversity is minimized, the use of adaptive modulation and coding may lead to great benefits by transmitting for each user on those bands where the channel experiences favourable conditions. For this permutation scheme, a smaller resource unit defined as nine contiguous subcarriers is used. This basic allocation unit is referred to as a bin. Each bin contains one pilot subcarrier (whose position is changed every OFDM symbol) and 8 data subcarriers. There are four types of AMC slots. The first is given by the collection of 6 consecutive bins (hence a 6×1 structure), the second has a 2×3 structure, and the third and the fourth are given by the 3×2 and the 1×6 structures.

3.2.1.4 Pilot and data allocation for the FUSC permutation scheme (Downlink)

For the FUSC permutation scheme, the symbol structure is constructed using pilot, data and zero subcarriers. Pilots and zero subcarriers are first allocated. The remaining subcarriers are then used as data subcarriers. 48 data subcarriers are later mapped to each subchannel. The subcarriers from each subchannel map to physical subcarriers placed equidistantly in the spectrum. For the FUSC scheme, one slot is defined as 1 subchannel per 1 OFDM symbol, thus giving the 48 data subcarriers.

In case of multiple transmitting antennas, the sets must be shared. Figure 3.2.3 and Figure 3.2.4 give an example of the location of the pilots within one cluster for two and four transmit antennas, respectively. As observed in both figures, the position of the pilot symbols from the variable set change each two OFDM symbols.

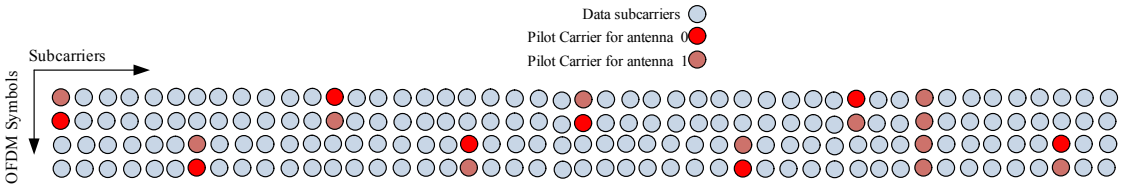

Figure 3.2.3: Cluster structure for STC FUSC using 2 antennas.

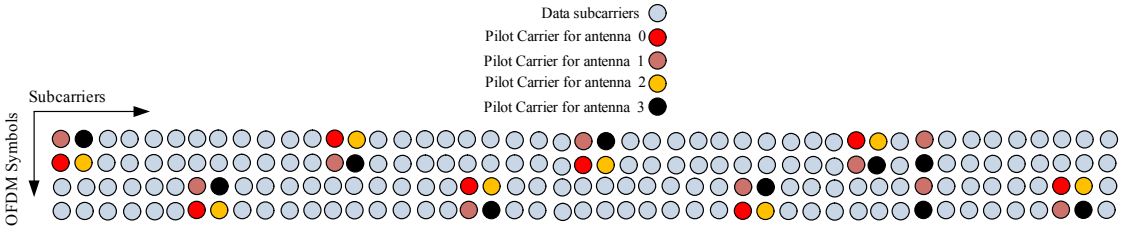

Figure 3.2.4: Cluster structure for STC FUSC using 4 antennas.

3.2.2 Filter bank multicarrier adaptation to WiMAX DPUSC structure

In OFDM systems to estimate the channel at a given frequency-time position (k_0,n_0), a complex pilot is transmitted at this position. At the receiver side the channel estimation is carried out by dividing the demodulated signal with the pilot's value which is considered known at the receiver. As it has been noticed, in FBMC/OQAM each subcarrier carries a real valued symbol but the density of the time-frequency lattice of sub-carriers is twice greater than in the classical OFDM, which means $T_{ofdm}=2\tau_0$ where τ_0 being the FBMC/OQAM symbol duration [49].

The downlink (DL) partial usage of subchannels (PUSC) configuration for data and pilot allocation in the CP-OFDM system is adapted in Figure 3.2.1(a) and Figure 3.2.1(b) for 2 antennas and 4 antennas, respectively. Figure 3.2.5(a) and Figure 3.2.5(b) show the specific associated configuration for an FBMC/OQAM system.

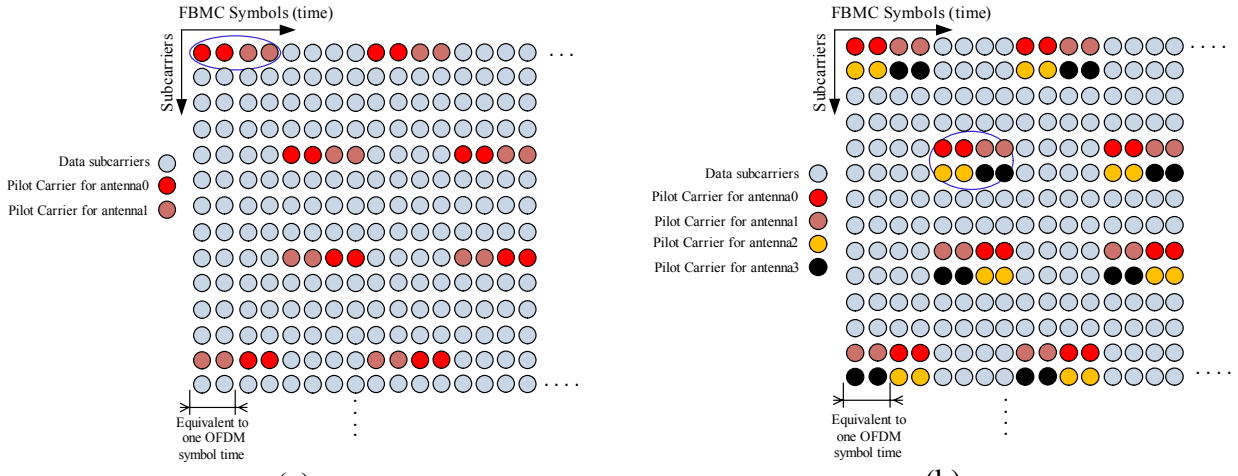

Figure 3.2.5: Cluster structure for STC PUSC adapted to FBMC using 2 antennas in (a), and 4 antennas in (b).

Let us consider the case where a communication system uses N_t antennas at the transmitter and N_r antennas at the receiver respectively. We assume that the filter bank configuration is that presented in [49] and used in [5]. Assume moreover, that the OQAM system is properly dimensioned, i.e. such

that the channel may be considered as invariant in a first-order neighborhood around the pilot antenna position (k_0,n_0) within each antenna transmitted communication frame.

Under the assumptions of low frequency selectivity for channel and a perfect time-frequency localization of the PHYDYAS reference filter bank in [49], the received signal at the N_r received antennas can be expressed as (1.2), where $\tilde{x}_{k,n}^{p} = d_{k,n}^{p} + ju_{k,n}^{p}$ is the AFB output from the p-th transmit antenna, with $d_{k,n}^{p}$ being the corresponding input symbol (primary part) and $ju_{k,n}^{p}$ the intrinsic interference from the surrounding time-frequency points (the secondary part). The latter is built out of the contributions of the neighbouring points [6]

3.2.2.1 Using the Pair of Pilots (POP) concept

The POP channel estimation method was investigated for the SISO case and based on the insertion of pairs of real-valued pilots (POP) at positions known at the receiver. In practice one can consider successive time positions having the same subcarrier index and where the channel is quasi-invariant. We extend and adapt the same principle to the multiple antennas case. Consider (1.2) with noise component neglected, for the case that $N_t > N_r$.

Denote by (k, n) and (k, n+1) two reference pilot positions. Then, we have:

:

$$\begin{cases} \tilde{\mathbf{y}}_{k.n}^{(c)} = \mathbf{H}_{k,n}^{(c)} \left(\mathbf{d}_{k,n} + j\mathbf{u}_{k,n} \right) \\ \tilde{\mathbf{y}}_{k.n+1}^{(c)} = \mathbf{H}_{k,n+1}^{(c)} \left(\mathbf{d}_{k,n+1} + j\mathbf{u}_{k,n+1} \right) \end{cases}$$

with channel component $\mathbf{H}_{k,n}^{(c)} = \mathbf{H}_{k,n}^{R} + j\mathbf{H}_{k,n}^{I}$ at the pilot antenna frequency-time position (k ,n), superscript c means “complex value”. The samples received at the N_r receive antennas will be expressed as,

$$\tilde{\mathbf{y}}_{k,n}^{(c)} = \begin{bmatrix} \tilde{y}_{k,n}^{(c)1} \\ \tilde{y}_{k,n}^{(c)2} \\ \vdots \\ \tilde{y}_{k,n}^{(c)N_r} \end{bmatrix} = \begin{bmatrix} H_{k,n}^{(c)1,1} & H_{k,n}^{(c)2,1} & \cdots & H_{k,n}^{(c)N_t,1} \\ H_{k,n}^{(c)1,2} & H_{k,n}^{(c)2,2} & & H_{k,n}^{(c)N_t,2} \\ \vdots & & & \\ H_{k,n}^{(c)1,N_r} & H_{k,n}^{(c)2,N_r} & & H_{k,n}^{(c)N_t,N_r} \end{bmatrix} \begin{bmatrix} d_{k,n}^{1} + ju_{k,n}^{1} \\ d_{k,n}^{2} + ju_{k,n}^{2} \\ \vdots \\ d_{k,n}^{N_t} + ju_{k,n}^{N_t} \end{bmatrix}$$

and

$$\tilde{\mathbf{y}}_{k,n+1}^{(c)} = \begin{bmatrix} \tilde{y}_{k,n+1}^{(c)1} \\ \tilde{y}_{k,n+1}^{(c)2} \\ \vdots \\ \tilde{y}_{k,n+1}^{(c)N_r} \end{bmatrix} = \begin{bmatrix} H_{k,n+1}^{(c)1,1} & H_{k,n+1}^{(c)2,1} & \cdots & H_{k,n+1}^{(c)N_t,1} \\ H_{k,n+1}^{(c)1,2} & H_{k,n+1}^{(c)2,2} & & H_{k,n+1}^{(c)N_t,2} \\ \vdots & & & \\ H_{k,n+1}^{(c)1,N_r} & H_{k,n+1}^{(c)2,N_r} & & H_{k,n+1}^{(c)N_t,N_r} \end{bmatrix} \begin{bmatrix} d_{k,n+1}^{1} + ju_{k,n+1}^{1} \\ d_{k,n+1}^{2} + ju_{k,n+1}^{2} \\ \vdots \\ d_{k,n+1}^{N_t} + ju_{k,n+1}^{N_t} \end{bmatrix} \quad (3.2.1)$$

Let that value C be the ratio between the imaginary and the real part of each $H_{k,n}^{(c)}$, i.e. $H_{k,n}^{(c)} = H_{k,n}^{R} + jH_{k,n}^{I}$, $C = H_{k,n}^{I} / H_{k,n}^{R}$ .Taking the real and imaginary part of each equation in (3.2.1), we obtain:

$$\begin{cases} \mathbf{y}_{k,n}^{R} = \mathbf{H}_{k,n}^{R}\mathbf{d}_{k,n} - (\mathbf{H}_{k,n}^{R} \otimes \mathbf{C})\mathbf{u}_{k,n} \\ \mathbf{y}_{k,n}^{I} = (\mathbf{H}_{k,n}^{R} \otimes \mathbf{C})\mathbf{d}_{k,n} + \mathbf{H}_{k,n}^{R}\mathbf{u}_{k,n} \\ \mathbf{y}_{k,n+1}^{R} = \mathbf{H}_{k,n+1}^{R}\mathbf{d}_{k,n+1} - (\mathbf{H}_{k,n+1}^{R} \otimes \mathbf{C})\mathbf{u}_{k,n+1} \\ \mathbf{y}_{k,n+1}^{I} = (\mathbf{H}_{k,n+1}^{R} \otimes \mathbf{C})\mathbf{d}_{k,n+1} + \mathbf{H}_{k,n+1}^{R}\mathbf{u}_{k,n+1} \end{cases} \quad (3.2.2)$$

Assuming that the channel is invariant, we may set $\mathbf{H}_{k,n+1}^{(c)} = \mathbf{H}_{k,n}^{(c)}$. Then by combining the above equations we are able to compute the values of **C**, and therefore estimate the coefficients of the channel $\mathbf{H}_{k,n}^{(c)} = \mathbf{H}_{k,n}^{R} + j\mathbf{H}_{k,n}^{I}$

For the SISO case this method does not require any knowledge of the prototype function in (3.2.2) and it can be used for preamble-based channel estimation [6], and even for the MIMO case. In presence of noise we will have,

$$\begin{cases} \tilde{\mathbf{y}}_{k,n}^{(c)} = \mathbf{H}_{k,n}^{(c)}(\mathbf{d}_{k,n} + j\mathbf{u}_{k,n}) + \boldsymbol{\eta}_{n,k} \\ \tilde{\mathbf{y}}_{k,n+1}^{(c)} = \mathbf{H}_{k,n+1}^{(c)}(\mathbf{d}_{k,n+1} + j\mathbf{u}_{k,n+1}) + \boldsymbol{\eta}_{k,n+1} \end{cases}$$

As in (3.2.2) following the real and the imaginary decomposition of the received signals an estimate for matrix **C** is obtained this time corrupted by the noise component. As in the SISO case in [6] it could be observed that the quality of the channel is directly linked with a certain vector $\boldsymbol{\nu}$ [5] which has a random behavior. If the power of $\boldsymbol{\nu}$ is high, the estimation will be good enough but if it is closed to zero, the noise is enhanced and the results will be poor.

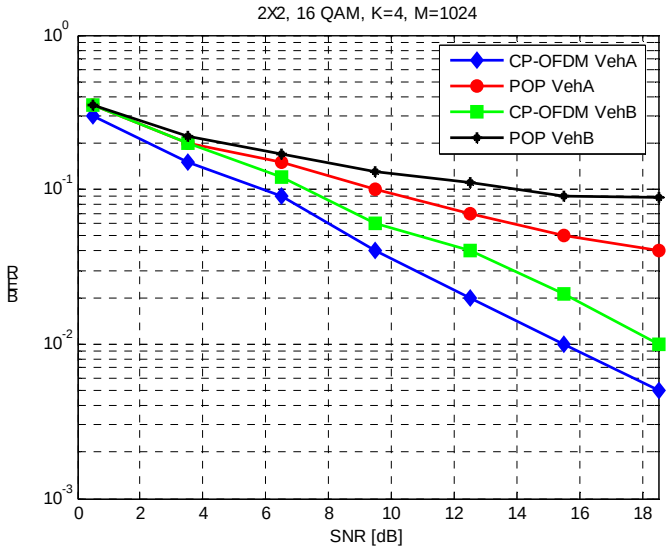

Figure 3.2.6: FBMC 2×2 performances vs CP-OFDM for Veh-A & Veh-B at 60Km/h, using adapted POP method to downlink PUSC. PHYDYAS reference filter bank; M=1024, K= 4, and 16 QAM modulation using ZF.

It can be seen in Figure 3.2.6 that the POP scheme adapted for MIMO FBMC exhibited a performance worse than the CP-OFDM schemes for both channels, Veh-A and Veh-B. A similar strategy for the pair values of (0, ± 1) for pilots have been adopted as in [5] for each antenna pilot pattern. Although a performance degradation is experienced by the CP-OFDM scheme in the Veh-B channel, the POP scheme still yields worse results in the Veh-A channel. Therefore, POP will not be considered for the PHYDYAS filter bank multicarrier system due to its bad performance compared with the conventional CP-OFDM scheme.

Note that referring to the downlink PUSC scheme, the advantage of the preamble has been taken into account, and the received signals are assumed perfectly synchronized. The interpolation process is carried out using two dimensional linear surface interpolation within the areas limited by the carriers and the symbols with pilot supports (*as the Matlab function griddata is used*). The remaining carriers and symbols are estimated using linear extrapolation. The simulations are run over 600 channel realizations. Note that a weak spatial correlation was assumed for both transmit and receive fading.

3.2.2.2 Using the adaptation of auxiliary pilot scheme

In the downlink PUSC mode illustrated in [5] for the SISO case, whether a regular placement of auxiliary pilots is adopted and the wider window of the filter bank components is used in the auxiliary pilot calculations. In case an auxiliary pilot is in the window of another auxiliary pilot,

recursive calculation of auxiliary pilots would be required, which may be somewhat inconvenient. However, by using a slightly modified pilot scheme, this difficulty can be avoided, and each of the auxiliary pilots can be calculated independently of the others. In the modified scheme presented below, the pilots are introduced using specific positions of pilot and auxiliary pilot per transmitted antenna as illustrated in Figure 3.2.7.

The transmultiplexer response $t_{k,n}$ is known from the filter bank design. If the prototype filter is designed with good frequency selectivity and roll-of factor $\alpha \leq 1$, the range includes k and both adjacent subcarriers, $k-1$ and $k+1$, in the frequency dimension. The range of n is [n-K, n+K] subcarrier samples with the typical overlapping factors (K) of 3 or 4.

As in [5] the auxiliary pilot position is denoted in the following as (k_a,n_a) and the auxiliary pilot is chosen in such a way that the secondary part of the pilot sample becomes zero. In the MIMO case this can be achieved by choosing the auxiliary pilot as

$$d^i_{k_a,n_a} = -\frac{\sum_{\substack{(k',n')\in\ \Omega_{\Delta k,\Delta n} \\ (k',n')\neq(k,n) \\ (k',n')\neq(k_a,n_a)}} d^i_{k',n'} t_{k-k',n-n'}}{t_{k-k_a,n-n_a}}$$

where superscript i corresponding to the i-th transmit antenna, and $\Omega_{\Delta k\ \Delta n}$ is the set of neighbouring symbol positions which have a significant effect on the pilot symbol at (k,n) frequency-time position. Note that it is preferable to choose the auxiliary pilot in such a way that the magnitude of the denominator is maximized. In typical filter bank designs, including the PHYDYAS reference filter bank, the choice for the auxiliary pilot (k_a,n_a) is the sample immediately following the pilot, i.e., (k ,n+1) or (k ,n-1).

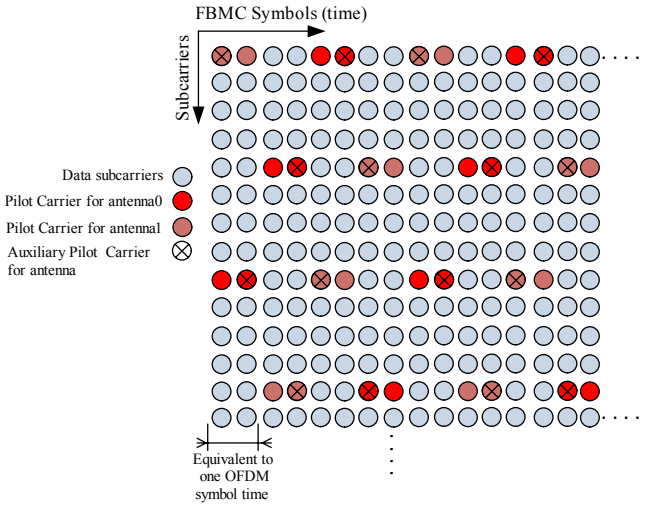

Figure 3.2.7: Pilot and pilot support (auxiliary pilot) allocation in FBMC for downlink PUSC pilot pattern, for 2 antennas.

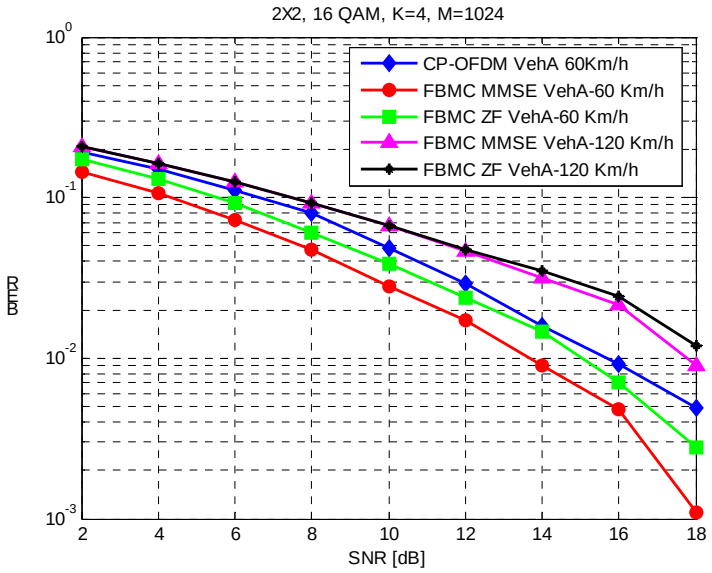

Figure 3.2.8: FBMC 2×2 channel estimation performances for Veh-A at different MS mobilities (60 and 120 km/h) using adapted auxiliary pilot method (Figure 3.2.7) vs. conventional CP-OFDM. PHYDYAS filter banks references; M=1024, K= 4, DPUSC, and 16 QAM modulation using MMSE and ZF.

In Figure 3.2.8 the received signals are assumed perfectly synchronized and not taking advantage of the downlink preamble. It can be observed that the use of the auxiliary pilot method in FBMC system outperforms the conventional CP-OFDM system. For the Veh-A channel case with 60Km/h the FBMC with Minimum Mean Square Error (MMSE) equalization clearly outperforms the CP-OFDM. Even using the zero forcing (ZF) equalization the performances are lightly better than the OFDM with ZF. The adapted approach in [4] and [5] eliminates the secondary interference from the neighbouring symbols onto a pilot antenna to perform pilot based channel estimation in an MIMO FBMC/OQAM system.

3.2.2.3 Using the Interference Approximation Method (IAM)

We have extended the concept to the MIMO case having two antennas at the transmitter (Figure 3.2.9(a) and .9(b)). As it can be seen in Figure 3.2.9 , for any pilot carrier symbol d_{k_0,n_0} located in the middle, d_{k_0,n_0-1} and d_{k_0,n_0+1} are also part of the pilot carrier allocation and hence the secondary part can be approximated. d_{k_0,n_0-1} and d_{k_0,n_0+1} are here named as "*Aided Pilot Carrier*" (APC) as they aid the middle antenna pilot carrier d_{k_0,n_0} to obtain an approximation of the interference due to the filter bank. The IAM method is based on the assumption that the contributions come only from the first order neighboring time-frequency points. Note that for the structures presented in Figure 3.2.9 we are dealing with a partial interference approximation as not all the interferences ($\Omega_{1,1}$) that affect the pilot $d_{k,n}$ are estimated. Here we are confined with the information from the (k, n-1), (k, n+1), (k -1, n), and (k +1, n) neighboring time-frequency positions (see Figure 3.2.9(b)).

We focus on the case where the pilot's positions (k, n-1), (k, n+1) for each antenna are forced to zero, forcing the largest interference weights caused by the PHYDYAS filter bank contributions ($|w_{k,n+1}|=|w_{k,n-1}|=0.5644$) to zero. The interference weights at the frequency-time positions (k_0-1, n_0), and (k+1,n) is $|w_{k-1,n}|=|w_{k+1,n}|=0.2393$ have relative lower value. This approach allows to maximize the modulus of the resulting pilot and hence to minimize the noise effect.

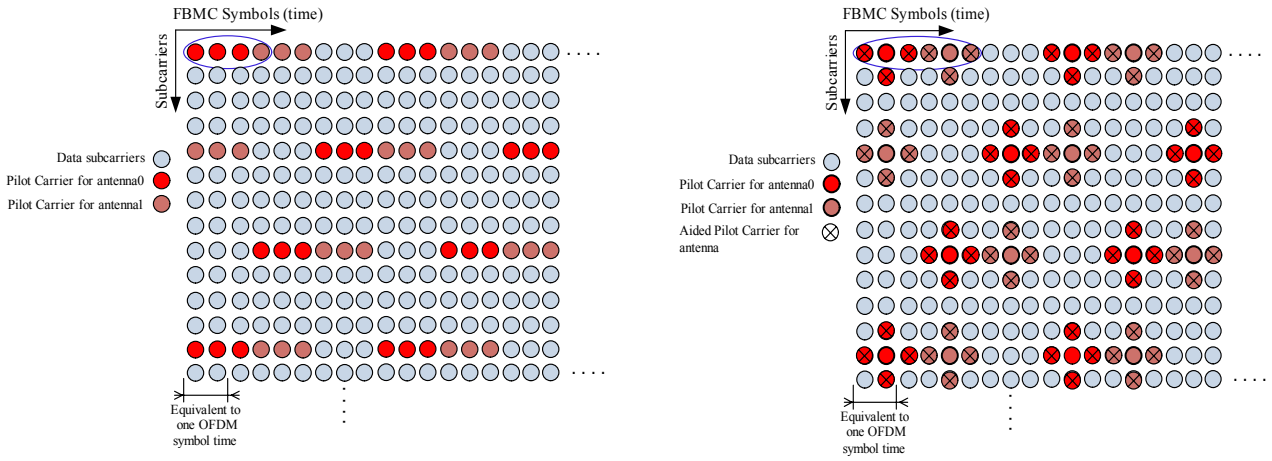

Figure 3.2.9: Pilot and pilot support using the IAM concept for FBMC in DL-PUSC using 2 antennas: (a) reserved allocation for pilots, (b) pilot and aided pilot carrier (APC) positions.

Figure 3.2.9(a)) presents the FBMC DL-PUSC adaptation for two antennas using the IAM concept, while Figure 3.2.9 (b) stand out the positions of the APC pilots for each antenna. Note that based on Figure 3.2.5(b) and Figure 3.2.9(b) an equivalent IAM arranged pilot structure could be achieved for four antennas.

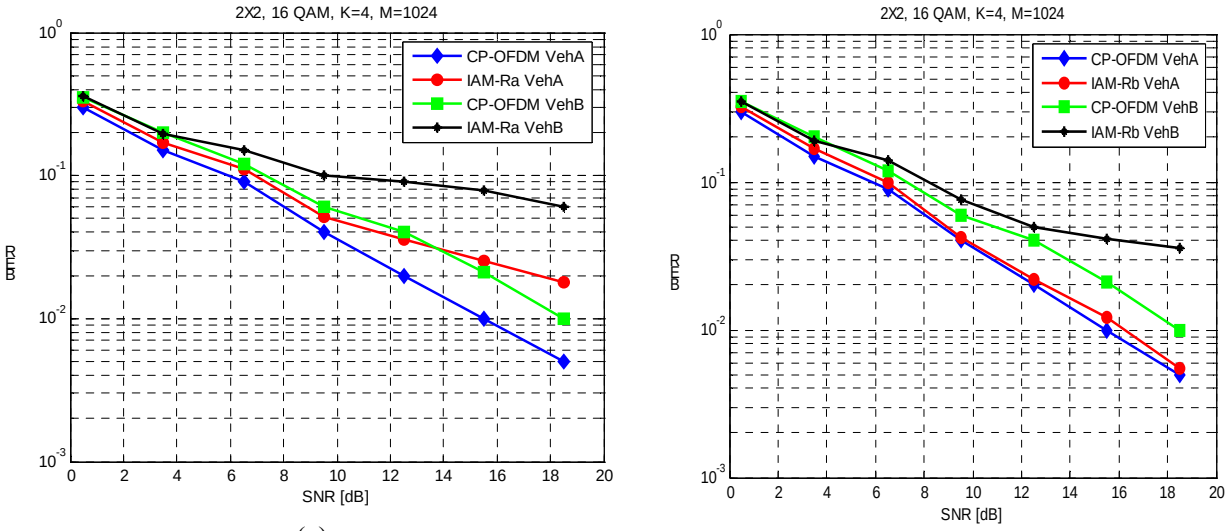

Figure 3.2.10. FBMC 2×2 performances vs CP-OFDM for Veh-A and Veh-B channels at 60 km/h, using adapted IAM method in DL-PUSC: (a) IAM-Ra; described scheme in Figure 3.2.9(a) for 2 antennas, (b) IAM-Rb; described scheme in Figure 3.2.9(b) for 2 antennas. PHYDYAS filter banks references; M=1024, K= 4, and 16 QAM modulation using ZF equalization.

In Figure 3.2.10, two variants of the adapted IAM-R scheme for 2 transmit antennas are presented. In the first case (Figure 3.2.10(a)), in IAM-Ra only 2 APC carriers are used to estimate the filter coefficients. We are dealing with a partial interference approximation as not all the interferences ($\Omega_{1,1}$) that affect the pilot $d^i_{k,n}$ could be estimated. The used values at [$d^i_{k,\,n-1}$ $d^i_{k,n}$ $d^i_{k,\,n+1}$] are [0 $d^i_{k,n}$ 0], with $d^i_{k,n} = \pm 1$ following the same alternation as in SISO systems [5].

It can be observed that the "IAM-Ra" scheme in Figure 3.2.10(a) performs similarly to CP-OFDM at sufficiently low SNR values, for SNR's lower than 8 dB in the case of a Veh-A channel, and lower

than 5 dB in the case of a Veh-B channel. Note that the error floor of IAM at high SNR's is observed as in SISO systems, due to the unavoidable intrinsic interference, which shows up at the weak noise regime.

However, it can be seen that a better result is achieved in Figure 3.2.10(b) "IAM-Rb" due to the use of more APC carriers, namely 4 aided pilots. For a Veh-A channel, very similar performance in terms of BER is achieved using the FBMC and the CP-OFDM schemes. The CP-OFDM scheme performs around ½ dB better than FBMC. For channels of higher frequency selectivity as the Veh-B, FBMC performs similarly with CP-OFDM up to an SNR of 12 dB. For higher values of SNR, CP-OFDM clearly outperforms the FBMC. The used values at $d^i_{k,n-1}$,and $d^i_{k,n+1}$ is 0 with $[d^i_{k+1,n}\ d^i_{k,n}\ d^i_{k-1,n}]$ following the same $\{\pm 1\}$ alternation as in [5]. Note that, still not all the interferences ($\Omega_{1,1}$) that affect the pilot $d^i_{k,n}$ could be estimated but almost the largest interference weights caused by the PHYDYAS filter bank contributions.

3.2.2.4 FBMC channel estimation using scattered pilots

Usually orthogonal pilot sequences are used to transmit over each of the N_t antennas in CP-OFDM systems. Using such pilot sequence it is possible to recover the channel coefficients for each pair of receive and transmit antenna. As for MIMO CP-OFDM systems, it is possible to choose orthogonal pilot sequences in the form $[P_1, P_2]$ over antenna # 1, and $[P'_1, P'_2]$ over antenna # 2 [11]. The assumption of constant channel over 2 consecutive symbols is fulfilled in the FBMC/OQAM. Adapting the proposed orthogonal pilot sequences in [11] to PHYDYAS FBMC specifications, we start from the equivalent DL-PUSC pilot pattern for 2 antennas at the transmitter in Figure 3.2.5(a), and we propose an adapted pilot structure in Figure 3.2.11(a).

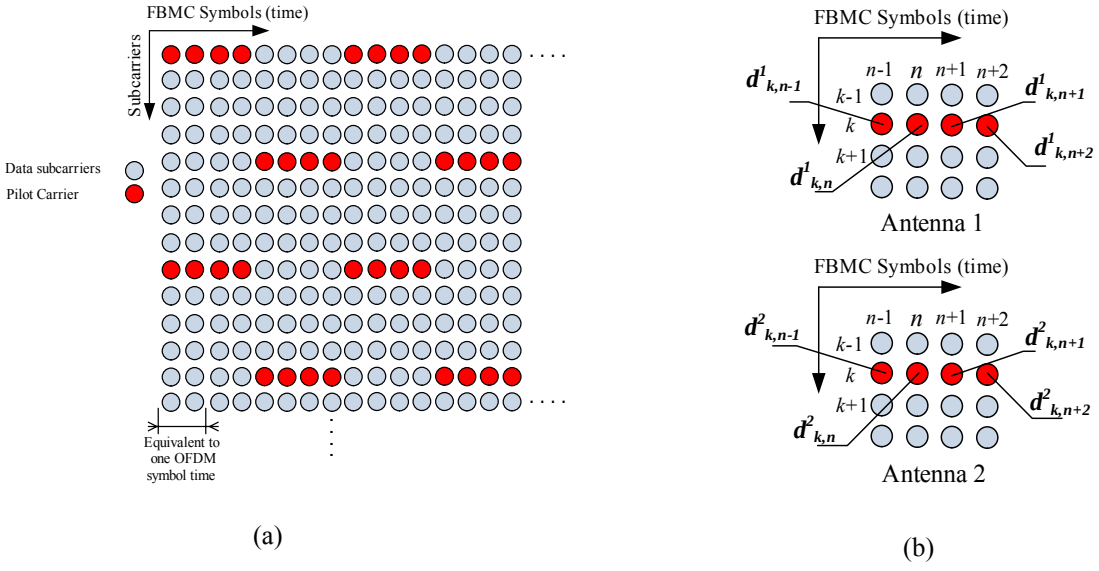

Figure 3.2.11: Simplified orthogonal pilot sequence in FBMC MIMO system with 2 transmit antennas: (a) general structure, (b) input pilots for each antenna.

Using the depicted scattered pilots in Figure 3.2.11, and using the PHYDYAS filter parameters in [5] we have assumed that the channel is quasi-static at least over four consecutive FBMC time symbols. The main objective as in [11] is to cancel the interference generated by the neighbouring symbols in Figure 3.2.11. First the orthogonality among the pilot sequences over the antennas could be created

by setting one of the pilots to zero. Secondly the interference is compensated by setting the value of one of the neighbours to the total of the intrinsic interference.

The cancellation of the interference is performed in two steps. First the $d^{i}_{k,n-1}$ symbols are determined to cancel the interference over the (k,n) position. Then the $d^{i}_{k,n+2}$ symbols are determined to cancel the interference over the *(k,n+1)* position. In Figure 3.2.11, it can be seen that $d^{i}_{k,n+2}$ is placed at position $(k, n+2)$ so by modifying the $d^{i}_{k,n+2}$ values does not generate interference over the (k, n) position (*same approach with that considered in subsection 3.2.2.2*). As a consequence this simplified 2-steps algorithm allows to cancel the intrinsic FBMC interference over both (k,n) and $(k,n+1)$ time-frequency positions. The values of $d^{2}_{k,n}$ and $d^{1}_{k,n+1}$ are fixed to 0. Note that this scattered pilot scheme in Figure 3.2.11 could be considered as a special case of the auxiliary antenna pilots scheme described in Figure 3.2.7.

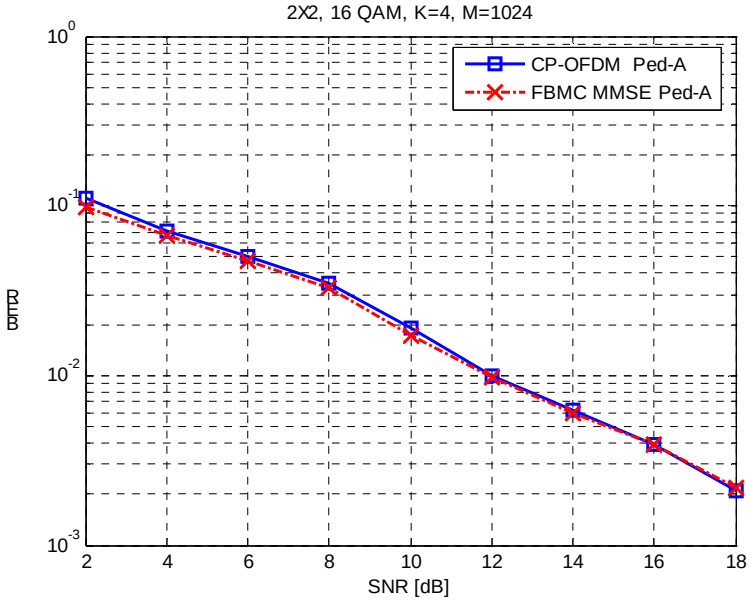

Figure 3.2.12: CP-OFDM and PHYDYAS FBMC comparison in 2x2 SDM case over Ped-A channel with non iterative MMSE receiver.

For the MIMO case, we compared the non iterative MMSE receiver performance in Figure 3.2.12 using Ped-A channel. For pedestrian channels (type A at 3 km/h), the FBMC performances is very similar to that of CP-OFDM. Due to the very low variability of this channel, the assumption of having 4 FBMC time symbols makes sense as the channel is quasi invariant. In the case of higher frequency selectivity channels, as the Veh-A/B, additional degradation in MIMO can occur in FBMC due the assumption of a constant channel over the symbols plus their first order neighbours.

3.3 Channel tracking

For system deployments which consider scenarios accounting for a certain degree of user mobility, the coherence time of typical channels is such that the channel coefficients cannot be longer assumed to be fixed for the purposes of system setup and symbol detection. If some partial statistical information about the channel is available, the frame-by-frame independent estimation of the channel can be improved by providing the system with specific channel tracking capabilities. Based on the presumed knowledge about the evolution in time of the wireless channel, the training pilots allocated for conventional estimation operation can be used to provide a sequential refinement of the channel estimate based on the Kalman filter recursion. In this subsection, details on the application of the Kalman recursion to a MIMO-FBMC system are described and first numerical simulation are provided.

Consider the conventional description of a mobile wireless channel in terms of the impulse response

$$h(t,\tau)=\sum_{p=0}^{P-1} c_p(t)\,\delta(\tau-\tau_p), \tag{3.3.1}$$

where P is the number of channel multipaths, and $c_p(t)$ and τ_p denote the complex gain and the delay of the pth path, respectively. The frequency response at time t is given by

$$H(t,f)=\sum_{p=0}^{P-1} c_p(t)\exp(-\mathrm{j}2\pi f\tau_p).$$

As a function of t and τ, the channel impulse response in (3.3.1) characterizes the amount of dispersion in time and frequency due to the delay spread and the time variability, respectively, of a given (frequency- and time-selective) fading channel.

Consider now the transmission of a baseband FBMC signal over M subcarriers and an ideal non-dispersive, noise-free channel, i.e.,

$$s(t)=\sum_{k=0}^{K-1}\sum_{n\in\mathbb{Z}} d_{k,n}\,p_{k,n}(t),$$

where

$$p_{k,n}(t)=\mathrm{j}^{k+n}(-1)^{kn}\exp\left(\mathrm{j}2\pi k\left(\Delta f t-\frac{L_p-1}{2M}\right)\right)p\left(t-n\frac{T}{2}\right),$$

with $p(t)$ being the impulse response of the L_p-tap prototype filter and T, the signaling interval, is the inverse of the subcarrier spacing Δf. In particular, L_pT is the length or time duration of the prototype and the FBMC system is such that $L_p=KM$, with $K=4$.

In a realistic scenario, the FBMC signal is transmitted over a noisy channel with impulse response given in (3.3.1) and noise contribution denoted here by $\eta(t)$. Then, the baseband received signal obtained after convolution with the channel impulse response can be expressed as [6]

$$r(t)=\sum_{k=0}^{M-1}\sum_{n\in\mathbb{Z}} d_{k,n}\int_0^{\Delta} h(t,\tau)\,p_{k,n}(t-\tau)\,d\tau+n(t), \tag{3.3.2}$$

where ✌ is the maximum delay spread. In the following, we assume that:

1) the channel can be considered to be flat at each subcarrier, which means that $1/(L_pT)$ is less than the coherence bandwidth of the channel $B_c=1/(2\Delta)$, and
2) the channel is constant over the duration of the prototype filter, or the prototype function is well-localized in the time-frequency plane.

Then, according to Assumption 1, the prototype function has relatively low variations in time over the interval $[0,\Delta]$, i.e., $p_{k,n}(t-\tau)\approx p_{k,n}(t)$. Therefore, (3.3.2) can be approximated as

$$r(t)=\sum_{k=0}^{M-1}\sum_{n\in\mathbb{Z}} d_{k,n}\,p_{k,n}(t)\,H_k(t)+n(t),$$

where

$$H_k(t)=\int_0^{\Delta} h(t,\tau)\exp(-\mathrm{j}2\pi k\Delta f\tau)\,d\tau.$$

On the other hand, according to Assumption 2, $H_k(t)\approx H_{k,n}(t)$, so that we finally can write

$$r(t) = \sum_{k=0}^{M-1} \sum_{n \in \mathbb{Z}} d_{k,n} p_{k,n}(t) H_{k,n}(t) + n(t).$$

Indeed, Assumptions 1 and 2 can be regarded as realistic in a practical WiMAX system, where the symbol duration is equal to [33] $72\mu s$ (fixed) or $48\mu s$ (mobile), and the minimum coherence bandwidth is equal to 0.1 MHz (center 9.1 GHz) and 3 MHz (center 5.3 GHz). Moreover, with a WiMAX characteristic minimum coherence time of 2ms (100 kmph), the channel cannot be considered to be fixed during the total duration of the frame, equal to 5 ms. Thus, under the previous assumptions, and assuming that the channel frequency response is constant over a sufficiently large number of subcarriers, demodulation over the k th subcarrier and the n th symbol period yields

$$\tilde{y}_{k,n} = H_{k,n}\left(d_{k,n} + ju_{k,n}\right) + \eta_{k,n},$$

where the noise contribution $\eta_{k,n}$ is correspondingly defined, and the term $ju_{k,n}$ represents a purely imaginary interference component that is intrinsic to the properties of the prototype function (see [5]). Based on the notion of *virtually transmitted symbols*, we define $\tilde{x}_{k,n} = d_{k,n} + ju_{k,n}$, and write

$$\tilde{y}_{k,n} = H_{k,n}\tilde{x}_{k,n} + \eta_{k,n}.$$

Note that for prototype functions that are sufficiently well-localized in the time-frequency plane, the intrinsic interference term $ju_{k,n}$ can be assumed to only depend on the neighbors of the symbol $d_{k,n}$ up to a certain, particularly low order, and the *auxiliary pilot* scheme reported previously can be employed to yield $u_{k,n} = 0$.

Consider now the overall system operation. On a frame-by-frame basis, and even at a finer scale as noted above for speeds of around 100kmph, the channel cannot be further considered to be fixed. Rather than estimating the channel independently in each frame, knowledge about the evolution in time of the wireless channel can be used to provide improved estimation and tracking capabilities of a WiMAX system. To that end, a sequential refinement of the estimation procedure based on a Kalman filter recursion for the purposes of channel tracking over time is presented next. In the sequel, the above channel estimation setting is considered. Furthermore, we assume that a number of scattered pilots are distributed over each frame such that the intrinsic interference is set to zero, or, otherwise, an estimate of it is provided.

3.3.1 Kalman filter

In the following, we describe the state-space model for frequency-domain estimation and tracking of the MIMO-FBMC channel[4]. Here, the wide-sense stationary uncorrelated scattering (WSSUS) channel model is considered for the channel impulse response corresponding to each transmit antenna. In order to describe the dynamics of the time-variant channel over successively transmitted WiMAX frames, a first-order auto-regressive (AR) model is applied. Accordingly, the state equation can be written for the ζ th iteration as

$$\mathbf{h}[\zeta] = \mathbf{A}_h[\zeta]\mathbf{h}[\zeta - 1] + \mathbf{v}[\zeta],$$

where $\mathbf{h}[\zeta]$ is a column vector containing the coefficients of the channel during the ζ th time interval at all the positions of the time-subcarrier tableaux where a transmitted pilot has been allocated. We remark that the time interval considered for channel update purposes solely depends on the dynamics of the latter and need not correspond to the frame duration. On the contrary, a finer temporal scale can be considered if the channel varies faster than the frame duration, as well as a coarser one if several frames may be assumed to be transmitted before the channel characteristics change.

[4]channel tracking in the time-domain has been reported in [45] to perform identically if the same channel dynamics are considered.

From the Jakes fading model, the autocorrelation of the k th subcarrier gain is

$$\mathsf{E}\left[H_k(t)H_k^*(t-s)\right] = J_0\left(2\pi f_d s T_{\text{int}erval}\right), \tag{3.3.3}$$

where $f_d = \upsilon/\lambda$ is the maximum Doppler frequency (υ is the terminal velocity and λ is the carrier wavelength), $T_{\text{int}erval}$ is the update time interval duration and $J_0(\cdot)$ is the zero-order Bessel function of the first kind. In the case of a first-order AR model, the transition matrix is given by a scaled identity matrix as $\mathbf{A}_h[\zeta] = a\mathbf{I}_M$, where a is obtained from the Jakes Doppler spectrum directly as (3.3.3). Auto-regressive models of higher order for the dynamics of multiple antenna multicarrier channels can also be considered (see discussion in [46]). In the latter case, the model parameters can be found by solving the Yule-Walker equation obtained from the Jakes Doppler spectrum. In general, note that the spectral norm of $\mathbf{A}_h[\zeta]$ is required to be smaller than one in order to ensure the stability of the system. Finally, the parameters of the state dynamics equation, especially the state transition matrix and covariance matrices of the noise and the channel, can also be estimated using the available samples of the measured channel (see, e.g., [47][48]). The state noise process $\mathbf{v}[\zeta]$ is assumed to be Gaussian and independent of the channel.

On the other hand, the measurement equation can be written as

$$\mathbf{r}[\zeta] = \mathbf{A}_c[\zeta]\mathbf{h}[\zeta] + \mathbf{w}[\zeta], \tag{3.3.4}$$

where $\mathbf{A}_c[\zeta]$ is a diagonal matrix containing the value of the pilots at the respective locations and the measurement noise process $\mathbf{w}[\zeta]$ is also assumed to be Gaussian and independent of the channel.

The previous state-space model can be used for channel tracking on single-input single-output (SISO) links. In particular, during the entire update time interval, for channel tracking purposes we assume from the discussion above that $[\tilde{\mathbf{y}}[\zeta]]_k = \tilde{y}_k = \tilde{y}_{k,n}$, as well as $[\mathbf{h}[\zeta]]_k = H_k = H_{k,n}$. Equivalently, the measurement noise vector $\eta[\zeta]$ is such that, for each ζ, its entries model the noise contribution over the subcarriers, namely, $[\eta[\zeta]]_k, k = 0,1,...,M-1$.

A straightforward extension is obtained for a single-input multiple-output (SIMO) link by considering the MN_r-dimensional vector

$$\mathbf{r}[\zeta] = \left[\mathbf{r}^{(1)}[\zeta]^T, \ldots, \mathbf{r}^{(N_r)}[\zeta]^T\right]^T, \tag{3.3.5}$$

where $\mathbf{r}^{(i)}[\zeta]$ is equivalently defined as the measurement corresponding to the i th sensor element of the antenna array at the receiver side. In order to account for system configurations with multiple antennas also at the transmitter side, consider the following model

$$\mathbf{r}^{(i)}[\zeta] = \sum_{j=1}^{N_t} \mathbf{A}_c^{(j)}[\zeta]\mathbf{h}^{(i,j)}[\zeta] + \mathbf{w}^{(i)}[\zeta], \quad i = 1, \ldots, N_r, \tag{3.3.6}$$

where $\mathbf{h}^{(i,j)}[\zeta]$ is an M -dimensional vector with the frequency response of the channel between the j th transmit antenna and the i th receive antenna, $\mathbf{A}_c^{(j)}$ is a diagonal matrix used with the pilot transmitted from the j th transmit antenna, and $\mathbf{w}^{(i)}[\zeta]$ is the measurement noise at the i th antenna. Morever, define the MN_t -dimensional vector $\mathbf{h}^{(i)}[\zeta] = \left[\mathbf{h}^{(i,1)}[\zeta]^T, \ldots, \mathbf{h}^{(i,N_t)}[\zeta]^T\right]^T$ and the $M \times MN_t$ matrix

$$\mathbf{\Lambda}_c[\zeta] = \left[\mathbf{A}_c^{(1)}[\zeta], \ldots, \mathbf{A}_c^{(N_t)}[\zeta]\right].$$

Then, we can write $\mathbf{r}^{(i)}[\zeta] = \sum_{j=1}^{N_t} \mathbf{A}_c^{(j)}[\zeta]\mathbf{h}^{(i,j)}[\zeta] + \mathbf{w}^{(i)}[\zeta], \quad i = 1,\ldots,N_r,$ (3.3.6) as

$$\mathbf{r}^{(i)}[\zeta] = \mathbf{\Lambda}_c[\zeta]\mathbf{h}^{(i)}[\zeta] + \mathbf{w}^{(i)}[\zeta], \quad i = 1,\ldots,N_r.$$

By stacking the measurements corresponding to all receive antennas as in (3.3.5), upon definition of the $MN_r \times MN_rN_t$ matrix

$$\mathbf{A}_c[\zeta] = \mathbf{I}_{N_t} \otimes \mathbf{\Lambda}_c[\zeta],$$

and the MN_rN_t-dimensional vector $\mathbf{h}[\zeta] = \left[\mathbf{h}^{(1)}[\zeta]^T,\ldots,\mathbf{h}^{(N_r)}[\zeta]^T\right]^T$, we can consider the tracking of a multiple-input multiple-output (MIMO) channel by directly using the model in (3.3.4).

For the general model in (3.3.4), based on the initial knowledge of the channel $\mathbf{h}[0]$ and its covariance matrix $\mathbf{P}[0]$, further channel estimates can be obtained by the Kalman filter recursion as follows:

1) State estimate prediction:

$$\mathbf{h}[\zeta+1|\zeta] = \mathbf{A}_h[\zeta]\mathbf{h}[\zeta|\zeta].$$

2) Error covariance update:

$$\mathbf{P}[\zeta+1|\zeta] = \mathbf{A}_h[\zeta]\mathbf{P}[\zeta|\zeta]\mathbf{A}_h[\zeta]^H + \mathbf{Q}[\zeta].$$

3) Kalman gain computation:

$$\mathbf{K}[\zeta+1] = \mathbf{P}[\zeta+1|\zeta]\mathbf{A}_c[\zeta+1]^H\left(\mathbf{A}_c[\zeta+1]\mathbf{P}[\zeta+1|\zeta]\mathbf{A}_c[\zeta+1]^H + \mathbf{R}[\zeta+1]\right)^{-1}.$$

4) Error covariance measurement update:

$$\mathbf{P}[\zeta+1|\zeta+1] = \left(\mathbf{I} - \mathbf{K}[\zeta+1]\mathbf{A}_c[\zeta+1]\right)\mathbf{P}[\zeta+1|\zeta].$$

5) State estimate measurement update:

$$\mathbf{h}[\zeta+1|\zeta+1] = \mathbf{h}[\zeta+1|\zeta] + \mathbf{K}[\zeta+1]\left(\mathbf{r}[\zeta+1] - \mathbf{A}_c[\zeta+1]\mathbf{h}[\zeta+1|\zeta]\right).$$

In the previous equations describing the Kalman recursion, $\mathbf{Q}[\zeta]$ and $\mathbf{R}[\zeta]$ are the covariance matrices of the state noise $\mathbf{v}[\zeta]$ and the measurement noise $\mathbf{w}[\zeta]$, respectively. In the state equation for the evolution of the multipath channel samples, the different taps are assumed to model mutually independent Rayleigh fading. Furthermore, the correlation between two consecutive samples of all taps is assumed to be the same and equal to a. In particular, as mentioned above, $\mathbf{A}_h[\zeta] = \mathbf{A}_h = a\mathbf{I}_M$. Moreover, if a constant training pilot sequence is transmited over the frames, then also $\mathbf{A}_c[\zeta] = \mathbf{A}_c$. Under the previous assumptions, the state noise covariance matrix is given by $\mathbf{Q}[\zeta] = \left(1-a^2\right)\mathbf{F}\mathbf{F}^H$, where $\mathbf{F}$ is an appropriately dimensioned Fourier matrix (see [45] for details).

Channel tracking on a MISO link has been numerically simulated for demonstration purposes. Results obtained by applying a Kalman filter recursion based on a temporal evolution model for the channel are compared with conventional least-squares (LS) channel estimation performed individually frame-by-frame (here, the frame duration has been considered as update time interval). Uncorrelated channels have been assumed, so that an extension to the MIMO case is straightforward by considering different parallel schemes for each antenna at the receiver side. Channel tracking on a MISO link has been numerically simulated for demonstration purposes. Results obtained by applying a Kalman filter recursion based on a temporal evolution model for the channel are compared with conventional least-squares (LS) channel estimation performed individually frame-by-frame. Uncorrelated channels have been assumed, so that an extension to the MIMO case is straightforward by considering different parallel schemes for each antenna at the receiver side.

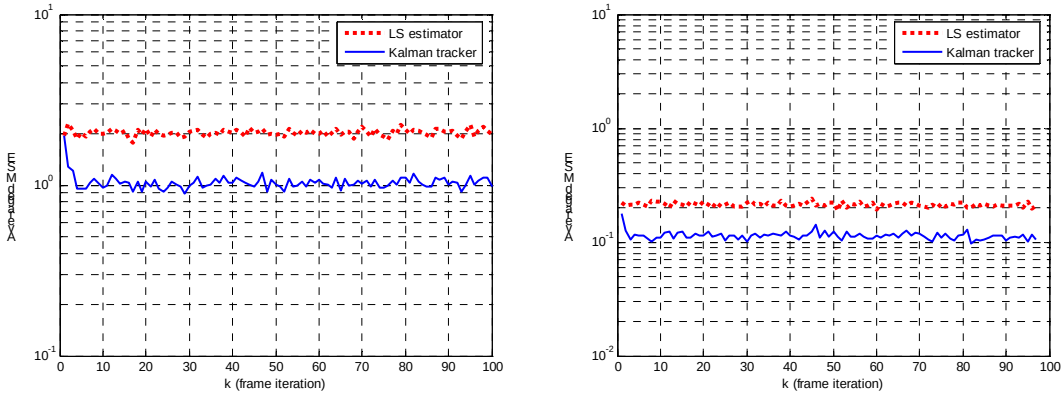

(a) (b)

Figure 3.3.1 Comparison of LS estimator and Kalman tracker on a MISO link. (a) SNR=0 dB, (b) SNR=10 dB

Regarding the implementation of the Kalman recursion, the associated computational complexity obviously depends on the rate of the channel coefficients update. This rate is determined by the time variability of the channel, so that the benefits from Kalman channel tracking are obtained at low computational costs in limited mobility scenarios. Moreover, it is interesting to note that for a certain degree of uncorrelation between channels, the channel tracking operation can be performed independently for the different antennas. Hence, in this case the computational cost is mainly due to the number of training or pilot subcarriers considered for filtering/tracking purposes.

3.4 Memory preloading

As far as initialization is concerned, the issue with the FBMC approach is the impulse response of the prototype filter which imposes a transition phase. We consider the system has 128 subcarriers and the synthesis filter bank (SFB) in the transmitter generates a real signal, which implies that 256 subcarriers are used altogether, to account for both positive and negative frequencies. The prototype filter length is $L_p = 1025$ and the symbol overlapping factor is $K = 4$. The impulse response of the prototype filter shown in Figure 3.4.1(a) provides the coefficients of the filter bank.

A crucial feature for the present topic is that the frequency response of the prototype filter is zero at the frequencies which are integer multiples of the sub-channel spacing, as shown in Figure 3.4.1(b). With this feature, at their center frequencies, the filters in the bank are independent.

The delay of the linear phase prototype filter is $\left(L_p - 1\right)/2 = 512$, which corresponds to 2 multicarrier symbols. When data are applied to the system, a transition phase of 2 symbols is introduced, as illustrated in Figure 3.4.2. The prototype filter transition phase for the preamble can be skipped and the transition phase for the data can be exploited to improve the estimations of the transmission parameters [39].

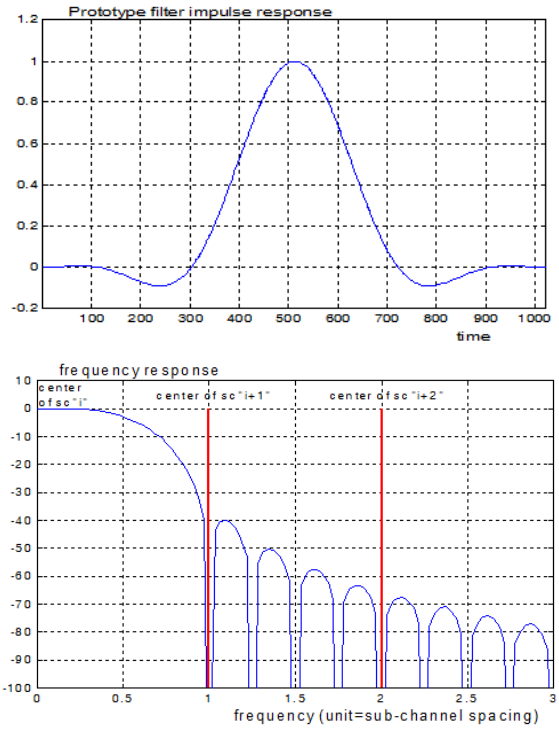

Figure 3.4.1 An example of prototype filter impulse response (a) and its frequency response and positioning of neighboring sub-channels (b)

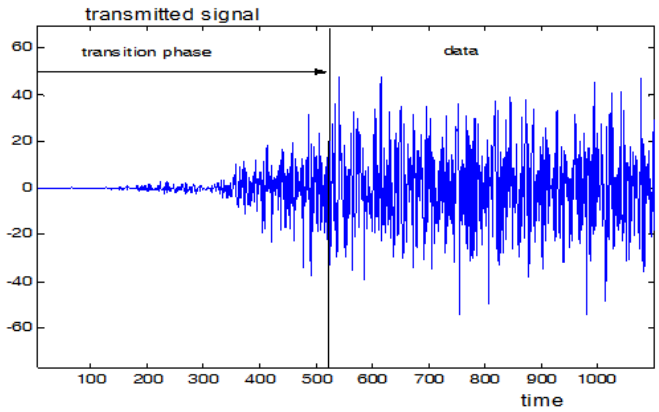

Figure 3.4.2. Transition phase in the transmitted signal

The SFB in the transmitter consists of the inverse FFT and the polyphase network (PPN), as shown in
Figure 3.4.3. The IFFT receives the set of data to be transmitted at each symbol and its output is propagated in the memories of the PPN at the symbol rate. The SFB output, s(m), is fed to the channel.

Now, if the same set of data is repeated at the input of the SFB, the same set of samples appears repeatedly at the output of the inverse FFT and it is stored in the memories of the polyphase network. Then, all the memories of the polyphase network contain the same set of samples. In these conditions, a periodic signal is generated by the SFB and fed to the channel. At the output of the channel, the received signal is periodic and the period is the multicarrier symbol duration. The structure of the analysis filter bank (AFB) in the receiver is shown in Figure 3.4.4. The received signal r(m) is fed to the memories of the PPN, which contain the same set of samples each. From the content of these memories, the receiver restores the transmitted data.

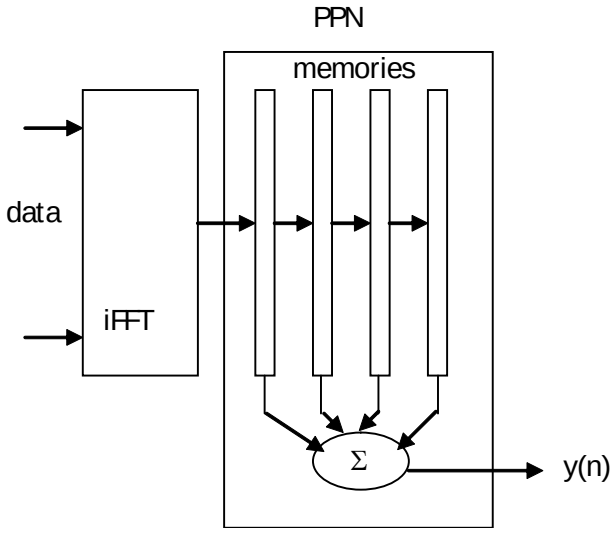

Figure 3.4.3. Structure of the SFB in the transmitter

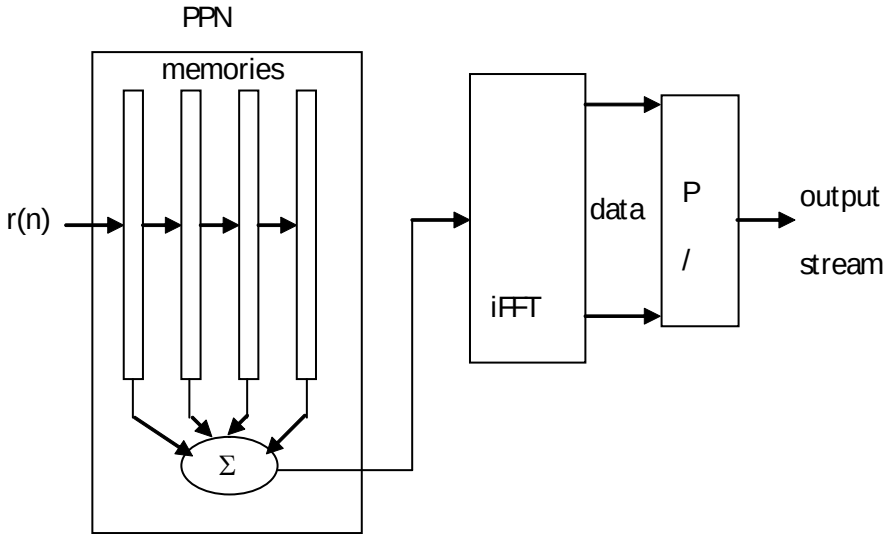

Figure 3.4.4. Structure of the AFB in the receiver

Now, if a periodic signal y(n) is to be generated without any transition phase, it is sufficient to preload the memories of the synthesis filter bank with the set of samples produced by the inverse FFT. Then, to demodulate the signal at the output of the channel without the transition phase, it is sufficient to fill the AFB memories with the first received set of samples corresponding to the symbol length. With this preloading technique, implemented in both the transmitter and the receiver, there is no transition phase for the preamble.

As concerns the data, they are not periodic and the transition phase must be kept if the highest level of performance is required. However, this transition phase can be included in the preamble.

3.4.1 Preloading with MIMO

In MIMO systems, a receiver is connected to several transmitters and the corresponding channel responses must be estimated. The case of 2 transmitters is shown in Figure 3.4.5.

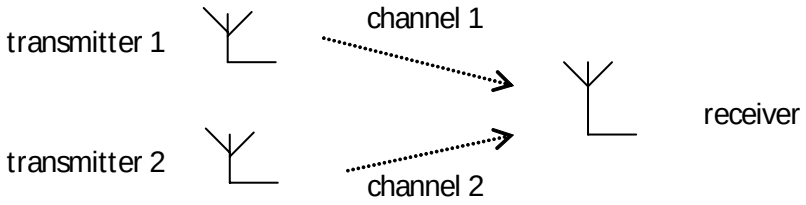

Figure 3.4.5. MIMO system (2×1)

With the memory preloading technique, it is possible to perform the measurements of two channels simultaneously, invoking the periodicity of the signals.

The frequency responses of adjacent filters in the bank are shown in Figure 3.4.6. At the center frequency of filter i, the responses of neighbouring filters $i-1$ and $i+1$ are null, as pointed out at the end of Section 1. Therefore, in the presence of constant signals at the synthesis filter bank inputs, there is no interference between the subcarriers. Then, it is possible to use the subcarriers with odd indices to estimate one of the 2 channels and the subcarriers with even indices to estimate the other channel. Finally, the channel responses at all the sub-channel center frequencies can be obtained through interpolation.

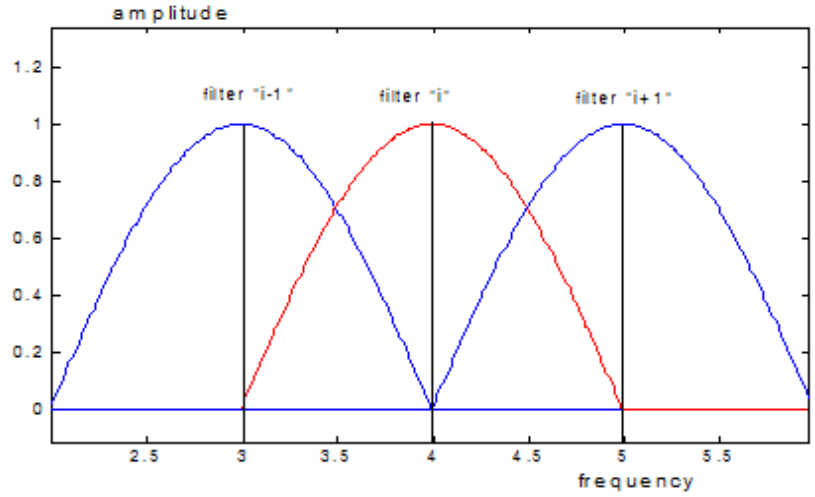

Figure 3.4.6. Frequency responses of neighbouring filters in the filter bank

The process is illustrated in Figure 3.4.7. In the simulation, two different channels with deep fading are used and the coefficient vectors are

$$\mathbf{h}_1 = [1 \quad 1 \quad 0.5 \quad -0.025 \quad 0.285]$$

$$\mathbf{h}_2 = [1 \quad -1 \quad 0.5 \quad 0.025 \quad 0.285]$$

At the output of the AFB in the receiver, single coefficient equalization is performed, using the FFT of impulse responses $\mathbf{h}_1$ and $\mathbf{h}_2$ for the subcarriers with odd and even indices respectively.

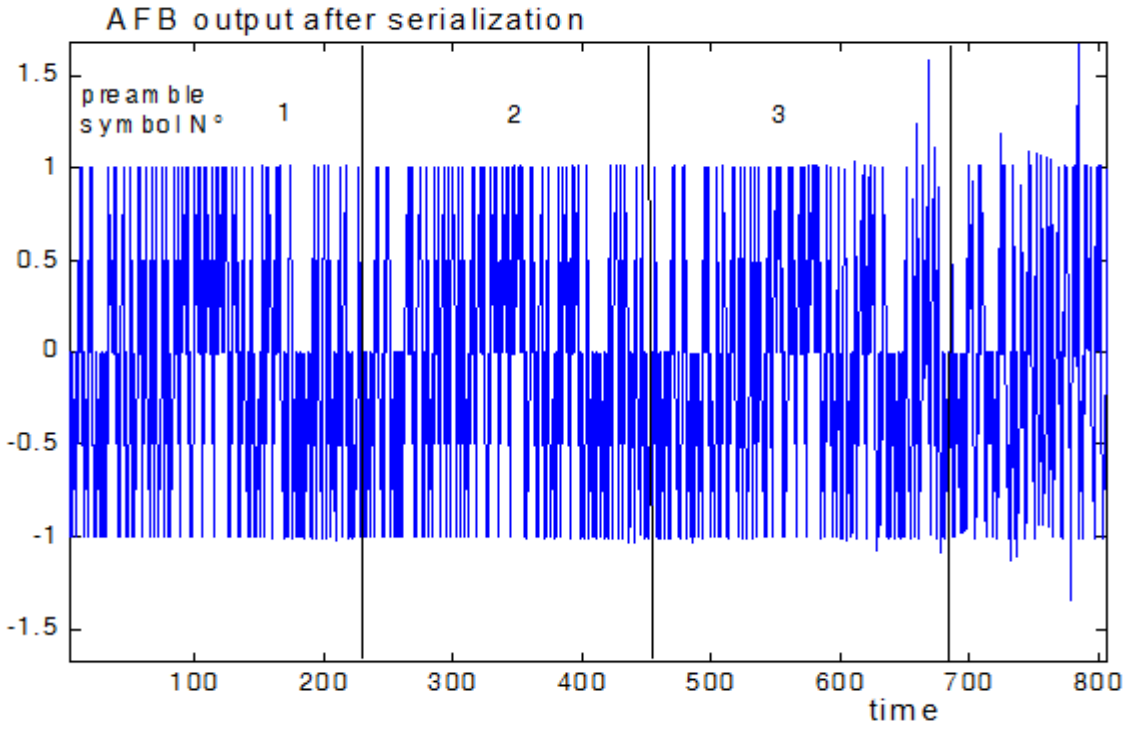

Figure 3.4.7. MIMO system (2x1) with frequency interleaved transmission

Figure 3.4.7. MIMO system (2×1) with frequency interleaved transmission

Clearly, the measurement is accurate, for the first symbol of the preamble.

The extension to MIMO systems with more transmitters can be achieved with a similar scheme. For example, in a 4×1 system, 4 interleaved groups of subcarriers can be allocated to the 4 transmitted signals. Of course, in that case, 3 frequency points have to be interpolated between two measured values.

If measurement of the channels at all the center frequencies is required, then multiple preloading can be implemented with the corresponding increase in the duration of the initialization phase.

Note that, in a MIMO system, the transmitted signals are synchronized. The time offset and the frequency offset are the same for all the received signals.

4 Equalization

Once the channel matrix has been measured, the sub-channel equalizer coefficients must be determined. A straightforward and simple approach for use at the beginning of a burst is the extension to the multiantenna case of the technique developed for the single antenna case and described in documents D2.1 and D2.2. Good results have been obtained with this technique for the single antenna case and equally good results can be expected in the MIMO case. The concept is presented below.

In the multiantenna case, the channel measurement process delivers the matrix **C**(i) for the sub-channel with index "i". Then, the procedure to calculate the coefficients is depicted in Figure 4.1, which is just a modified version of Figure 3.14 in document D2.2.

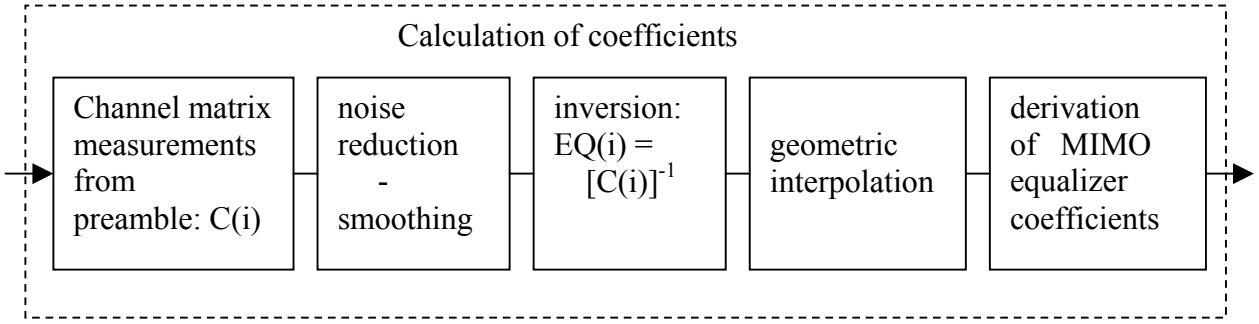

Figure 4.1. Procedure to compute the MIMO equalizer coefficients at the beginning of the burst

The matrix **C**(i) is assumed to be square and invertible. In case of a single coefficient, the equalizer matrix **EQ**(i) is just the inverse of the channel matrix **C**(i). Since the measurements have been performed in the center frequency of the sub-channels, equalization is achieved at these frequencies. Now, if more coefficients are envisaged, equalization can be achieved at more frequencies in the sub-channels. Interpolation in the complex frequency domain provides the intermediate values and the coefficients for each branch of each equalizer are obtained through inverse FFT or any equivalent method.

This concept has been validated and its performance is compared to the general equalization techniques which are presented in this section, with their performance in the MIMO-FBMC context. First, in section 4.1, the equalization for MIMO-FBMC using spatial multiplexing is studied. In addition to the simple one-tap MIMO-OFDM equalizer applied to MIMO-FBMC, we consider the MMSE, successive interference cancellation (SIC), ordered SIC (OSIC) and two stage OSIC (TS-OSIC) equalizers. Next, in section 4.2, we analyze diversity reception with complex finite impulse response (CFIR) subcarrier equalizers that are designed using frequency sampling technique according to maximal ratio combining (MRC) principle, In section 4.3, the linear decision-feedback (L-DF) equalizer and the widely-linear decision-feedback (WL-DF) equalizer are applied to MIMO FBMC/OQAM systems.

4.1 MMSE MIMO-FBMC equalization

Spatial multiplexing is considered here, which means that we use several antennas at both sides of the communication link and each antenna sends its own information, independent from the other antennas. Moreover, we assume that the MIMO channel is time invariant, or at least approximately constant on the duration of an estimation block. We denote by $h_{ij}[m]$ the mth tap of the channel impulse response (CIR) between the ith transmit antenna and the jth receive antenna, i.e. $\mathbf{h}_{ij} = [h_{ij}[0], h_{ij}[1], \ldots, h_{ij}[\nu]]$. We assume that all channels have the same length $\nu + 1$. Moreover, let $\mathbf{q}_{k\ell}^{ij} = [q_{k\ell}^{ij}[0], q_{k\ell}^{ij}[1], \cdots, q_{k\ell}^{ij}[L_q]]$, $L_q = \lfloor \frac{2L+\nu}{M/2} \rfloor$, represent the impulse response resulting from the convolution between $g_\ell[m]$, $h_{ij}[m]$ and $f_k[m]$ downsampled by the factor $\frac{M}{2}$, i.e.

$$q_{k\ell}^{ij}[n] = (g_\ell * h_{ij} * f_k)[m]_{\downarrow \frac{M}{2}} \tag{4.1.1}$$

where $g_k[m]$ and $f_k[m]$ are the synthesis and analysis filters for the kth subchannel, respectively. It is the impulse response from a symbol on transmit antenna i and subchannel ℓ to the received output on antenna j and subchannel k.

The received signal at the output of the AFB for the kth subchannel of the jth receive antenna can thus be expressed as

$$y_k^j[n] = \sum_{i=1}^{N_t} \sum_{t=0}^{M-1} (q_{kt}^{ij}[n] \star v_t^i[n]) + \eta_k^j[n],\ j = 0, ..., N_r \text{ and } k = 0, ..., M-1 \qquad (4.1.2)$$

where $v_t^i[n] = d_k^i[n]\theta_k[n]$ with $\theta_k[n] = j^{k+n}$ and $d_k^i[n]$ are the real data symbols transmitted on the kth subcarrier over the ith transmit antenna, obtained by converting the real and imaginary parts of the complex input symbols $a_k^i[l]$ into real data symbols. Note that the rate of $a_k^i[l]$ is $\frac{1}{T}$ whereas that of $d_k^i[n]$ is $\frac{2}{T}$, where $T = \frac{1}{\Delta f}$ and Δf is the subcarrier spacing. $\eta_k^j[n]$ represents the additive white noise $\eta^j[n]$ at the jth receive antenna, filtered by the analysis filter $f_k[m]$ and downsampled by a factor of $\frac{M}{2}$ as shown in Figure 1.3. It is given by

$$\eta_k^j[n] = \sum_{m=-\infty}^{\infty} \eta^j[m] f_k[n\tfrac{M}{2} - m]. \qquad (4.1.3)$$

We assume that the noise is spatially and temporally decorrelated and independent from the transmitted symbols, i.e.

$$E[\eta^i[m-\ell]\eta^j[m-\tau]^*] = \delta_{ij}\delta_{\ell\tau}\sigma_\eta^2 \quad \text{and} \quad E[v_k^i[n]\eta^j[m]^*] = 0$$

Given that, in FBMC systems, the interference in each subchannel comes mainly from the adjacent subchannels and the interference from the other subchannels can be neglected [52][13], $y_k^j[n]$ can be approximated by

$$y_k^j(n) \approx \sum_{i=1}^{N_t} \sum_{t=k-1}^{k+1} (q_{kt}^{ij}[n] \star v_t^i[n]) + \eta_k^j[n],\ j = 0, ..., N_r \text{ and } k = 0, ..., M-1 \qquad (4.1.4)$$

where for each receive antenna $j = 1,..., N_r$ and for each subchannel $k = 0, ..., N-1$, we only kept terms corresponding to the subchannel of interest, k, and directly adjacent subchannels $k-1$ and $k+1$.

In the case of frequency selective MIMO channels, the received signal at the output of each analysis filter of each receive antenna consists of a mixture of the signal of interest, inter-symbol interference (ISI) and inter-carrier interference (ICI) from all the transmit antennas. In order to recover the different streams of information sent on the different antennas and subchannels, an equalizer is necessary at the receiver. Here we are particularly interested in per-subchannel equalization. In order to compute the equalizers, it is easier to consider the matrix formulation. Stacking L_{eq} consecutive observations on a given subchannel and given receive antenna, where L_{eq} represents the equalizer length, (4.1.4) can be written in matrix notation as follows

$$\mathbf{y}_k^j[n] = \sum_{t=k-1}^{k+1} \mathbf{Q}_{kt}^j \mathbf{v}_t[n] + \mathbf{B}_k \eta^j[m] \qquad (4.1.5)$$

where $\mathbf{y}_k^j[n] = [y_k^j[n], y_k^j[n-1], ..., y_k^j[n-L_{eq}+1]]^T$ is the stacked received vector for antenna j and subchannel k, $\mathbf{v}_t[n] = [\mathbf{v}_t^1[n]^T, \mathbf{v}_t^2[n]^T, ..., \mathbf{v}_t^{N_t}[n]^T]^T$ is the vector of transmitted symbols with $\mathbf{v}_t^i[n] = [v_t^i[n], v_t^i[n-1], ..., v_t^i[n-L_q-L_{eq}+1]]^T$, $i = 1, ..., N_t$, and $\mathbf{Q}_{kt}^j = [\mathbf{Q}_{kt}^{1j}\ \mathbf{Q}_{kt}^{2j}\ \ldots\ \mathbf{Q}_{kt}^{N_t j}]$ is the stacked matrix containing all the convolution matrices $\mathbf{Q}_{kt}^{ij}$ of size $L_{eq} \times (L_q + L_{eq})$ constructed from the row vectors of impulse reponses $\mathbf{q}_{k\ell}^{ij} = [q_{k\ell}^{ij}[0], q_{k\ell}^{ij}[1], ..., q_{k\ell}^{ij}[L_q]]$. $\mathbf{Q}_{kt}^{ij}$ is given by

$$\mathbf{Q}_{kt}^{ij} = \begin{bmatrix} q_{kt}^{ij}[0] & q_{kt}^{ij}[1] & \cdots & q_{kt}^{ij}[L_q] & 0 & \cdots & 0 \\ 0 & q_{kt}^{ij}[0] & q_{kt}^{ij}[1] & \cdots & q_{kt}^{ij}[L_q] & \ddots & \vdots \\ \vdots & \ddots & \ddots & \ddots & & \ddots & 0 \\ 0 & \cdots & 0 & q_{kt}^{ij}[0] & q_{kt}^{ij}[1] & \cdots & q_{kt}^{ij}[L_q] \end{bmatrix} \quad (4.1.6)$$

$\eta^j[m]$ is the additive noise present at the input of the jth antenna and $\mathbf{B}_k$ is an $L_{eq} \times (L + (L_{eq} - 1)M/2)$ convolution matrix constructed from the cascade of $f_k[m]$ and $\downarrow \frac{M}{2}$ (see Figure 1.3). It is given by:

$$\mathbf{B}_k(i,(i-1)\frac{M}{2}+1:(i-1)\frac{M}{2}+L_p) = f_k(:), \quad i = 1,2,...,L_{eq}$$

4.1.1 Frequency domain equalizer

A simple one-tap MIMO-FBMC equalizer can be calculated as in the case of MIMO-OFDM, where the equalization is carried out in the frequency domain. In this case we suppose, for each subchannel, that the selective channel between each receive antenna and transmit antenna is reduced to a single tap. Therefore, for each subchannel the system can be considered as a MIMO flat fading channel and the equalizer is a simple matrix. Let H_k^{ij} denote the gain between the i th transmit antenna and the j th receive antenna for the kth subchannel, it is given by

$$H_k^{ij} = \sum_{m=0}^{\nu} h_{ij}[m] e^{-\frac{j2\pi km}{M}} \quad (4.1.7)$$

Let $\mathbf{H}_k = [H_k^{ij}]$, $i = 1,\cdots,N_t$ and $j = 1,\cdots,N_r$, denote the MIMO flat fading channel for subchannel k, i.e.

$$\mathbf{H}_k = \begin{bmatrix} H_k^{11} & H_k^{21} & \cdots & H_k^{N_t 1} \\ H_k^{12} & H_k^{22} & \cdots & H_k^{N_t 2} \\ \vdots & \vdots & \ddots & \vdots \\ H_k^{1N_r} & H_k^{2N_r} & \cdots & H_k^{N_t N_r} \end{bmatrix}$$

Now, as in MIMO-OFDM, the equalizer, $\mathbf{W}_k$, for the kth subchannel considering the MMSE criterion is given by

$$\mathbf{W}_{k-MMSE} = \mathbf{H}_k(\mathbf{H}_k\mathbf{H}_k^H + \frac{1}{\sigma_v^2}\mathbf{R}_{\eta\eta})^{-1} \quad (4.1.8)$$

where $\mathbf{R}_{\eta\eta} = \sigma_\eta^2 \mathbf{I}$ is the noise covariance matrix obtained using the fact that the noise, at the antenna inputs, is spatially decorrelated.

The ZF equalizer is obtained by letting the SNR tends to infinity in (4.1.8), which results in

$$\mathbf{W}_{k-ZF} = \mathbf{H}_k(\mathbf{H}_k\mathbf{H}_k^H)^{-1} \quad (4.1.9)$$

Finally the transmitted symbols on the kth subchannel are estimated by applying either the MMSE equalizer or ZF equalizer. In the case of the MMSE equalizer we have

$$\begin{bmatrix} \tilde{v}_k^1[n] \\ \tilde{v}_k^2[n] \\ \vdots \\ \tilde{v}_k^{N_t}[n] \end{bmatrix} = \mathbf{W}_{k-MMSE}^H \begin{bmatrix} y_k^1[n] \\ y_k^2[n] \\ \vdots \\ y_k^{N_r}[n] \end{bmatrix} \quad (4.1.10)$$

An estimation of the transmitted symbols $a_k^i[n]$ can easily be computed from $\tilde{v}_k^i[n]$ as can be seen in Figure 1.3, where $\tilde{v}_k^i[n]$ are passed through the OQAM demodulator. We have

$$\tilde{d}_k^i[n] = Re\{\theta_k[n]^* \tilde{v}_k^i[n]\} \tag{4.1.11}$$

and

$$\tilde{a}_k^i[l] = \tilde{d}_k^i[2l] + j\tilde{d}_k^i[2l+1] \tag{4.1.12}$$

Finally $\hat{a}_k^i[l]$ is obtained by taking a hard decision on $\tilde{a}_k^i[l]$.

This kind of equalizer is suitable for mildly selective MIMO channels, where for each subchannel the MIMO channel can be considered as flat. More selective channels however require more sophisticated methods.

4.1.2 MMSE MIMO-FBMC equalizer

As said before, for more selective channels, the frequency domain equalizer presented previously does not provide a satisfactory performance and hence more complex equalizers have to be considered. A common solution is to use the MMSE equalizer which we derive here for MIMO-FBMC using spatial multiplexing. We stack the vectors $\mathbf{y}_k^j[n]$, for the different receive antennas $j = 1, ..., N_r$, in $\mathbf{y}_k[n]$ and we get

$$\mathbf{y}_k[n] = \sum_{t=k-1}^{k+1} \mathbf{Q}_{kt}\mathbf{v}_t[n] + \overline{\mathbf{B}}_k\eta[m] \tag{4.1.13}$$

where $\mathbf{y}_k[n] = [\mathbf{y}_k^1[n]^T, \mathbf{y}_k^2[n]^T, ..., \mathbf{y}_k^{N_r}[n]^T]^T$, $\overline{\mathbf{B}}_k = diag[\mathbf{B}_k, \mathbf{B}_k, ..., \mathbf{B}_k]$, $\eta[m] = [\eta^1[m]^T, \eta^2[m]^T, ..., \eta^{N_r}[m]^T]^T$, and

$$\mathbf{Q}_{kt} = \begin{bmatrix} \mathbf{Q}_{kt}^{11} & \mathbf{Q}_{kt}^{21} & \cdots & \mathbf{Q}_{kt}^{N_t 1} \\ \mathbf{Q}_{kt}^{12} & \mathbf{Q}_{kt}^{22} & \cdots & \mathbf{Q}_{kt}^{N_t 2} \\ \vdots & \vdots & \ddots & \vdots \\ \mathbf{Q}_{kt}^{1N_r} & \mathbf{Q}_{kt}^{2N_r} & \cdots & \mathbf{Q}_{kt}^{N_t N_r} \end{bmatrix} \tag{4.1.14}$$

with $\mathbf{Q}_{kt}^{ij}$ given by

$$\mathbf{Q}_{kt}^{ij} = \begin{bmatrix} q_{kt}^{ij}[0] & q_{kt}^{ij}[1] & \cdots & q_{kt}^{ij}[L_q] & 0 & \cdots & 0 \\ 0 & q_{kt}^{ij}[0] & q_{kt}^{ij}[1] & \cdots & q_{kt}^{ij}[L_q] & \ddots & \vdots \\ \vdots & \ddots & \ddots & \ddots & & \ddots & 0 \\ 0 & \cdots & 0 & q_{kt}^{ij}[0] & q_{kt}^{ij}[1] & \cdots & q_{kt}^{ij}[L_q] \end{bmatrix} \tag{4.1.6}$$

As shown in [52], [13] and [14], and due to the structure of the system, the equalizer for OQAM only keeps either the real or the imaginary part of the output, depending on the symbol and subchannel indices. It is thus better to optimize it directly on the corresponding output. Let $\mathbf{W}_k = [\mathbf{w}_k^1 \ \ldots \ \mathbf{w}_k^{N_t}]$ be the MIMO equalizer for the kth subchannel. Then, the equalizer outputs can be written as

$$\tilde{\mathbf{v}}_k[n] = \mathbf{W}_k^H \mathbf{y}_k[n] \tag{4.1.15}$$

where $\tilde{\mathbf{v}}_k[n] = [\tilde{v}_k^1[n] \ \ldots \ \tilde{v}_k^{N_t}[n]]^T$.

At the output of the equalizer, due to the OQAM modulation, we are interested only in either the real part or the imaginary part of the output depending on the indices k and n. We have

$$Re\{\tilde{\mathbf{v}}_k[n]\} = Re\{\mathbf{W}_k^H \mathbf{y}_k[n]\} = Re\{\mathbf{W}_k^T\} Re\{\mathbf{y}_k[n]\} + Im\{\mathbf{W}_k^T\} Im\{\mathbf{y}_k[n]\}, \text{ for } k+n \text{ even}$$
$$Im\{\tilde{\mathbf{v}}_k[n]\} = Im\{\mathbf{W}_k^H \mathbf{y}_k[n]\} = Re\{\mathbf{W}_k^T\} Im\{\mathbf{y}_k[n]\} - Im\{\mathbf{W}_k^T\} Re\{\mathbf{y}_k[n]\}, \text{ for } k+n \text{ odd}$$

The whole system and equalization problem can be rewritten using only real matrices and vectors, by taking into account the structure of the OQAM modulation. In order to obtain this particular formulation, we express $Re\{\mathbf{y}_k[n]\}$ and $Im\{\mathbf{y}_k[n]\}$ as follows

$$Re\{\mathbf{y}_k[n]\} = \sum_{t=k-1}^{k+1} Re\{\overline{\mathbf{Q}}_{kt}\} \overline{\mathbf{v}}_t[n] + Re\{\overline{\mathbf{B}}_k \eta[m]\}$$
$$Im\{\mathbf{y}_k[n]\} = \sum_{t=k-1}^{k+1} Im\{\overline{\mathbf{Q}}_{kt}\} \overline{\mathbf{v}}_t[n] + Im\{\overline{\mathbf{B}}_k \eta[m]\}$$

where the matrix $\overline{\mathbf{Q}}_{kt}$ and vector $\overline{\mathbf{v}}_t[n]$ are obtained in the following way: consider the product of $\mathbf{Q}_{kt}$ and $\mathbf{v}_t[n]$; each column of $\mathbf{Q}_{kt}$ corresponds, in this product, to an entry of $\mathbf{v}_t[n]$. The entries of $\mathbf{v}_t[n]$ are either purely real or purely imaginary. Now the product can be kept identical by removing the factor $j = \sqrt{-1}$ from the purely imaginary entries of $\mathbf{v}_t[n]$ and applying it to the corresponding columns of $\mathbf{Q}_{kt}$. This is how matrix $\overline{\mathbf{Q}}_{kt}$ and vector $\overline{\mathbf{v}}_t[n]$ are obtained. They are such that the product is the same as with the initial matrices, but the new vector $\overline{\mathbf{v}}_t[n]$ is now purely real. After taking the real and imaginary parts of the output, the above equations are obtained.

The MMSE equalizer is computed by minimizing the mean square error on $Re\{\tilde{\mathbf{v}}_k[n]\}$ for $k+n$ even or $Im\{\tilde{\mathbf{v}}_k[n]\}$ for $k+n$ odd. It is easily seen that the MMSE equalizer for purely real symbols ($k+n$ even) and purely imaginary symbols ($k+n$ odd) are identical, so we only consider the real case. For $k+n$ even, we get the compact expression

$$Re\{\tilde{\mathbf{v}}_k[n]\} = \overline{\mathbf{W}}_k^T \overline{\mathbf{y}}_k[n] \tag{4.1.16}$$

where

$$\overline{\mathbf{W}}_k = \begin{bmatrix} Re\{\mathbf{W}_k\} \\ Im\{\mathbf{W}_k\} \end{bmatrix} \tag{4.1.17}$$

and

$$\overline{\mathbf{y}}_k[n] = \begin{bmatrix} Re\{\mathbf{y}_k[n]\} \\ Im\{\mathbf{y}_k[n]\} \end{bmatrix} = \sum_{t=k-1}^{k+1} \overline{\overline{\mathbf{Q}}}_{kt} \overline{\mathbf{v}}_t[n] + \overline{\overline{\mathbf{B}}}_k \overline{\eta}[m]$$

where

$$\overline{\overline{\mathbf{Q}}}_{kt} = \begin{bmatrix} Re\{\overline{\mathbf{Q}}_{kt}\} \\ Im\{\overline{\mathbf{Q}}_{kt}\} \end{bmatrix}, \overline{\overline{\mathbf{B}}}_k = \begin{bmatrix} Re\{\overline{\mathbf{B}}_k\} & -Im\{\overline{\mathbf{B}}_k\} \\ Im\{\overline{\mathbf{B}}_k\} & Re\{\overline{\mathbf{B}}_k\} \end{bmatrix} \text{and } \overline{\eta}[m] = \begin{bmatrix} Re\{\eta[m]\} \\ Im\{\eta[m]\} \end{bmatrix} \tag{4.1.18}$$

For selective channels, the optimal equalizer delays may be different for the different subchannels and symbol streams (or antennas). Hence we introduce a specific delay denoted as $\Delta_{k,i}$, $i = 1, ..., N_t$,

for the kth subchannel and ith symbol stream (or transmit antenna). Now the MSE criterion to be minimized, for $k+n$ even, can be expressed as[5]

$$E[\|\mathbf{e}_k\|^2] = E[\|\overline{\mathbf{W}}_k^T \overline{\mathbf{y}}_k[n] \ - \mathbf{v}_{k,\Delta}[n]\|^2] \tag{4.1.19}$$

where $\mathbf{e}_k = \overline{\mathbf{W}}_k^T \overline{\mathbf{y}}_k[n] - \mathbf{v}_{k,\Delta}[n]$, and $\mathbf{v}_{k,\Delta_k}[n] = [v_k^1[n-\Delta_{k,1}], v_k^2[n-\Delta_{k,2}], ..., v_k^{N_t}[n-\Delta_{k,N_t}]]^T$, $0 \le \Delta_{k,i} \le L_q + L_{eq} - 1$. The equalizer delays may be optimized independently for each subchannel and output to minimize the MSE.

By using the orthogonality principle, the MSE in (4.1.19) is minimized when

$$E[\mathbf{e}_k[n]\overline{\mathbf{y}}_k[n]^T] = \mathbf{0} \tag{4.1.20}$$

Then

$$E[(\overline{\mathbf{W}}_k^T \overline{\mathbf{y}}_k[n] - \mathbf{v}_{k,\Delta}[n])\overline{\mathbf{y}}_k[n]^T] = \mathbf{0} \tag{4.1.21}$$

Afterwards

$$\overline{\mathbf{W}}_k^T E[\overline{\mathbf{y}}_k[n]\overline{\mathbf{y}}_k[n]^T] = E[\mathbf{v}_{k,\Delta}[n]\overline{\mathbf{y}}_k[n]^T] \tag{4.1.22}$$

to yield

$$\overline{\mathbf{W}}_k^T = \mathbf{R}_{\mathbf{v}_{k,\Delta}\overline{\mathbf{y}}_k} \mathbf{R}_{\overline{\mathbf{y}}_k\overline{\mathbf{y}}_k}^{-1} \tag{4.1.23}$$

where $\mathbf{R}_{\overline{\mathbf{y}}_k\overline{\mathbf{y}}_k} = E[\overline{\mathbf{y}}_k[n]\overline{\mathbf{y}}_k[n]^T]$ is the covariance matrix of $\overline{\mathbf{y}}_k[n]$ and $\mathbf{R}_{\mathbf{v}_{k,\Delta}\overline{\mathbf{y}}_k} = E[\mathbf{v}_{k,\Delta}[n]\overline{\mathbf{y}}_k[n]^T]$ is the covariance matrix of vectors $\mathbf{v}_{k,\Delta}[n]$ and $\overline{\mathbf{y}}_k[n]$.

Using the fact that, for uncorrelated entries of $\overline{\mathbf{v}}_i[n]$ and $\overline{\eta}[m]$, $E[\overline{\mathbf{v}}_i[n]\overline{\mathbf{v}}_j[n]^T] = \delta_{ij}\sigma_v^2\mathbf{I}$, and $\mathbf{R}_{\overline{\eta}\overline{\eta}} = \frac{\sigma_\eta^2}{2}\mathbf{I}$ and $E[\overline{\mathbf{v}}_i[n]\overline{\eta}[m]^T] = \mathbf{0}$, and after some developments and simplifications, we get

$$\mathbf{R}_{\overline{\mathbf{y}}_k\overline{\mathbf{y}}_k} = \sigma_v^2 \sum_{i=k-1}^{k+1} \overline{\overline{\mathbf{Q}}}_{ki}\overline{\overline{\mathbf{Q}}}_{ki}^T + \frac{\sigma_\eta^2}{2}\overline{\overline{\mathbf{B}}}_k\overline{\overline{\mathbf{B}}}_k^T \tag{4.1.24}$$

On the other hand we have

$$\mathbf{R}_{\mathbf{v}_{k,\Delta}\overline{\mathbf{y}}_k} = \sum_{i=k-1}^{k+1} E[\mathbf{v}_{k,\Delta}[n]\overline{\mathbf{v}}_i[n]^T]\overline{\overline{\mathbf{Q}}}_{ki}^T + E[\mathbf{v}_{k,\Delta}[n]\overline{\eta}[m]^T]\overline{\overline{\mathbf{B}}}_k^T \tag{4.1.25}$$

Using the fact that $E[\mathbf{v}_{k,\Delta}[n]\overline{\eta}[m]^T] = \mathbf{0}$ and $E[\mathbf{v}_{k,\Delta}[n]\overline{\mathbf{v}}_i[n]^T] = \delta_{ki}\sigma_v^2\mathbf{P}_{k,\Delta}$ where $\mathbf{P}_{k,\Delta}(i,j) = \delta_{j,(i-1)N_t+\Delta_{k,i}+1}$, we get

$$\mathbf{R}_{\mathbf{v}_{k,\Delta}\overline{\mathbf{y}}_k} = \sigma_v^2\mathbf{P}_{k,\Delta}\overline{\overline{\mathbf{Q}}}_{kk}^T \tag{4.1.26}$$

Finally, substituting (4.1.24) and (4.1.26) into (4.1.23), we obtain

[5] Note that for $k+n$ odd, the use of the imaginary part in (4.1.16) and (4.1.19) leads to the same equalizer.

$$\overline{\overline{\mathbf{W}}}_{k,MMSE}^{T} = \mathbf{P}_{k,\Delta}\overline{\overline{\mathbf{Q}}}_{kk}^{T}(\sum_{i=k-1}^{k+1}\overline{\overline{\mathbf{Q}}}_{ki}\overline{\overline{\mathbf{Q}}}_{ki}^{T} + \frac{\sigma_\eta^2}{2\sigma_v^2}\overline{\overline{\mathbf{B}}}_k\overline{\overline{\mathbf{B}}}_k^{T})^{-1} \tag{4.1.27}$$

Therefore, from (4.1.17), by unstacking $\overline{\mathbf{W}}_{k,MMSE}$, we get

$$\mathbf{W}_{k,MMSE} = \overline{\mathbf{W}}_{k,MMSE}(1 : L_{eq}N_r, :) + j\overline{\mathbf{W}}_{k,MMSE}(L_{eq}N_r + 1 : 2L_{eq}N_r, :) \tag{4.1.28}$$

Note that in (4.1.28) we used a Matlab notation where $\ell : m$ denotes the ℓth to the mth entries of a vector, and : denotes all the entries of a vector.

Now the outputs of the equalizer for the kth subchannel are given by

$$\tilde{\mathbf{v}}_k[n] = \mathbf{W}_k^H\mathbf{y}_k[n] \tag{4.1.29}$$

In order to recover the transmitted complex symbol streams from $\tilde{\mathbf{v}}_k[n] = [\tilde{v}_k^1[n], \tilde{v}_k^2[n], \ldots, \tilde{v}_k^{N_t}[n]]^T$ we perform the OQAM demodulation

$$\tilde{d}_k^i[n] = Re\{\theta_k[n]^*\tilde{v}_k^i[n]\}, i = 1, \ldots, N_t \tag{4.1.30}$$

and

$$\tilde{a}_k^i[l] = \tilde{d}_k^i[2l] + j\tilde{d}_k^i[2l+1], i = 1, \ldots, N_t \tag{4.1.31}$$

Finally $\hat{a}_k^i[l]$ is obtained by taking a hard decision on $\tilde{a}_k^i[l]$.

Remark: The ZF equalizer follows directly from (4.1.27) by letting $\sigma_\eta^2 = 0$.

Here is a brief summary of the main steps for computing the MMSE equalizer for each subchannel. We assume that the MIMO channel, the transmitted symbol variance and the noise variance are known (perfectly estimated).

1. Obtain the convolution matrix $\mathbf{Q}_{kt}^{ij}$ using some channel estimation method. $\mathbf{B}_k$ can be computed using the equation before Section 4.1.1.
2. Compute the matrix $\mathbf{Q}_{kt}$ using (4.1.14) and the matrix $\overline{\mathbf{B}}_k$ from $\mathbf{B}_k$ (see (4.1.13)).
3. Compute $\overline{\mathbf{Q}}_{kt}$ by shifting the complex number $j = \sqrt{-1}$ from the imaginary entries of $\mathbf{v}_t[n]$ (see (4.1.13)) into the corresponding columns of $\mathbf{Q}_{kt}$.
4. Compute the matrices $\overline{\overline{\mathbf{Q}}}_{kt}$ and $\overline{\overline{\mathbf{B}}}_k$ using (4.1.18).
5. Compute the equalizer $\mathbf{W}_{k,MMSE}$ using (4.1.27) and (4.1.28).

4.1.3 Successive interference cancellation (SIC) for MIMO-FBMC

Here we propose to adapt the successive interference cancellation (SIC) technique [15] to our context, i.e., MIMO-FBMC. The idea behind the SIC is to recover the symbol streams coming from the different antennas in a sequential way. The first step consists in extracting the first symbol stream using an MMSE equalizer, or any other equalizer. Then we subtract the contribution of the already recovered stream from the received signal and so on. This obviously requires some channel estimation, and is susceptible to error propagation, so the effect of channel estimation errors need to be investigated. In MIMO-FBMC, given that there is interference from adjacent subchannels, for each subchannel k we subtract not only the recovered symbol stream from other antennas corresponding to subchannel k but also the contributions of the symbol streams of the adjacent

subchannels $k-1$ and $k+1$. The interest of this technique is that, once channel estimation is available, and provided that error propagation can be kept small, it provides an easy way to improve the performance of any equalizer. In this section, we will investigate the application of this technique to the MMSE equalizer, and to the frequency sampling (FS) equalizer described in deliverable D3.1 [5].

The SIC technique for MIMO FBMC is briefly described in the following steps

Step 1: Recover the first symbol stream. We first need to compute the equalizer according to the frequency domain, MMSE or ZF methods. Let $\mathbf{w}_k$ be the first column of such an equalizer. Then

$$\tilde{v}_k^1[n] = \mathbf{w}_k^H \mathbf{y}_k[n]\,, k = 0, \ldots, M-1 \tag{4.1.32}$$

As described in the previous section, the decision $\hat{a}_k^1[l]$ on the corresponding symbol can easily be computed from $\tilde{v}_k^1[n]$. Let us suppose that the decision on $\hat{a}_k^1[l]$ is correct, i.e. $\hat{a}_k^1[l] = a_k^1[l]$.

Step 2: Remodulate $a_k^1[l]$ to get $v_k^1[n]$ according to the OQAM modulation technique. Let $\mathbf{v}_k^1[n] = [v_k^1[n], v_k^1[n-1], ..., v_k^1[n-L_q-L_{eq}+1]]^T$. Now we can subtract the contribution of $\mathbf{v}_k^1[n]$, $\mathbf{v}_{k-1}^1[n]$ and $\mathbf{v}_{k+1}^1[n]$ from the received signal $\mathbf{y}_k[n]$ as follows

$$\mathbf{y}_k^-[n] = \mathbf{y}_k[n] - \sum_{i=k-1}^{k+1} \begin{bmatrix} \mathbf{Q}_{ki}^{11} \\ \mathbf{Q}_{ki}^{12} \\ \vdots \\ \mathbf{Q}_{ki}^{1N_r} \end{bmatrix} \mathbf{v}_i^1[n] = \sum_{i=k-1}^{k+1} \mathbf{Q}_{ki}^- \mathbf{v}_i^-[n] + \overline{\mathbf{B}}_k \eta[m] \tag{4.1.33}$$

where $\mathbf{y}_k^-[n]$ is the received vector after removing the contribution of $\mathbf{v}_i^1[n],\ i = k-1, k, k+1$, $\mathbf{v}_i^-[n] = [\mathbf{v}_i^2[n]^T, ..., \mathbf{v}_i^{N_t}[n]^T]^T$, and

$$\mathbf{Q}_{ki}^- = \begin{bmatrix} \mathbf{Q}_{ki}^{21} & \cdots & \mathbf{Q}_{ki}^{N_t 1} \\ \mathbf{Q}_{ki}^{22} & \cdots & \mathbf{Q}_{ki}^{N_t 2} \\ \vdots & \ddots & \vdots \\ \mathbf{Q}_{ki}^{2N_r} & \cdots & \mathbf{Q}_{ki}^{N_t N_r} \end{bmatrix}$$

This step obviously requires the estimation of the convolution matrices $\mathbf{Q}_{kt}^{ij}$. These can be obtained by channel estimation procedures as described in WP3. They are also necessary for the design of most equalizers and hence SIC does not require any additional estimation methods. Several simple equalization schemes do not need the estimation of the full matrix, particularly for mildly selective channels. In this case, the SIC technique might not be indicated as simple equalization already performs well.

Step 3: Go to step 1 and recover the second stream and so on until the recovery of all the transmitted streams.

It is clear, from the above steps, that the SIC recovers the transmitted streams in a deflatory mode. Therefore, if all the decisions of each recovered stream are correct, i.e., no error propagation after recovering the ith stream, the system model becomes equivalent to a system with $N_t - i$ transmit

antennas and N_r receive antennas leading to an increased diversity. In general there might be error propagation and the performance might not benefit from full diversity.

4.1.4 Ordered SIC (OSIC) for MIMO-FBMC

In order to improve the performance and minimize the error propagation problem we propose to consider the ordered SIC technique [15]. The idea behind it is that at each layer the stream with the highest signal to interference plus noise ratio (SINR) is selected for detection and subsequent subtraction. The OSIC algorithm is almost the same as the SIC algorithm and only few changes are required. However, in contrast to the SIC receiver, the order of subtraction may be different from one subchannel to another depending on the SINR's of each subchannel. Hence the subtraction of the contribution of the adjacent subchannels often becomes impossible. Suppose, for subchannel k and without loss of generality, that the first stream has the highest SINR, then equation (4.1.33) in step 2 of the SIC becomes

$$\mathbf{y}_k^-[n] = \mathbf{y}_k[n] - \begin{bmatrix} \mathbf{Q}_{kk}^{11} \\ \mathbf{Q}_{kk}^{12} \\ \vdots \\ \mathbf{Q}_{kk}^{1N_r} \end{bmatrix} \mathbf{v}_k^1[n] = \mathbf{Q}_{kk}^- \mathbf{v}_k^-[n] + \sum_{i=k-1, i\neq k}^{k+1} \mathbf{Q}_{ki}\mathbf{v}_i[n] + \overline{\mathbf{B}}_k \eta[m] \quad (4.1.34)$$

Then we use $\mathbf{y}_k^-[n]$ to compute the equalizer for the remaining streams. Subsequently we select the equalizer that provides the highest SINR. After detecting the stream at the output of this equalizer, as seen in SIC (see steps 1 and 2), we subtract its contribution from $\mathbf{y}_k^-[n]$ by applying (4.1.34). We repeat this process until all streams are recovered. Note that, in order to determine the stream with the best SINR, it is theoretically necessary to compute the equalizer for each stream and then determine which one has the best performance. Doing so substantially increases the complexity of OSIC with respect to the initial SIC technique as new equalizers have to be computed for all streams at each step. In practice, it is better to use approximate evaluations of the SINR on each stream.

4.1.5 Two Stage OSIC (TS-OSIC) for MIMO-FBMC

In order to further improve the performance of the OSIC receiver we propose to use the two stage OSIC (TS-OSIC). The main idea behind the TS-OSIC is that after applying the OSIC algorithm one time, subtraction of the contribution of the adjacent subchannels from the subchannel of interest becomes possible. Once the contribution of the adjacent subchannels is removed we can apply the OSIC algorithm a second time to enhance the performance. Let

$$\mathbf{y}_k^{'}[n] = \mathbf{y}_k[n] - \sum_{i=k-1, i\neq k}^{k+1} \mathbf{Q}_{ki}\mathbf{v}_i[n] = \mathbf{Q}_{kk}\mathbf{v}_k[n] + \overline{\mathbf{B}}_k \eta[m], \quad k = 0, ..., M-1 \quad (4.1.35)$$

represent the received signal after subtracting the contribution of the adjacent subchannels using the decisions $\mathbf{v}_i[n]$, $i = 0, ..., M-1$ resulting from applying the OSIC algorithm in the first stage. In the second stage we apply the OSIC algorithm again but this time on $\mathbf{y}_k^{'}[n]$. This means that the interference coming from adjacent subchannels is always cancelled using the results of the first stage, and the interference coming from the subchannel of interest is cancelled using the OSIC technique in the second stage. It is worth noting that the equalizer computation in (4.1.27) is simplified in the second stage since the terms corresponding to the adjacent subchannels can be ignored, i.e.

$$\overline{\overline{\mathbf{W}}}_{k,MMSE}^T = \mathbf{P}_{k,\Delta}\overline{\overline{\mathbf{Q}}}_{kk}^T(\overline{\overline{\mathbf{Q}}}_{kk}\overline{\overline{\mathbf{Q}}}_{kk}^T + \tfrac{\sigma_\eta^2}{2\sigma_v^2}\overline{\overline{\mathbf{B}}}_k\overline{\overline{\mathbf{B}}}_k^T)^{-1} \quad (4.1.36)$$

Note that the TS-OSIC requires a high computational complexity and is currently not suitable for a practical implementation.

4.1.6 Simulations

Remark: Given the number and complexity of the implemented algorithms, simulations considering the simulation parameters corresponding to the WiMAX scenario will be provided later on. Here we will just consider parameters that allow comparing the algorithms.

In this section we will assess the performance of the presented algorithms and CP-OFDM by comparing them in terms of bit error rate (BER). Unless otherwise specified, we consider the following simulation parameters: $M = 64$ carriers, overlapping factor $K = 4$, 16-QAM modulation. The CP length for CP-OFDM system is $M/4$. The MIMO FIR channels are chosen randomly. All simulation results are averaged over 200 independent realizations. It is difficult to obtain a fair comparison with CP-OFDM as the systems have different characteristics, and all parameters can thus not be made equal. We still have provided results for CP-OFDM however in order to obtain a rough idea of the achievable performance. In the present simulation scenario, the CP-OFDM system has been normalized for the same Eb/N0 as the FBMC system. As a result, and since CP-OFDM uses the cyclic prefix, it should be noted that its throughput rate is smaller than that of the FBMC system.

In what follows we refer to the extension to MIMO case of the frequency sampling equalizer presented in [2] by Frequency Sampling (FS) MIMO-FBMC equalizer. The considered equalizer length is 3. A brief description of the Frequency Sampling (FS) MIMO-FBMC equalizer is given in section 4.2.4.

Figure 4.1.1 compares the algorithms in terms of BER. We consider $N_t = 2$, $N_r = 2$ and $\nu = 9$, i.e. each channel between two antennas has $\nu + 1 = 10$ taps. The MMSE and FS equalizer length is 3. From this figure we can see that, for low SNR, all the equalizers approximately have the same performance. For high SNR we notice that the TS-OSIC-MMSE and OSIC-MMSE provide the best performance which was expected. The SIC technique and the different variations all bring some small performance improvements, both in the MMSE and FS case. CP-OFDM has a better performance for high SNR, but it should be noted that its throughput rate is smaller than that of the FBMC system. It is worth noting that the SIC technique applied to the FS equalizer is not sufficient to reach the performance of the MMSE equalizer. For this type of channel, at high SNR, the simple one-tap frequency domain equalizer has substantially lower performance.

In Figure 4.1.2 we consider $N_t = 3$, $N_r = 3$. With respect to the 2x2 MIMO system, more diversity is available. Clearly the SIC technique is able to take advantage (at least partly) of this diversity and provides larger improvements for larger number of parallel streams. Once again, the different variations all bring noticeable performance improvements.

In Figure 4.1.3 we consider a situation where the number of receive antennas is greater than the number of transmit antennas, namely $N_t = 2$ and $N_r = 3$. First of all, we observe that using more antennas at the receiver than at the transmitter considerably improves the performance. Regarding the comparison of the algorithms, the general behavior is similar to what was observed above.

In Figure 4.1.4 and Figure 4.1.5 we investigate the effect of the channel length on the performance of the algorithms for $E_b / N_0 = 20dB$ and $E_b / N_0 = 30dB$, respectively. These figures plot BER versus channel length ν+1 for $N_t = 3$, $N_r = 3$ and 16-QAM modulation. We observe that for a short channel (length 2 or 3) the MMSE and FS equalizers almost provide the same performance. The SIC based techniques in itself brings some small improvement. The OSIC and TS-OSIC further improve the performance slightly. For more selective channels, the MMSE seems to be able to cope better with the created interference, and all MMSE-based algorithms are better than the frequency domain

and FS equalizers. For CP-OFDM, the performance is good as long as the channel length is smaller than the CP, but then degrades rapidly for longer channels. It is worth nothing that SIC based techniques are interesting even for short channels especially when a large number of antennas is considered. Moreover, we observe that, for $E_b / N_0 = 20dB$ (Figure 4.1.4), the algorithms are less sensitive to the channel length compared to the case $E_b / N_0 = 30dB$ (Figure 4.1.5).Therefore, for low SNR the channel length slightly affects the performance of the algorithms.

Figure 4.1.5illustrates the effect of the equalizer length on the performance of the MMSE based algorithms, MMSE, SIC-MMSE and OSIC-MMSE. We consider $L_{eq} = 1, 2, 4, 6$ and 8, $N_t = 3$, $N_r = 3$, $E_b / N_0 = 30dB$ and 16-QAM modulation. We observe that increasing the equalizer length, more than 4, moderately improves the performance. Moreover, as we have already seen in figures Figure 4.1.1 to Figure 4.1.5 the OSIC-MMSE is better than the SIC-MMSE which is in its turn better than the MMSE equalizer.

For future works, the effect of channel estimation errors on this technique needs to be investigated, and in particular the potential risk of error propagation. For long channels, the number of taps to be estimated also needs to be investigated.

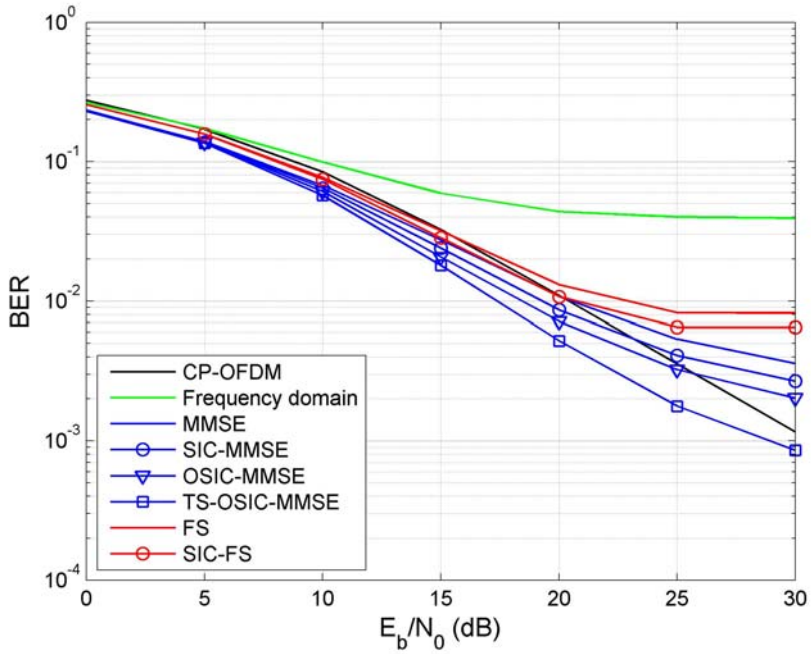

Figure 4.1.1. BER versus E_b/N_0. Comparison of equalizers. 16-QAM, $N_t = 2$, $N_r = 2$ and channel length $\nu + 1 = 10$. $L_{eq} = 3$ for both MMSE and FS.

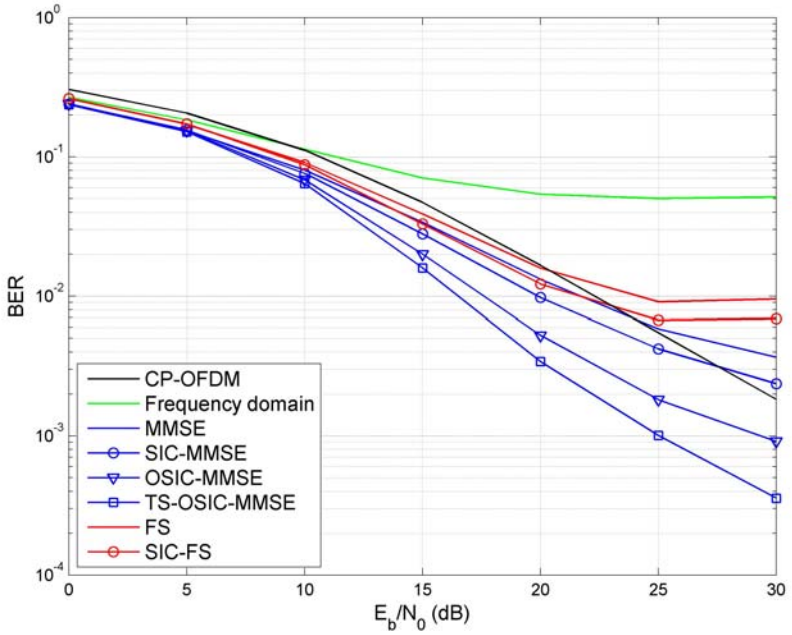

Figure 4.1.2. BER versus E_b/N_0. Comparison of equalizers. 16-QAM, $N_t = 3$, $N_r = 3$ and channel length $\nu + 1 = 10$. $L_{eq} = 3$ for both MMSE and FS.

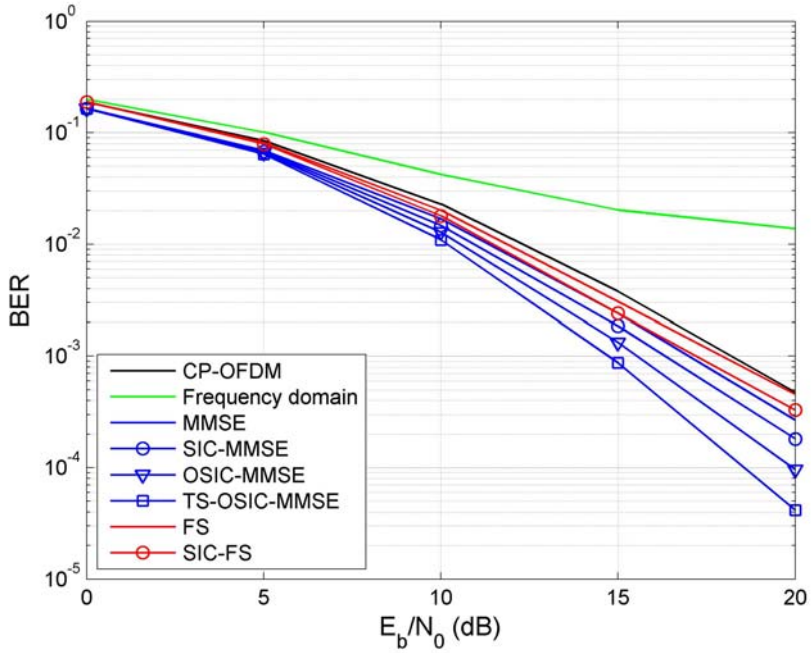

Figure 4.1.3. BER versus E_b/N_0. Comparison of equalizers. 16-QAM, $N_t = 2$, $N_r = 3$ and channel length $\nu + 1 = 10$. $L_{eq} = 3$ for both MMSE and FS.

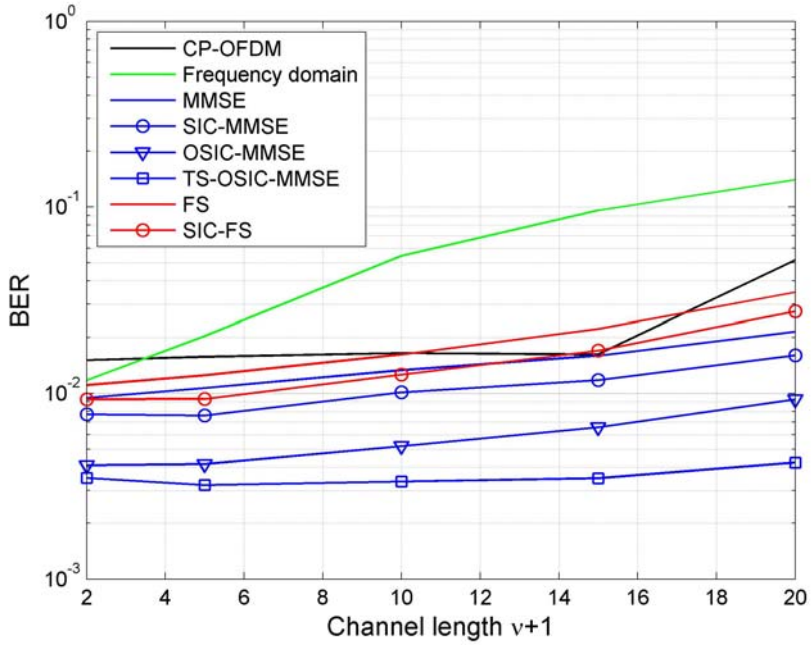

Figure 4.1.4. BER versus channel length $\nu + 1$. Effect of the channel length on the performance of the equalizers. 16-QAM, $N_t = 3$, $N_r = 3$, $L_{eq} = 3$ and E_b/N_0=20dB.

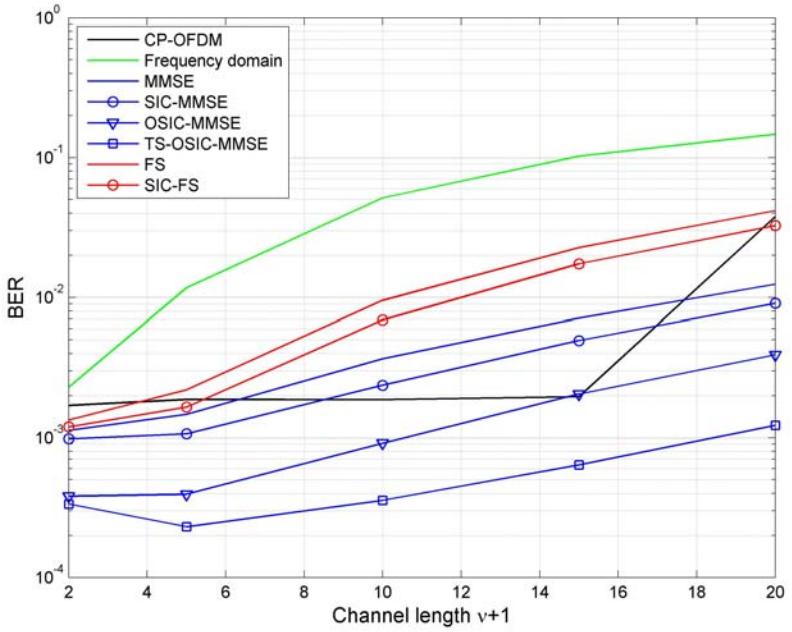

Figure 4.1.5. BER versus channel length $\nu + 1$. Effect of the channel length on the performance of the equalizers. 16-QAM, $N_t = 3$, $N_r = 3$, $L_{eq} = 3$ and $E_b/N_0 = 30dB$.

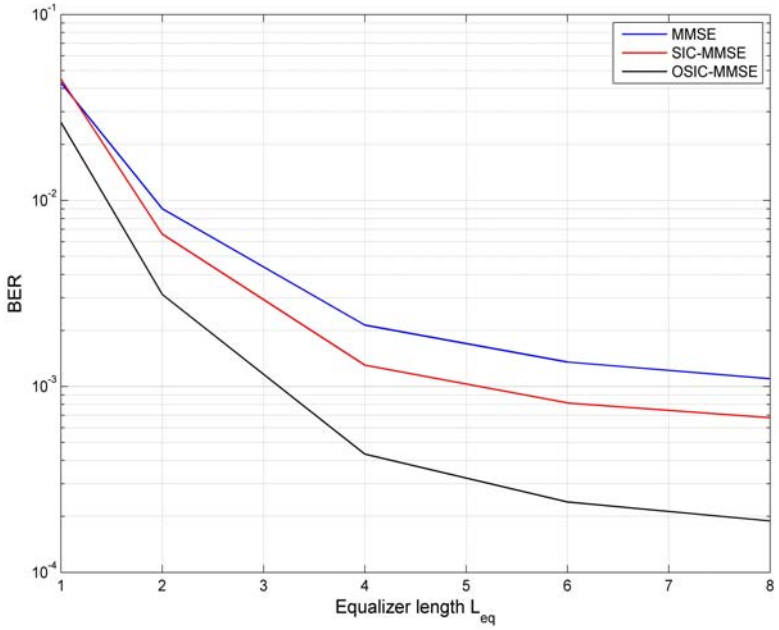

Figure 4.1.6 BER versus equalizer length L_{eq} . Effect of the equalizer length on the performance of the equalizers. 16-QAM, $N_t = 3$, $N_r = 3$, $\nu + 1 = 10$ and $E_b/N_0 = 30dB$.

4.2 Diversity equalization with Maximal Ratio Combining

The content of this contribution is organized as follows. In Section 4.2.1, the frequency sampling-based per-subcarrier equalizer design scheme is extended to receive diversity context. Section 4.2.2 gives some operational insights of the developed diversity equalization scheme. In Section 4.2.3, the performance of the described technique is analyzed through uncoded bit-error-rate simulations over various multipath channel models. Moreover, the impact of fractional time delay on the required equalizer filter order is investigated. Finally, Section 4.2.4 discusses the possibilities to extend the developed algorithm to other multi-antenna configurations.

4.2.1 Per-subcarrier equalization according to MRC

The fundamental philosophy of the maximal ratio combiner is to maximize the output SNR (that is, the effective SNR after combining) by weighting each diversity branch signal with a factor that is proportional to the instantaneous SNR in the respective antenna [16]. Moreover, in order to enable coherent summation of the branch signals, weighting factors that co-phase the different antenna signals prior combining are required. This can be achieved if channel state information is available in the receiver.

The block diagram in Figure 4.2.1 shows the structure of the FBMC receiver for $1 \times Q$ antenna diversity scheme to be analyzed. Channel equalization is performed in the receiver using per-subcarrier processing by means of complex finite impulse response

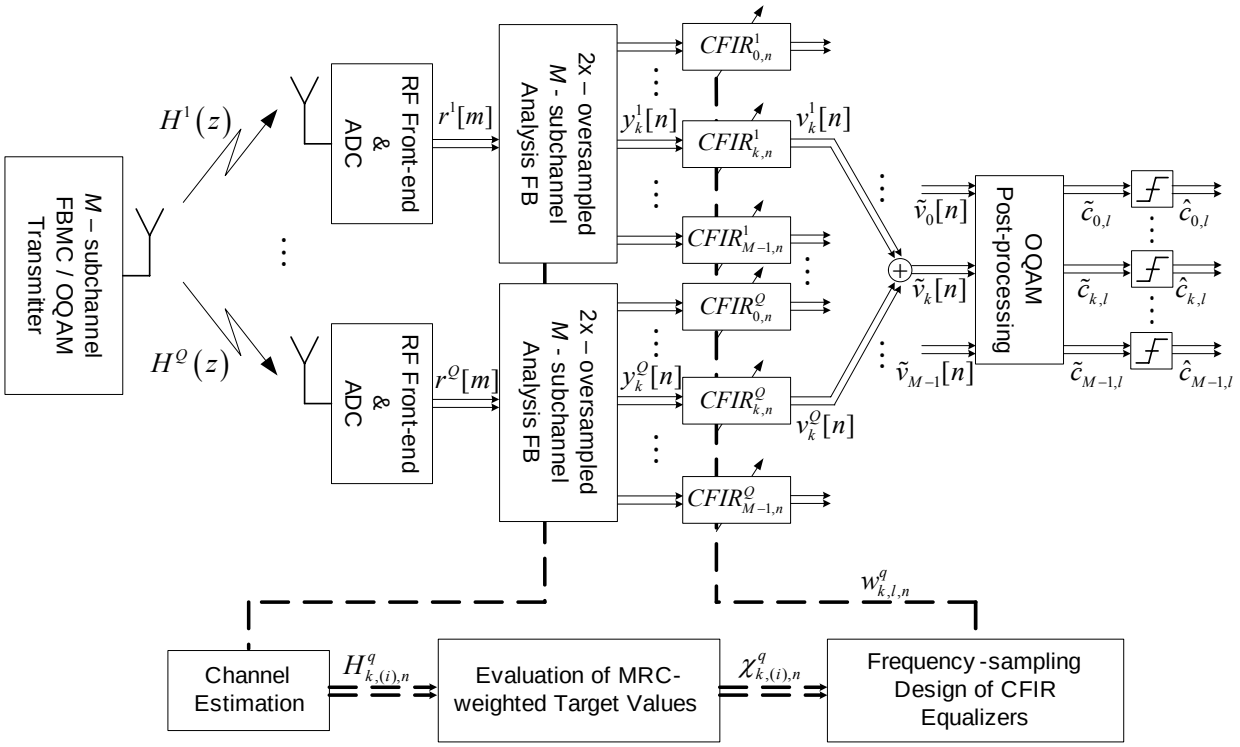

Figure 4.2.1. FBMC receiver structure for maximal ratio combined diversity reception with frequency sampling-designed subcarrier equalizers. Solid lines: signal flow; dashed lines: information flow.

(CFIR) filters. Furthermore, we consider the equalizer coefficient derivation based on the frequency sampling technique described in detail in [5].

We assume that the channel estimator can provide information on the channel transfer function at a set of target frequency points chosen in the selected mode of frequency sampling design. In general, the number of frequency points of interest within a subcarrier bandwidth, has a one-to-one relation to the length of the CFIR subcarrier equalizer filter. Typically, 1-tap and 3-tap structures are considered. For the latter structure, channel estimates at double resolution compared to the subcarrier spacing $\Delta f = 1/T$ are required. In the following description of diversity equalization, CFIRs with three taps are considered.

Let us denote the complex coefficient of the generally time-variant channel frequency response experienced by the kth subcarrier on the qth antenna branch during the nth OQAM sub-symbol by

$$H_{k,(i),n}^q, \text{ for } k \in M_u, \text{ and } i = 0, 1, 2, \tag{4.2.1}$$

where the subscript (i) is used to index the target frequency points within a subcarrier band. Specifically, the subscript index $i = 1$ corresponds to the subcarrier center frequency, whereas the indexes $i = 0$ and $i = 2$ refer to the lower and the upper passband edge frequencies, respectively.
Moreover, we express the time-variant transfer function of a 3-tap CFIR equalizer for the kth subcarrier on the qth antenna branch as

$$W_{k,n}^q(z) = w_{k,0,n}^q z + w_{k,1,n}^q + w_{k,2,n}^q z^{-1}, \tag{4.2.2}$$

where a non-causal form is used for notational convenience.

Now the MRC principle is applied in a subcarrier-by-subcarrier manner and pointwise to each of the three target frequency points considered in 3-tap CFIR frequency sampling-design. The resulting maximal ratio-weighted target frequency response values at the frequency sampling-design points then become

$$\chi^q_{k,(i),n} = \frac{\left(H^q_{k,(i),n}\right)^*}{\sum_{q=1}^{Q}\left|H^q_{k,(i),n}\right|^2}, \tag{4.2.3}$$

where $|.|$ and $(.)^*$ denote the magnitude and the conjugate-operation of the complex argument, respectively.

The subcarrier equalizers operate at the low rate (i.e., at the OQAM sub-symbol rate $2/T$ after decimation by $M/2$) and process the channel distorted subcarrier sequences $y^q_k[n]$. The target frequency points indexed with subscripts (0), (1), and (2) correspond at the low rate to the frequency points $-\pi/2$, 0 and $\pi/2$, respectively. The CFIR transfer function in Eq. (4.2.2) will then be evaluated at these frequency points, yielding a system of three equations (in the general case, the number of equations equals the number of taps L_{eq} in the CFIR filter) that relates the equalizer frequency response at the target frequency points $\chi^q_{k,(i),n}$ and the three (in the general case L_{eq}) complex filter coefficients $\{w^q_{k,0,n}, w^q_{k,1,n}, w^q_{k,2,n}\}$. When this system of equations is solved for the unknown filter coefficients, the following closed-form expressions for the MRC-optimized CFIR filter coefficients can be derived:

$$\begin{aligned}
w^q_{k,0,n} &= \left[\left(-1+j\right)\chi^q_{k,(0),n} + 2\chi^q_{k,(1),n} + \left(-1-j\right)\chi^q_{k,(2),n}\right]/4 \\
w^q_{k,1,n} &= \left[\chi^q_{k,(0),n} + \chi^q_{k,(2)n}\right]/2 \\
w^q_{k,2,n} &= \left[\left(-1-j\right)\chi^q_{k,(0),n} + 2\chi^q_{k,(1),n} + \left(-1+j\right)\chi^q_{k,(2),n}\right]/4.
\end{aligned} \tag{4.2.4}$$

The low rate sample sequence at the output of the CFIR filter for the kth subcarrier on the qth antenna branch can then be expressed as

$$v^q_k[n] = \sum_{l=0}^{2} w^q_{k,l,n} y^q_k[n-l]. \tag{4.2.5}$$

The diversity equalized sample sequence is finally obtained by combining (through coherent summation) the CFIR filtered sequences from different antenna branches, i.e.,

$$\tilde{v}_k[n] = \sum_{q=1}^{Q} v^q_k[n], \tag{4.2.6}$$

for $k \in M_u$.

4.2.2 Operational insights

Let us investigate the operation of MRC diversity equalization in detail. Figure 4.2.2(a)- (d) illustrate the 3-tap CFIR operation in an exemplary 1×3 SIMO case. The series of subfigures (a)-(c) show the channel response (solid line), the equalizer response (dashdot line), the compensated response (dashed line), and the target frequency points (circle markers) for the different diversity branches. The subfigure (d) shows the effective transfer function after combining the branch signals. Equalizer performance is demonstrated for an arbitrarily chosen subchannel k in terms of a randomly picked instantaneous channel snapshot drawn from the Vehicular-B channel model. Responses are shown over the subcarrier bandwidth of $2/T$ in width (twice the subcarrier spacing). Behavior is shown both in terms of the magnitude (left) and the phase (right). A number of observations can be made:

i. The equalizer responses are forced to go through the target values defined by (4.2.3) based on the channel estimates in (4.2.1).

ii. The magnitude terms of the target values among different diversity branches will be assigned according to the channel state (condition) of each particular branch with respect to channel states in other branches. Therefore, the assigned magnitude is higher for diversity branch with channel estimates of larger magnitudes and vice versa. The normalization factor (the denominator) in (4.2.3), common to all diversity branches, will guarantee unity magnitude for the effective post-combining transfer function at the target frequency points.

iii. The equalizer response forces the phase of the compensated response to go through zero at the target frequency points. This is how the co-phasing of the different diversity branches is constructed into the equalizer solution.

iv. As a consequence of the previous two observations, the equalizer output signals will be added together coherently to maximize the post-combining SNR.

v. The 3-tap CFIR equalizer is clearly able to compensate for frequency-selective channel responses to a significant extent.

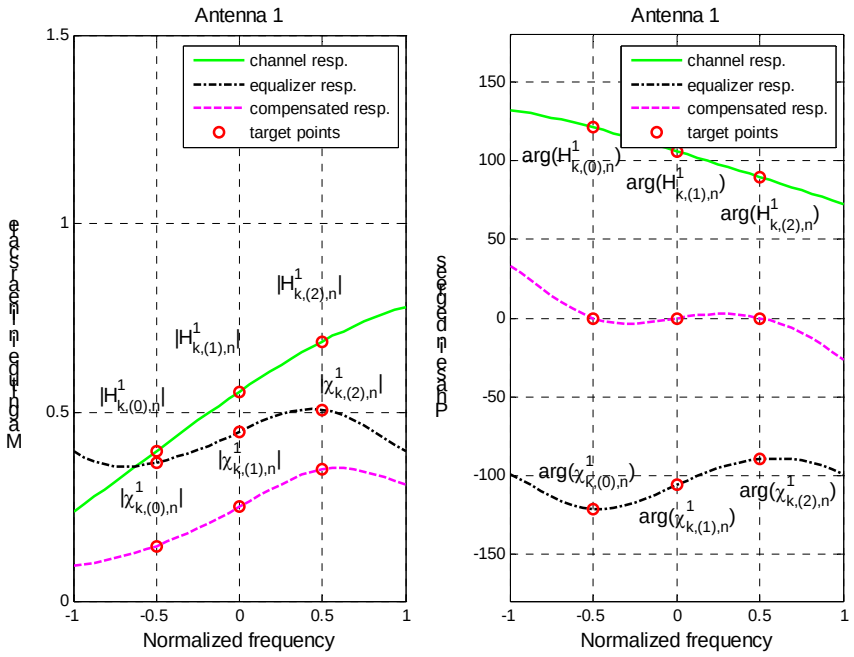

(a)

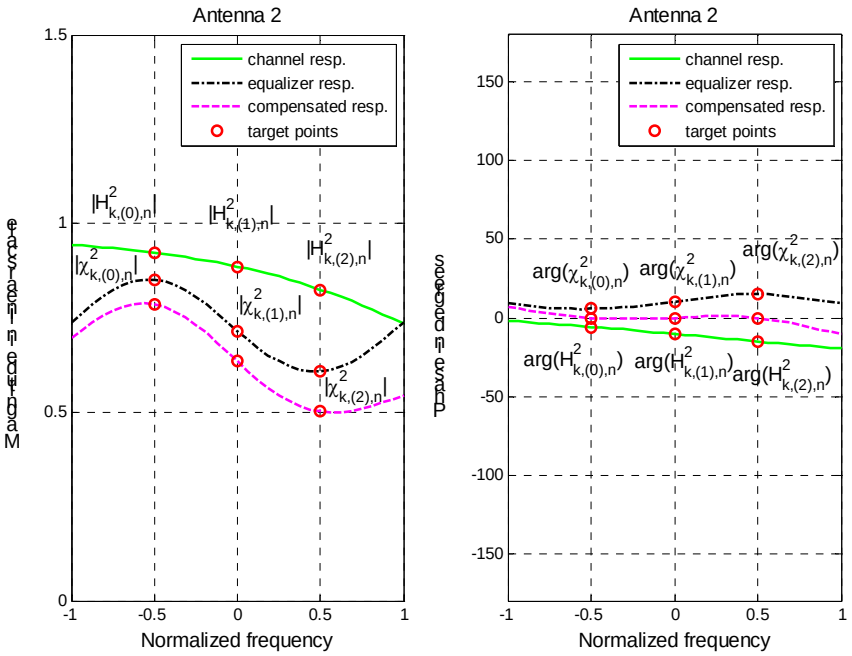
Antenna 2
channel resp.
equalizer resp.
compensated resp.
target points
Normalized frequency
Antenna 2
channel resp.
equalizer resp.
compensated resp.
target points
Normalized frequency

(b)

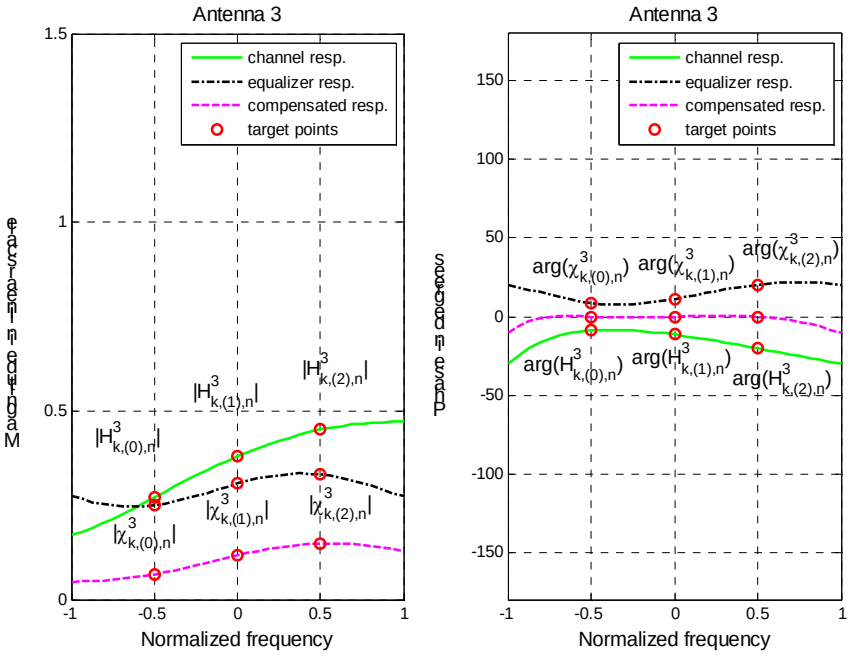
Antenna 3
channel resp.
equalizer resp.
compensated resp.
target points
Normalized frequency
Antenna 3
channel resp.
equalizer resp.
compensated resp.
target points
Normalized frequency

(c)

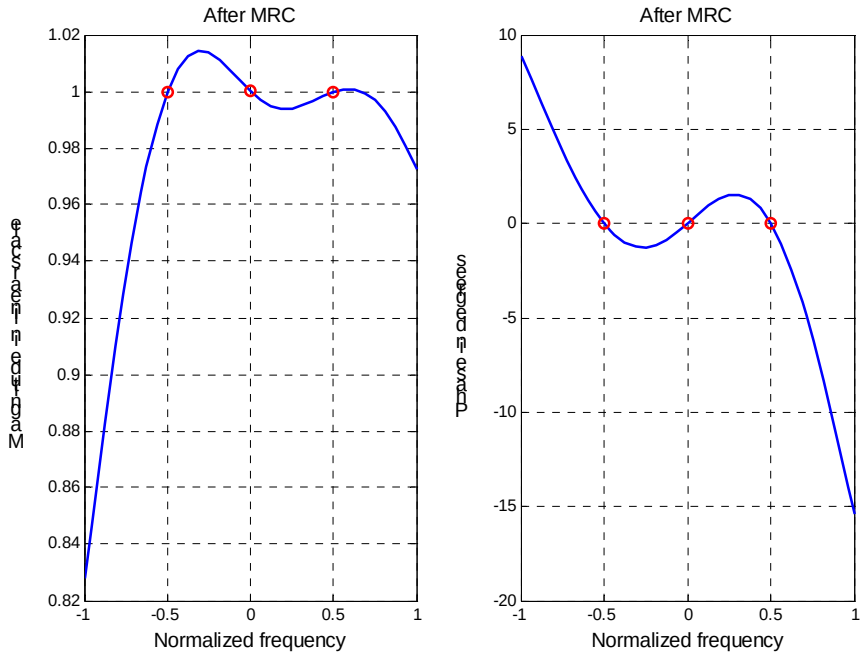

(d)

Figure 4.2.2. Operational details of MRC diversity equalization with frequency sampling–designed 3-tap CFIR per-subcarrier filters. Magnitude (left) and phase (right) compensation for arbitrary subcarrier k on different antenna braches (a)-(c) and the effective response after combining the diversity branches (d).

4.2.3 Numerical performance evaluations

Numerical performance evaluations for the FBMC modulation with the diversity equalization scheme described above have been carried out. Uncoded bit error rate (BER) simulations were performed for FBMC transmission according to PHYDYAS parametrization. Specifically, a sampling rate of $f_s = 11.2$ MHz and a filter bank with $M = 1024$ subcarriers, and a 10 MHz system band were assumed. As for the prototype, an NPR lowpass filter with an overlapping factor of $K = 4$ and designed according to the frequency sampling technique described in [17] was considered. BER metrics were estimated by transmitting 3000 frames, each of approximately 5 ms in duration and carrying 53 OQAM multicarrier symbols from the 64-QAM alphabet, over the Vehicular A (Veh-A), the Extended Vehicular A (Veh-AE), and the Vehicular B (Veh-B) multipath channels. In the simulations, random quasi-static channel instances of the above models with AWGN were considered. Moreover, perfect channel information (PCI) in the receiver was assumed. The effect of timing error in terms of fractional time delay was also addressed. Receive diversity was tested in 1×2 ($Q = 2$) and 1×4 ($Q = 4$) antenna configurations. Also the performance curves for 1×1 SISO ($Q = 1$, no diversity) case are shown for comparison. Simulations were carried out using both 1-tap and 3-tap complex FIR equalizers.

Figure 4.2.3(a), 3(b), and 3(c) show the uncoded BER as a function of energy per bit to noise spectral density ratio (E_b/N_o) for the Veh-A, the Veh-AE, and the Veh-B channel, respectively. For these simulations, fractional time delay was not included in the system model (w/o FTD). As a general observation we can say that the diversity reception provides considerable SNR gain (that is, the given error rate is achieved with less transmit energy), when compared to the single antenna receiver structure. This is true regardless of the channel model considered. Moreover, while the 1-tap and 3-

tap CFIR structures obtain approximately equal performance in the Veh-A channel, the 3-tap structure shows increasing benefit over the 1-tap structure for Veh-AE and Veh-B channels with increasing delay spread (and therefore for decreasing coherence bandwidth). This is due to the fact that for these models the channel frequency responses show significant selectivity over the subcarrier bandwidth that the single tap equalizer is unable to compensate. The 3-tap structure, on the other hand, is able to perform frequency selective channel equalization as demonstrated in the previous section.

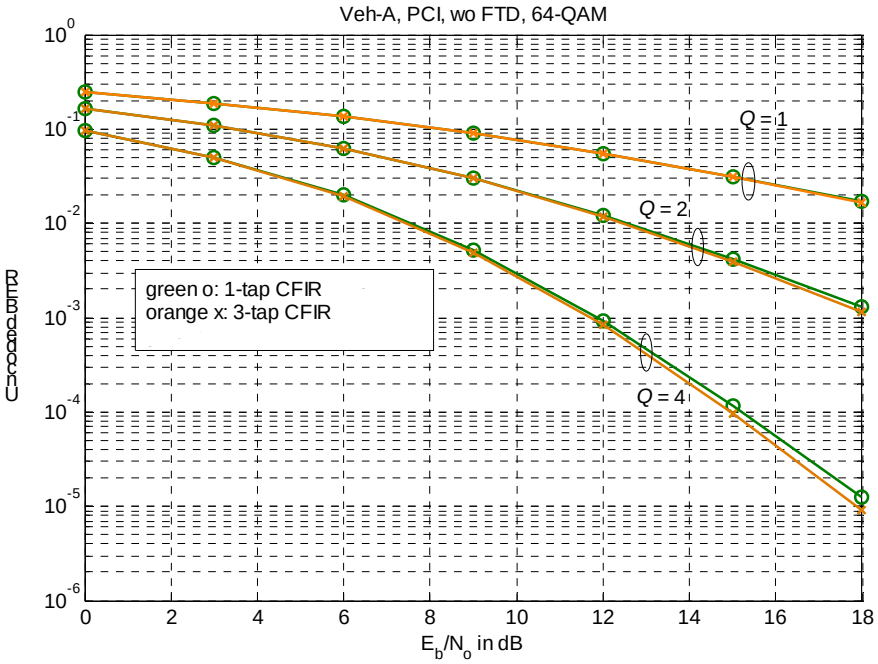

(a)

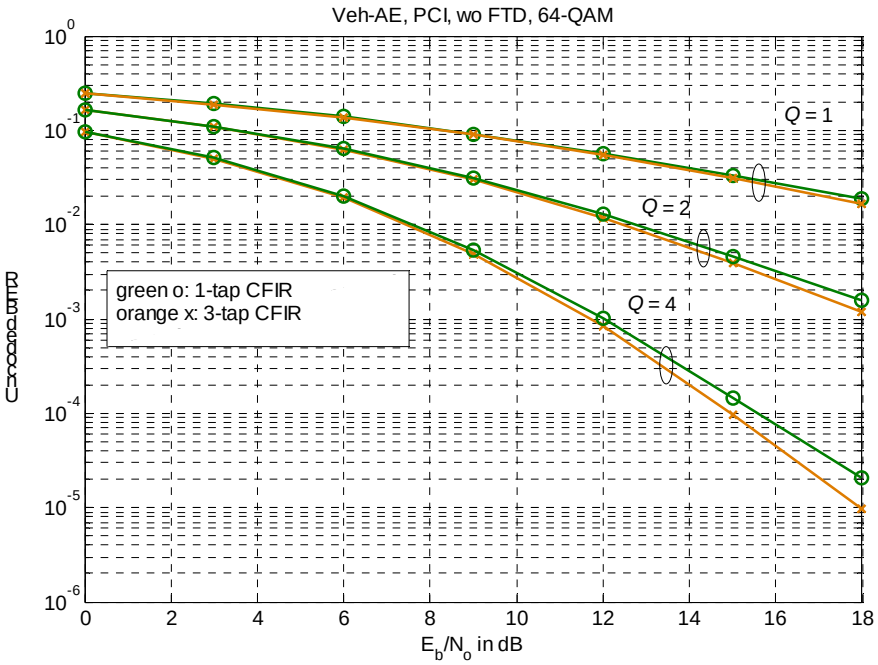

(b)

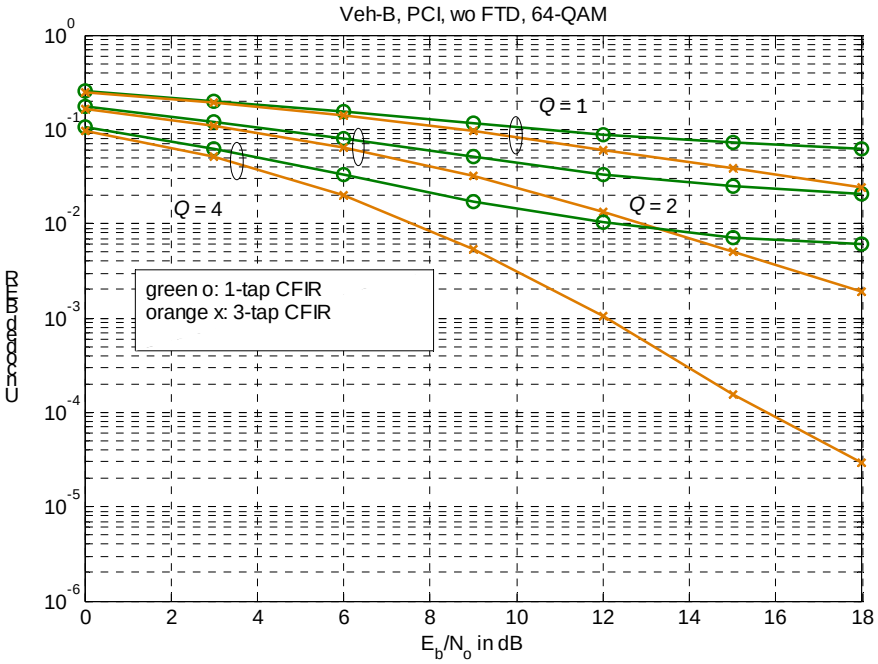

(c)

Figure 4.2.3. Uncoded bit-error-rate performance for FBMC system exploiting receive diversity of order $Q = 2$ and $Q = 4$ for transmission over (a) Veh-A, (b) Veh-AE, and (c) Veh-B multipath channels, respectively. Perfect channel information and timing synchronization is assumed in the receiver. 64-QAM modulation.

Timing offset introduces a linearly frequency-dependent phase response over the signal band, resulting in frequency-selective subcarrier responses even for multipath channel profiles that otherwise would impose approximately flat-fading responses. This timing offset needs to be appropriately compensated for in order to recover the orthogonality among the neighboring subcarriers, a condition necessary to guarantee sufficient signal quality for low error rates prior detection. Here, we consider a frequency domain compensation of the timing offset by means of 3-tap CFIR subcarrier equalizers. Figure 4.2.4(a) and (b) show the uncoded BER for FBMC receiver exploiting diversity reception over the Veh-AE channel model when fractional time delay of $\tau = 0.05$ (approximately 25 samples) and $\tau = 0.1$ (approximately 50 samples), respectively, is additionally included in the system model. Perfect knowledge of the fractional delay is assumed in the receiver. Moreover, recall that without a timing offset, the performance with 1-tap and 3-tap equalizers are approximately equal when a 64-QAM transmission over the Veh-AE channel is considered (see Fig. 4.2.3(b) for clarification). Figure 4.2.4(a) and (b) clearly show that even fairly modest timing offsets severely degrade the system performance unless not properly compensated for. This is in fact the case with the 1-tap equalizer that is only capable of frequency-flat processing and therefore fails to compensate for the phase slope within the subcarrier band. The 3-tap structure (and multitap structures in general), on the other hand, provides performance very close to that obtained in the ideally synchronized case (also shown as reference for 3-tap structure). These results demonstrate the feasibility of performing the timing adjustment in the frequency domain using frequency sampling-designed multitap per-subcarrier equalizers. Moreover, with the described approach, the timing offset can be compensated at virtually no additional cost in contrast to approaches where separate processing (circuitry) for timing adjustment is applied.

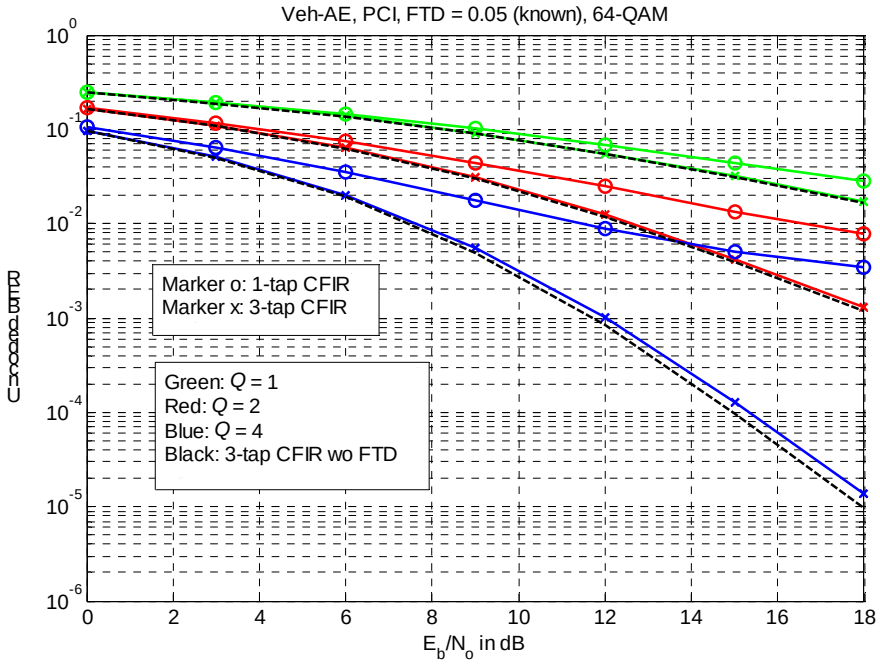

(a)

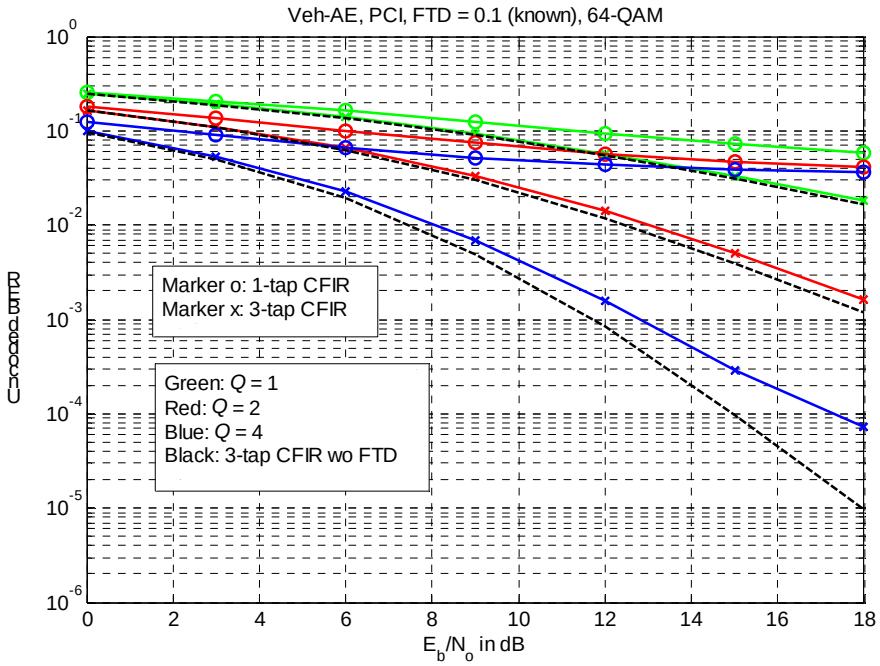

(b)

Figure 4.2.4. Uncoded bit-error-rate performance for FBMC system exploiting receive diversity of order $Q = 2$ and $Q = 4$ for transmission over Veh-AE multipath channel when fractional time delay (FTD) of (a) $\tau = 0.05$ and (b) $\tau = 0.1$, respectively, is included in the system model. Perfect channel information and knowledge on the FTD is assumed in the receiver. 64-QAM modulation.

4.2.4 Extension to other multi-antenna configurations

The structure of Figure 4.2.1 can be generalized to other linear multiantenna receiver configurations in case of mildly frequency selective subcarriers.

Assume that the complex frequency responses at time n from transmitter antenna p to receiver antenna q at frequency point (i) of subcarrier k , $H_{k,(i),n}^{p,q}$ are available. Assume further that for each (i) and k, the weights $\chi_{k,(i),n}^{p,q}$ for frequency-flat MIMO solution can be calculated from $H_{k,(i),n}^{p,q}$. Then the corresponding equalizer coefficients can be calculated as in (4.2.4) using $\chi_{k,(i),n}^{p,q}$ as the target response values.

5 MIMO Techniques for FBMC

MIMO techniques combine nicely with OFDM and sophisticated algorithms have been developed in that context. A key characteristic of FBMC is the possibility to have independent (non overlapping) sub-carriers. Therefore, two situations may occur in FBMC transmission:

1. The subcarriers do not overlap, which occurs when a user exploits a single subcarrier or when the interleaved Carrier Assignment Scheme (CAS) is employed. Then, QAM modulation can be used, the MIMO context is similar to OFDM and the same techniques can be implemented.
2. The subcarriers overlap and offset QAM modulation is used. This situation corresponds to the search for maximum throughput. Then, the OFDM techniques must be adapted and specific schemes must be elaborated.

The PHYDYAS project is essentially concerned with the second situation. In the following sections, the two main approaches of the MIMO concept are briefly reviewed and an introduction is provided for their application in the FBMC context. These two approaches are basically:
- Spatial Multiplexing (SM): Increasing the throughput by transmitting different streams of data over the different antennas.
- Spatial Diversity (SD): Improve the robustness of the transmission by transmitting the same data with coding over the different antennas.

5.1 Spatial multiplexing

Spatial multiplexing using layered space-time coding techniques increases spectral efficiency and enable to communicate at higher data rates. An architecture which theoretically achieves the capacity in an independent Rayleigh scattering environment was proposed as BLAST in [22]. Difficulties in implementation of the original Diagonal-BLAST (D-BLAST) led to a simplified architecture called V-BLAST [29] where each layer is associated with a certain transmit antenna.

5.2 Diversity techniques

The full spatial diversity gain is obtained by using Space Time Code (STC). The primary purpose of STC is to ensure that a given data will be transmitted by all the transmitted antennas such that the data will encounter all channel attenuation coefficients, thus leading to more reliable detection. STC is divided into two classes: Space Time Trellis Codes (STTC) and Space Time Block Codes (STBC).

- In STTC codes, the data to be transmitted are coded in such a way that the minimum distance between block transmitted is maximized at the decoding side [26]. STTC codes provide two benefits: the diversity gain, as the data is send by all the transmitted antennas, and the coding gain, by maximizing the distance. The main drawback is that it requires a high decoding complexity implemented in general by a Viterbi decoder. This complexity grows exponentially with the number of antennas.
- On the other hand, STBC's [27][25] purpose is to design transmission data so the received signal could be writen as orthogonal sequences. Therefore, the best decoding in terms of error probability is obtained with a simple linear decoder. Thus, STBC present in general lower complexity than STTC. However, STBC do not provide a coding gain.

STC codes have already been combined with CP-OFDM leading to good performances. In this family, the simplest scheme, restricted to the case of 2 transmit antennas and a single receive antenna, is the so-called "Alamouti" scheme [20]. To begin with, the application of this scheme to FBMC is considered.

5.2.1 Alamouti scheme with FBMC

The FBMC modulator transmits real data, which correspond either to the real or the imaginary part of complex data. That is, we can view the real transmitted data $d_{k,n}$ at subcarrier index k and time instant n as:

- $d_{k,2n} = \Re\{c_{k,2n}\}$ and $d_{k,2n+1} = \Im\{c_{k,2n}\}$

where $c_{k,n}$ is the complex data. Therefore, if we apply the Alamouti scheme to the $c_{k,n}$ complex data, we have:

- At antenna 0: $\begin{cases} c^0_{k,2n} & = c_{k,n} \\ c^0_{k,2n+1} & = -(c_{k,n+1})^* \end{cases}$
- At antenna 1: $\begin{cases} c^1_{k,2n} & = c_{k,n+1} \\ c^1_{k,2n+1} & = c^*_{k,n} \end{cases}$

This leads to the following input real data:

$$\begin{cases} d^0_{k,2n} & = \Re\{c_{k,n}\}, d^1_{k,2n} = \Re\{c_{k,n+1}\} \\ d^0_{k,2n+1} & = \Im\{c_{k,n}\}, d^1_{k,2n+1} = \Im\{c_{k,n+1}\} \\ d^0_{k,2n+2} & = -\Re\{(c_{k,n+1})^*\} = -\Re\{c_{k,n+1}\} = -d^1_{k,2n} \\ d^1_{k,2n+2} & = \Re\{(c_{k,n})^*\} = \Re\{c_{k,n})\} = d^0_{k,2n} \\ d^0_{k,2n+3} & = -\Im\{(c_{k,n+1})^*\} = \Im\{c_{k,n+1}\} = d^1_{k,2n+1} \\ d^1_{k,2n+3} & = \Im\{(c_{k,n})^*\} = -\Im\{c_{k,n}\} = -d^0_{k,2n+1} \end{cases} \tag{5.2.1}$$

At the single received antenna side, the demodulated signal can be written as:

$$y_{k,n} = H^{0,0}_{k,n}(d^0_{k,n} + ju^0_{k,n}) + H^{1,0}_{k,n}(d^1_{k,n} + ju^1_{k,n}) + \eta_{k,n}$$

where $\eta_{k,n}$ is the noise component at the sub-carrier k and time instant n. Thus the transmission of the real data given in (5.2.1), leads to the received/demodulated signal:

$$\begin{cases} y_{k,2n} & = H^{0,0}_{k,2n}(d^0_{k,2n} + ju^0_{k,2n}) + H^{1,0}_{k,2n}(d^1_{k,2n} + ju^1_{k,2n}) + \eta_{k,2n} \\ y_{k,2n+1} & = H^{0,0}_{k,2n+1}(d^0_{k,2n+1} + ju^0_{k,2n+1}) + H^{1,0}_{k,2n+1}(d^1_{k,2n+1} + ju^1_{k,2n+1}) + \eta_{k,2n+1} \\ y_{k,2n+2} & = H^{0,0}_{k,2n+2}(d^0_{k,2n+2} + ju^0_{k,2n+2}) + H^{1,0}_{k,2n+2}(d^1_{k,2n+2} + ju^1_{k,2n+2,1}) + \eta_{k,2n+2} \\ y_{k,2n+3} & = H^{0,0}_{k,2n+3}(d^0_{k,2n+3} + ju^0_{k,2n+3}) + H^{1,0}_{k,2n+3}(d^1_{k,2n+3} + ju^1_{k,2n+3,1}) + \eta_{k,2n+3} \end{cases}$$

The purpose now is to recover the data $c_{k,n}$ from the above equation. We assume the channel invariant over the time of interest i.e.

$$H^{0,0}_{k,2n} = H^{0,0}_{k,2n+1} = H^{0,0}_{k,2n+2} = H^{0,0}_{k,2n+3} = h_{k,1}$$
$$H^{1,0}_{k,2n} = H^{1,0}_{k,2n+1} = H^{1,0}_{k,2n+2} = H^{1,0}_{k,2n+3} = h_{k,2}$$

Then, we have:

$$\underbrace{\begin{bmatrix} y_{k,2n} \\ (y_{k,2n+2})^* \end{bmatrix}}_{\mathbf{y}_{2n}} = \begin{bmatrix} h_{k,1} & h_{k,2} \\ (h_{k,2})^* & -(h_{k,1})^* \end{bmatrix} \begin{bmatrix} d^0_{k,2n} \\ d^1_{k,2n} \end{bmatrix} + \begin{bmatrix} h_{k,1} & h_{k,2} & 0 & 0 \\ 0 & 0 & (h_{k,2})^* & -(h_{k,1})^* \end{bmatrix} \begin{bmatrix} ju^0_{k,2n} \\ ju^1_{k,2n} \\ -ju^1_{k,2n+2} \\ ju^0_{k,2n+2} \end{bmatrix} + \underbrace{\begin{bmatrix} \eta_{k,2n} \\ (\eta_{k,2n+2})^* \end{bmatrix}}_{\boldsymbol{\eta}_{k,2n}}$$

and

$$\underbrace{\begin{bmatrix} y_{k,2n+1} \\ (-y_{k,2n+3})^* \end{bmatrix}}_{\mathbf{y}_{2n+1}} = \begin{bmatrix} h_{k,1} & h_{k,2} \\ (h_{k,2})^* & -(h_{k,1})^* \end{bmatrix} \begin{bmatrix} d^0_{k,2n+1} \\ d^1_{k,2n+1} \end{bmatrix} + \begin{bmatrix} h_{k,1} & h_{k,2} & 0 & 0 \\ 0 & 0 & (h_{k,2})^* & -(h_{k,1})^* \end{bmatrix} \begin{bmatrix} ju^0_{k,2n+1} \\ ju^1_{k,2n+1} \\ ju^1_{k,2n+3} \\ -ju^0_{k,2n+3} \end{bmatrix} + \underbrace{\begin{bmatrix} \eta_{k,2n+1} \\ (\eta_{k,2n+2})^* \end{bmatrix}}_{\boldsymbol{\eta}_{k,2n+1}}$$

Thus, the decoding of $(d^0_{k,2n}, d^1_{k,2n})^T$ and $(d^0_{k,2n+1}, d^1_{k,2n+3})^T$ are done in the same manner. Let us focus on the detection of $(d^0_{k,2n}, d^1_{k,2n})^T$. If we compute:

$$\underbrace{\begin{bmatrix} z_{k,2n} \\ z_{k,2n+2} \end{bmatrix}}_{\mathbf{z}_{2n}} = \Re\left\{ \begin{bmatrix} (h_{k,1})^* & h_{k,2} \\ (h_{k,2})^* & -(h_{k,1}) \end{bmatrix} \begin{bmatrix} y_{k,2n} \\ (y_{k,2n+2})^* \end{bmatrix} \right\},$$

we obtain:

$$\mathbf{z}_{2n} = (|h_{k,1}|^2 + |h_{k,2}|^2) \begin{bmatrix} d^0_{k,2n} \\ d^1_{k,2n} \end{bmatrix} + \underbrace{\Im\{h^*_{k,1} h_{k,2}\} \begin{bmatrix} -u^1_{k,2n} + u^0_{k,2n+2} \\ u^0_{k,2n} + u^1_{k,2n+2} \end{bmatrix}}_{\mathbf{t}_{k,2n}} + \mathbf{v}_{k,2n},$$

where $\mathbf{v}_{k,2n}$ is the noise term given by:

$$\mathbf{v}_{k,2n} = \Re\left\{ \begin{bmatrix} (h_{k,1})^* & h_{k,2} \\ (h_{k,2})^* & -(h_{k,1}) \end{bmatrix} \begin{bmatrix} \eta_{k,2n} \\ (\eta_{k,2n+2})^* \end{bmatrix} \right\}$$

Consequently, $\mathbf{t}_{k,2n}$ is an interference term, which is not present in classical Alamouti decoding scheme. This term is canceled when $\mathrm{Im}\{h^*_{k,1} h_{k,2}\} = 0$. , which implies that the channels are proportional and the proportionality factor is real. Therefore, alternative schemes will be developed for FBMC to fully exploit the spatial diversity while providing a simple decoding process.
The delay diversity approach is presented in section 5.2. But, as an introduction to the processing, zero delay is considered first.

5.2.2 The zero-delay case

The transmission of two real symbols over two consecutive carriers is as follows:

$$d^1_{k,n} = d_1 \quad d^1_{k+1,n} = jd_2$$
$$d^2_{k,n} = d_1 \quad d^2_{k+1,n} = jd_2$$

Then, the received signal in the first subchannel states as

$$y_1 = (d_1 + ju_1)h_1 + (d_1 + ju_1)h_2 + \eta_1$$

where η_1 is the noise term received in the subchannel 1, and u_1 accounts for all the interference components that arise from the filterbank usage, where this interference comes from the two adjacent subchannels and time instants. On the other hand, the received signal in the second subchannel is as

$$y_2 = (u_2 + jd_2)h_1 + (u_2 + jd_2)h_2 + \eta_2$$

The receiver now has two different input signals, one on each subchannel, where each input results into a spatial combination of each one of the two parts d_1 and d_2 of the same symbol.
At the receiver side, some processing can be accomplished to deal with the output from subchannel 1, so that we can obtain the following expression with d_1 and without any component from d_2, as follows:

$$z_1 = Re\{h_1^H\ y_1 + h_2\ y_1^H\} = \left(|h_1|^2 + 2Re\left(h_1^H h_2\right) + |h_2|^2\right) d_1 + Re\left(h_1^H \eta_1\right) + Re\left(h_2 \eta_1^H\right) \qquad (5.2.2)$$

where we can see that all the interference terms u_1 are removed thanks to the receiver processing. This is actually a great step as 8 interfering terms have disappeared. The price for that is some dependence on the channel phase due to the $\mathrm{Re}\left\{h_1^* h_2\right\}$ term, that can show positive and negative values depending on the instantaneous channel conditions of both h_1 and h_2. Notice that the information in d_1 is received with a great spatial antenna gain as it benefits from both h_1 and h_2. Moreover, the data component d_1 is received without any other data components, so that with the simple Matched Filter (MF) receiver, the data can be efficiently extracted. Obviously, this single equation is enough for the detection of d_1 but we still need another one for d_2. Also some proposal is required to deal with the channel phase effect, as will be later seen.

Applying a different processing at the receiver side for subchannel 2 in order to retrieve the d_2 component, we obtain the following equation.

$$z_2 = \mathrm{Im}\left\{h_1^H\ y_2 + h_2^H\ y_2\right\} = \left(|h_2|^2 + 2Re\left(h_1^H h_2\right) + |h_1|^2\right) d_2 + \mathrm{Im}\left(h_1^H \eta_2\right) + \mathrm{Im}\left(h_2^H \eta_2\right) \qquad (5.2.3)$$

where we also notice that there is not any interference term in the equation. As we saw in (5.2.2), a channel phase dependence is also present for the detection of d_2.

From the previous two equations, the detection of d_1 and d_2 seems to be solved as no more FBMC/OQAM interfering terms are shown in the equations. The problem that we remain to solve is the channel phase effect due to the $\mathrm{Re}\left\{h_1^* h_2\right\}$ term. Notice that the channel phase effect can be positive or negative, where the receiver is interested in a positive value for the channels phase effect, so that the decoding process is improved.

The zero delay scheme could be applied with opportunistic transmission, if we define the user with the best channel conditions as the one who shows a positive and high value for the $\mathrm{Re}(h_1^H h_2)$ term, so that its selection enables the following condition

$$\left(|h_2|^2 + 2Re\left(h_1^H h_2\right) + |h_1|^2\right) > \left(|h_2|^2 + |h_1|^2\right)$$

to guarantee that the phase channel effect is always beneficial to the system performance. Therefore, the opportunistic transmission is looking for scheduling the user showing

$$\max_{over\ all\ user} \left(|h_2|^2 + 2Re\left(h_1^H h_2\right) + |h_1|^2\right)$$

As the two parts of the symbol have to be detected with the same spatial diversity effect in both (5.2.2) and (5.2.3) then the same gains are obtained for the two parts of the symbol (i.e. d_1 and $d_{2\,2}$).

5.2.3 Single delay STTC in FBMC with 2 antennas.

As already mentioned, STTC enables also to exploit the diversity. A classical approach to diversity consists of introducing a delay between the signals transmitted by the different antennas [25]. This is often referred to as single delay STTC.

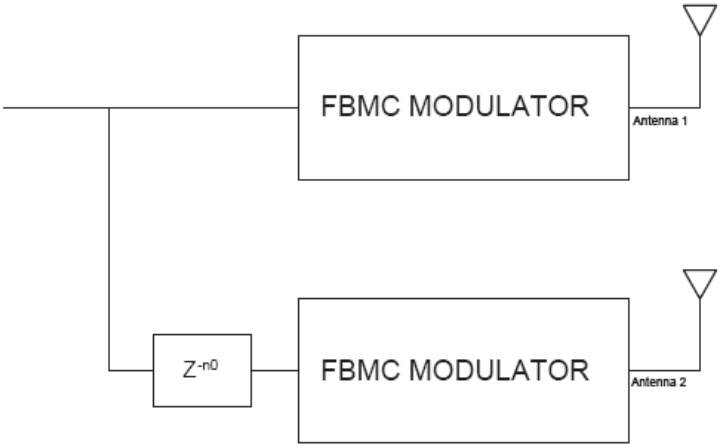

Figure 5.2.1: FBMC Single delay STTC transmitter

Let us consider the single delay STTC scheme with 2 antennas as shown in Figure 5.2.1. The real data to be transmitted are modulated by an FBMC modulator and transmitted by the first antenna. The same stream of data is delayed by $n_0 = 2$ before being modulated by the second FBMC modulator and transmitted by the second antenna. The delay $n_0 = 2$ is taken as to have the same delay as with a CP-OFDM system although a delay of $n_0 = 1$ could be chosen. We denote by $a_{k,n}$ the real data from the main stream of data at frequency k and time index n. Thus, at a given subcarrier k, the transmission is given by:

- At antenna 0: $d^0_{k,n} = a_{k,n}$
- At antenna 1: $d^1_{k,n} = a_{k,n-2}$.

At the receive side, the demodulated signal can be written as:

$$\begin{aligned}\tilde{y}_{k,n} &= H^{0,0}_{k,n}(d^0_{k,n} + ju^0_{k,n}) + H^{1,0}_{k,n}(d^1_{k,n} + ju^1_{k,n}) + \eta_{k,n} \\ &= H^{0,0}_{k,n}(a_{k,n} + ju^0_{k,n}) + H^{1,0}_{k,n}(a_{k,n-2} + ju^1_{k,n}) + \eta_{k,n},\end{aligned}$$

where $\eta_{k,n}$ is the noise component at the subcarrier k and time instant n. As the same stream of data is transmitted over the two antennas, we have:

$$u^1_{k,n} = u^0_{k,n-2} = u_{k,n-2}.$$

Moreover, if we assume a channel constant over time, i.e., $H^{0,0}_{k,n} = h_{k,1}$, $H^{1,0}_{k,n} = h_{k,2}$, we get:

$$\tilde{y}_{k,n} = h_{k,1}(a_{k,n} + ju_{k,n}) + h_{k,2}(a_{k,n-2} + ju_{k,n-2}) + \eta_{k,n}.$$

The problem now is how we recover the useful data $a_{k,n}$. Based on the work published in [21], noting $z_{k,n+2} = \mathrm{Re}\left\{(h_{k,2})^* \tilde{y}_{k,n} + (h_{k,1})^* \tilde{y}_{k,n+2}\right\}$, we get:

$$\begin{aligned} z_{k,n+2} &= \mathrm{Re}\left\{(h_{k,2})^* \tilde{y}_{k,n} + (h_{k,1})^* \tilde{y}_{k,n+2}\right\} \\ &= |h_{k,2}|^2 a_{k,n-2} + 2\mathrm{Re}\left\{h_{k,1}^* h_{k,2}\right\} a_{k,n} + |h_{k,1}|^2 a_{k,n+2} + \underbrace{\mathrm{Re}\left\{(h_{k,2})^* \eta_{k,n} + (h_{k,1})^* \eta_{k,n+2}\right\}}_{\mu_{k,n+2}} \end{aligned}$$

Then if we denote:

$$\mathbf{z}_1 = \begin{bmatrix} z_{k,0} & z_{k,2} & \cdots & z_{k,L_f-2} \end{bmatrix}^T,\ \mathbf{a}_1 = \begin{bmatrix} a_0 & a_2 & \cdots & a_{L_f-2} \end{bmatrix}^T$$

$$\mathbf{z}_2 = \begin{bmatrix} z_{k,1} & z_{k,3} & \cdots & z_{k,L_f-1} \end{bmatrix}^T,\ \mathbf{a}_2 = \begin{bmatrix} a_1 & a_3 & \cdots & a_{L_f-1} \end{bmatrix}^T$$

$$\boldsymbol{\mu}_1 = \begin{bmatrix} \mu_{k,0} & \mu_{k,2} & \cdots & \mu_{k,L_f-2} \end{bmatrix}^T,\ \boldsymbol{\mu}_2 = \begin{bmatrix} \mu_{k,1} & \mu_{k,3} & \cdots & \mu_{k,L_f-1} \end{bmatrix}^T$$

Thus, we have:

$$\mathbf{z}_1 = \underbrace{\begin{bmatrix} |h_{k,1}|^2 & 0 & \cdots & \cdots & \cdots & 0 \\ 2\mathrm{Re}\{h_{k,1}h_{k,2}^*\} & |h_{k,1}|^2 & \ddots & \cdots & \cdots & \vdots \\ |h_{k,2}|^2 & 2\mathrm{Re}\{h_{k,1}h_{k,2}^*\} & |h_{k,1}|^2 & 0 & \cdots & 0 \\ 0 & \ddots & \ddots & \ddots & \ddots & \vdots \\ \vdots & \ddots & \ddots & \ddots & \ddots & 0 \\ 0 & \cdots & 0 & |h_{k,2}|^2 & 2\mathrm{Re}\{h_{k,1}h_{k,2}^*\} & |h_{k,1}|^2 \end{bmatrix}}_{\mathbf{H}} \mathbf{a}_1 + \boldsymbol{\mu}_1$$

$$\mathbf{z}_2 = \underbrace{\begin{bmatrix} |h_{k,1}|^2 & 0 & \cdots & \cdots & \cdots & 0 \\ 2\Re\{h_{k,1}h_{k,2}^*\} & |h_{k,1}|^2 & \ddots & \cdots & \cdots & \vdots \\ |h_{k,2}|^2 & 2\mathrm{Re}\{h_{k,1}h_{k,2}^*\} & |h_{k,1}|^2 & 0 & \cdots & 0 \\ 0 & \ddots & \ddots & \ddots & \ddots & \vdots \\ \vdots & \ddots & \ddots & \ddots & \ddots & 0 \\ 0 & \cdots & 0 & |h_{k,2}|^2 & 2\mathrm{Re}\{h_{k,1}h_{k,2}^*\} & |h_{k,1}|^2 \end{bmatrix}}_{\mathbf{H}} \mathbf{a}_2 + \boldsymbol{\mu}_2$$

The decoding of $\mathbf{a}_1$ or $\mathbf{a}_2$ is done in the same manner therefore we focus only on the decoding of $\mathbf{a}_1$. An evaluation of the maximum likelihood performance can be done to assess the bound of this STTC chain. Extension of this scheme to higher number of antennas (3,4) and an analysis of more complex STTC schemes can also be considered.

6 Overview and conclusion

In the multiantenna context, the prototype filter impulse response has the same impact as in the single antenna case and, therefore, the techniques developed for single antenna can be extended to MIMO.

Again, two transition phases can be present, related to the preamble symbols and the data symbols.
If appropriate, the preamble transition can be eliminated by the memory preloading technique, recalled in section 3.4. Similarly, it can be reduced by the burst shortening scheme introduced in document D2.1.
A simple method to exploit the single antenna techniques is the frequency multiplexing of the signals of the transmitter antennas, as mentioned in section 3.4.1. The approach leads CFO and timing delay estimation and also to the measurement of the channel matrix elements, except that an additional interpolation step is necessary to get the full channel estimation. A key advantage is that there is no cascading of preambles for the measurements of the channel matrix elements.

If timing offset estimation in the time domain is desired, then the joint ML technique can be invoked and it is described in section 2 for multiple antennas. Next, if the transition phase of the data symbols is to be eliminated or reduced, the auxiliary pilot scheme is used, as described in section 2.2 for CFO and timing offset estimation and in sections 3.1 and 3.2 for channel estimation.

Concerning scattered pilot/auxiliary pilot pairs in a scenario with multiple transmit antennas, it is necessary that the pilots be alotted to the different transmit antennas in such a way that, when one antenna sends a pilot, the others are silent. It was found out that the pilot quality remains good in the synchronized scheme, and the pilot-based synchronization schemes developed for the single-antenna case can be expected to perform well also in multi-antenna transmission. In multiuser MIMO schemes (like collaborative spatial multiplexing of WiMAX), this pilot model shows some level of robustness, tolerating carrier frequency differences approaching 5% of subcarrier spacing and timing offsets approaching 5 % of OQAM symbol interval while maintaining 20 dB pilot MSE.

For an initial channel estimate based on preamble, we have investigated a number of methods for both *full* and *sparse* preambles. It was seen that FBMC offers a significant improvement in estimation accuracy, for low and moderate SNR values. At high SNR regimes, the well-known error floor (due to the intrinsic interference) again prevails and FBMC is then outperformed by CP-OFDM. As expected, the crossing point is moved to higher SNR values as the number of subcarriers increases. It should be noted that, as confirmed in the simulations (Figure 3.1.6), with the *optimal* one-symbol preamble there is practically no significant interference neither in frequency nor in time direction, and hence the error floor is not an issue. Although only 1.5 complex symbols are used, the obtained estimation performance is significantly better than all the other schemes considered.

In subsection 3.2, several pilot schemes for two and four antennas have been adapted to the FBMC scheme following the DL-PUSC basis in WiMAX standard. Obtained performance results concerning the POP scheme makes it inappropriate for filter bank applications and compared with the conventional OFDM scheme neither similar or better performances are achieved. The IMR-b scheme achieves better results than the POP due the use of more APC carriers, exactly 4 aided pilots. Using the IAMb in Veh-A channel very similar performance in terms of BER is achieved with FBMC scheme and OFDM. Note that using the IAM-b, still not all the interferences ($\Omega_{1,1}$) that affect the pilot $d^{i}_{k,n}$ could be estimated but almost the largest interference weights caused by the PHYDYAS filter bank contributions. However the use of auxiliary pilots with one help pilot carrier to cancel the interference within the secondary part seems an interesting candidate to be used in FBMC, as it achieves the same performances as the OFDM and outperforms it using a MMSE equalization. The adapted approach for DL-PUSC mode eliminates the secondary interference from the neighbouring symbols onto the antenna pilot. The use of scattered pilot combines the auxiliary technique and the APC approach, the antenna's pilot positions are overlapped and their values combined such that the pilot position doesn't suffer the effect of the surrounding interference due to the largest weights of the PHYDYAS filter. In pedestrian channel the FBMC performances using scattered pilots are very similar to CP-OFDM.

The issue of channel tracking in case of high mobility combines nicely with the adaptation capability of FBMC and a Kalman filter approach is presented in section 3.3, showing a 3 dB gain in mean square error power.

Now, once the channel measurements are available, the sub-channel equalizer coefficients can be derived through a straight application of the schemes reported in documents D2.1 and D2.2. For comparison purposes, the MMSE classical techniques are recalled in section 4.1.2.

With FBMC, due to the presence of the sub-channel equalizers, it is possible to implement more sophisticated techniques, involving the successive interference cancellation principle, as described in sections 4.1.3-6. Simulations show that gains can be obtained at high SNR values.

The frequency-sampling based method for subcarrier equalizer design was extended to antenna diversity reception in SIMO transmission and also to the MIMO case. Three-tap subcarrier equalizers were shown to provide significant performance gain over 1-tap equalizers with increasing channel delay spread and/or significant timing offsets. The frequency sampling based MIMO solution provides a good tradeoff between complexity and performance when there is modest frequency selectivity with the subcarrier bandwidth.

The present document is related to the beginning of the work in WP4. In the next phase, the MIMO techniques will be developed. An introduction to these techniques is provided in section 5, which is a transition to the work which will be reported in the next deliverable.

7 References

[1] T. Fusco, A. Petrella, and M. Tanda, "Data-aided symbol timing estimation for multiple access OFDM/OQAM systems," accepted for presentation at *ICC-2009*, Dresden, Germany, June 14-18, 2009.

[2] Deliverable 2.1, "Data-aided synchronization and initialization (single antenna)" ICT-211887 PHYDYAS, July 2008.

[3] N. Zorba, "Spatial diversity within the OQAM-OFDM systems," Centre Tecnologic de Telecomunicacions de Catalunya (CTTC).

[4] J.-P. Javaudin, D. Lacroix, and A. Rouxel, "Pilot-aided channel estimation for OFDM/OQAM," *Proc. VTC-2003 (Spring)*, pp. 1581-1585, April 2003.

[5] Deliverable 3.1, "Transmit/receive processing (single antenna)," ICT-211887 PHYDYAS, July 2008.

[6] C. Lélé, J.-P. Javaudin, R. Legouable, A. Skrzypczak, and P. Siohan, "Channel estimation methods for preamble-based OFDM/OQAM modulations," *Proc. EW'07*, Paris, France, April 2007.

[7] F. Schaich, "Framing in WiMAX," PHYDYAS internal report, Feb. 2008.

[8] Air interface for Fixed Broadband Wireless Access Systems, IEEE Standard for Local and Metropolitan Area Networks, IEEE 802.16-2004, June 2004.

[9] Amendment 2 and Corrigendum 1 to IEEE Std. 802.16-2004, IEEE Std. 802.16e-2005, Feb. 2006.

[10] M. El Tabach, J.-P. Javaudin, and M. Hélard, "Spatial data multiplexing over OFDM/OQAM modulations," *Proc. ICC'2007*, pp 4201-4206, 24-28 June 2007, Glasgow, Scotland.

[11] J.-P. Javaudin and Yiqi Jiang, "Channel estimation in MIMO OFDM/OQAM," *Proc. SPAWC-2008*, Recife, Pernambuco, Brazil, July 6-9, 2008.

[12] T. Karp and N. J. Fliege, "Modified DFT filter banks with perfect reconstruction," *IEEE Trans. Circuits and Systems II*, vol. 46, no. 11, pp. 1404-1014, Nov. 1999.

[13] G. Lin, L. Lundheim, and N. Holte, "On efficient equalization for OFDM/OQAM systems," *10th International OFDM Workshop*, Hamburg, Germany, Aug. 2005.

[14] D. S. Waldhauser, L. G. Baltar, and J. A. Nossek, "MMSE subcarrier equalization for filter bank based multicarrier systems," *Proc. SPAWC-2008*, Recife , Brazil, 6-9 July 2008.

[15] A. Paulraj, R. Nabar, and D. Gore, *Introduction to Space-Time Wireless Communications*, Cambridge University Press, 2003.

[16] J.G. Proakis, *Digital Communications*, 4th Edition, McGraw-Hill, 2001.

[17] M. G. Bellanger, "Specification and design of a prototype filter for filter bank based multicarrier transmission," *Proc. ICASSP'01*, Salt Lake City, USA, May 2001, pp. 2417-2420.
[18] N. Al-Dhahir and A. H. Sayed, "The finite-length multi-input multi-output MMSE DFE," *IEEE Trans. Signal Processing*, vol. 48, Oct. 2000.
[19] D. Mattera, L. Paura, and F. Sterle, "Widely linear decision-feedback equalizer for time-dispersive linear MIMO channels," *IEEE Trans. Signal Processing*, vol. 53, July 2005.
[20] S. M. Alamouti, "A simple transmit diversity technique for wireless communications," *IEEE Journal on Selected Areas in Communications*, vol. 16, no. 8, pp. 1451 – 1458, Oct. 1998.
[21] M. G. Bellanger, "Transmit diversity in multicarrier transmission using OQAM modulation," *Proc. ISWPC-2008*, Santorini (Greece), May 2008.
[22] G. J. Foschini, "Layered space-time architecture for wireless communications in a fading environment when using multiple antennas," *Bell Laboratories Technical Journal*, vol. 1, pp 41-59, 1996.
[23] G. J. Foschini, G. D. Golden, R. A. Valenzuela, and P. W. Wolniansky, "Simplified processing for high spectral efficiency wireless communications employing multi-element arrays," *IEEE Journal on Selected Areas in Communications*, vol. 17, no. 11, pp. 1841-1852, Nov. 1999.
[24] R. V. Nee, A. V. Zelst, and G. Awater, "Maximum likelihood decoding in a space division multiplexing system," *Proc. VTC- 2000 (Spring)*, May 2000.
[25] N. Seshadri and J. H. Winters, "Two signaling schemes for improving the error performance of frequency division duplex (FDD) transmission systems using transmitter antenna diversity," *Int. J. Wireless Inform. Networks*, vol. 1, no. 1, Jan. 1994.
[26] V. Tarokh, N. Seshadri, and A. R. Calderbank, "Space – time codes for high data rate wireless communication: Performance criterion and code construction," *IEEE Trans. Information Theory*, Vol. 44 (2), March 1998.
[27] V. Tarokh, H. Jafarkhani, and A. R. Calderbank, "Space – time block coding for wireless communications: Performance results," *IEEE Trans. Information Theory*, vol. 17, no. 3, March 1999.
[28] S. Verdú, *Multiuser Detection*, Cambridge University Press, 1998.
[29] P. W. Wolniansky, G. J. Foschini, G. D. Golden, and R. A. Valenzuela, "An architecture for realizing very high data rates over rich-scattering wireless channel," *Proc. URSI International Symposium on Signals, Systems, and Electronics*, pp. 295-300,1998.
[30] A. V. Zelst, "Space division multiplexing algorithms," *Proc. 10th Mediterranean Electrotechnical Conference (MELECON)*, May 2000.
[31] E. Kofidis, D. Katselis, A. Rontogiannis, and S. Theodoridis, "Preamble-based channel estimation methods for OFDM/OQAM systems," PHYDYAS internal report.
[32] E. Kofidis, D. Katselis, A. Rontogiannis, and S. Theodoridis, Preamble-based channel estimation methods for OFDM/OQAM systems: The MIMO case," PHYDYAS internal report.
[33] J. G. Andrews, A. Ghosh, and R. Muhamed, *Fundamentals of WiMAX: Understanding Broadband Wireless Networking*, Prentice-Hall, 2007
[34] C. Lélé, P. Siohan, and R. Legouable, "2 dB better than CP-OFDM with OFDM/OQAM for preamble-based channel estimation," *Proc. ICC'08*, Beijing, China, May 19-23, 2008.
[35] F. Schaich, "Preamble (DL) and sounding zone (UL)," PHYDYAS internal report.
[36] R. Negi and J. Cioffi, "Pilot tone selection for channel estimation in a mobile OFDM system," *IEEE Trans. Consumer Electronics*, vol. 44, no. 3, pp. 1122-1128, Aug. 1998.
[37] J. Rinne and M. Renfors, "Pilot spacing in orthogonal frequency division multiplexing systems on practical channels," *IEEE Trans. Consumer Electronics*, vol. 42, no. 2, pp. 959-962, Nov. 1996.
[38] I. Barhumi, G. Leus, and M. Moonen, "Optimal training design for MIMO-OFDM systems in mobile wireless channels," *IEEE Trans. Signal Processing*, vol. 51, no. 6, pp. 1615-1624, June 2003.

[39] M. G. Bellanger, "Initialization in FBMC transmission systems: The memory preloading technique," PHYDYAS internal report.
[40] H. Minn and N. Al-Dhahir, "Optimal training signals for MIMO OFDM channel estimation," *IEEE Trans. Wireless Communications*, vol. 5, no. 5, pp. 1158-1168, May 2006.
[41] Z. Wu, J. He, and G. Gu, "Design of optimal pilot-tones for channel estimation in MIMO-OFDM systems," *Proc. IEEE Wireless Communications and Networking Conf. (WCNC'05)*, New Orleans, LA, March 13-17, 2005.
[42] K. Yu, M. Bengtsson, and B. Ottersten, "MIMO channel models," pp. 271-292 in T. Kaiser et al. (eds.), *Smart Antennas - State of the Art*, Hindawi, 2005.
[43] S. L. Loyka, "Channel capacity of MIMO architecture using the exponential correlation matrix," *IEEE Communications Letters*, vol. 5, no. 9, pp. 369–371, Sept. 2001.
[44] G. L. Stüber, J. R. Barry, S. W. McLaughlin, Y. Li, M. A. Ingram, and T. G. Pratt, "Broadband MIMO-OFDM wireless communications," *Proc. IEEE*, vol. 92, no. 2, pp. 271-294, Feb. 2004.
[45] C. Zhenlan and D. Dahlhaus, "Time versus frequency domain channel tracking using Kalman filters for OFDM systems with antenna arrays," *Proc. VTC-2003 (Spring)*, April 22-25, 2003.
[46] T. Roman, *Advanced Receiver Structures for Mobile MIMO Multicarrier Communication Systems*, Ph.D. Thesis, Signal Processing Laboratory, Helsinki University of Technology, 2006.
[47] D. Schafhuber, G. Matz, and F. Hlawatsch, "Kalman tracking of time-varying channels in wireless MIMO-OFDM systems," *Proc. 37th Asilomar Conf. on Signals, Systems, and Computers*, Nov. 2003.
[48] M. Enescu, T. Roman, and V. Koivunen, "State-space approach to spatially correlated MIMO OFDM channel estimation," *Signal Processing*, vol. 87, no. 9, Sept. 2007.
[49] M. G. Bellanger, "PHYDYAS reference filter bank," PHYDYAS internal report.
[50] D. Lacroix and J.-P. Javaudin, "A new channel estimation method for OFDM/OQAM," *OFDM Workshop*, 2002.
[51] "Multi-user MIMO OFDM for next generation of wireless", Special Issue of Proceedings of the IEEE, vol.95, N°7, July 2007
[52] A. M. Wyglinski, P. Kabal and F. Labeau, "Variable-length subcarrier equalizers for multicarrier systems", *in Proc. IEEE Vehicular Technology Conference*, Los Angeles, CA, Sep. 2004